Performance Analysis of Matrix Fuel for a Passive Pressure Tube Light Water Reactor

by

Brett T. Mattingly

B.S., Electrical Engineering
Clarkson University, 1992

Submitted to the Department of Nuclear Engineering
in Partial Fulfillment of the Requirements for the Degree of

Master of Science in Nuclear Engineering

at the
Massachusetts Institute of Technology
June 1995

Signature of Author _____
Department of Nuclear Engineering

Certified by _____
Professor Neil E. Todreas
Department of Nuclear Engineering
Thesis Advisor

Certified by _____ 5/21/95
Dr. Scott A. Simonson
Research Scientist, Department of Nuclear Engineering
Thesis Advisor

Certified by _____
Professor Michael J. Driscoll
Department of Nuclear Engineering
Thesis Reader

Accepted by _____
Professor Allan F. Henry
Chairman, Department Committee on Graduate Students
Department of Nuclear Engineering

Performance Analysis of Matrix Fuel for a Passive Pressure Tube Light Water Reactor

by
Brett T. Mattingly

Submitted to the Department of Nuclear Engineering on May 24, 1995
in Partial Fulfillment of the Requirements for the Degree of
Master of Science in Nuclear Engineering

ABSTRACT

Thermal analyses were performed on two different fuel designs for use in the Passive Pressure Tube Light Water Reactor (PTLWR). From the results of these analyses and comprehensive literature reviews, an experimental program was designed and implemented to begin to examine the usefulness of using SiC coated graphite in a LWR.

The PTLWR fuel was designed to survive a loss of primary coolant accident without fuel damage. In order to achieve this, the fuel configurations incorporate high density, isotropic graphite which acts as a temporary heat sink in the initial stages of an accident. In these designs graphite is coated with SiC to prevent significant oxidation at high temperatures. The ability of a SiC coating to protect graphite was examined experimentally. Limited results indicate that an intact SiC coating can protect graphite from oxidation in a steam atmosphere at 1000°C for several hours. Microcracks in SiC coatings, caused by quench cooling of the SiC coated graphite, reduce the oxidation protection offered by SiC layers. However, some protection from rapid graphite oxidation is provided by a partially intact SiC layer. Thus, the goal of SiC providing protection for the graphite during a hypothetical accident sequence in a PTLWR appears promising.

Perhaps the more challenging issue to be overcome is the performance of SiC coated graphite during normal reactor operation. The specific water chemistry in a nuclear reactor during normal operation, if not chosen carefully, is detrimental to SiC coatings. Good corrosion performance of SiC under normal conditions appears feasible if lithium is avoided in the primary chemistry.

The most important issue that has been identified by this work is that of water infiltration into graphite through SiC coating defects. During rapid power changes, or initial stages of an accident, water that has penetrated the graphite can flash to steam. This can cause the SiC coating to crack and spall, thus exposing graphite surfaces to an oxidizing environment. It must be shown that this issue can be overcome through manufacturing control, quality assurance inspections, and the selection of an appropriate coating technology that will withstand in-service conditions.

Thesis Supervisors:	Prof. Neil E. Todreas	Dr. Scott A. Simonson
Titles:	Professor of Nuclear and Mechanical Engineering	Research Scientist

Dedication

For Norma Eleanor Bliss

April 1914 - July 1994

"Love will be remembered long after memories are forgotten."

Acknowledgments

The sponsorship of this study by the U.S. Department of Energy is acknowledged and greatly appreciated.

There are several people who helped me to complete the work in this thesis. First and foremost is Pavel Hejzlar who developed the initial concept for the specific reactor designs that were investigated. My work grew essentially out of a small area of his broader concept. I thank him for the many hours of technical assistance and constant communication, not to mention the help with unruly computer codes.

Second is Dr. Scott Simonson who has spent many hours helping me with the experimental work. His insight into experimental problems and graduate student motivation have made this thesis more than merely a science project. It has been a real pleasure to work with him. I must also thank his wife for allowing me to take so much of his time.

I sincerely thank Prof. Neil E. Todreas and Prof. Michael J. Driscoll for their support and technical direction throughout this endeavor. Without their expertise this project would never have been started.

The following people provided materials or equipment necessary to the success of the experimental work. Ernesto Cabello, Dr. Gordon Kohse, Yakov Ostrovsky, Prof. Ronald G. Ballinger, and Peter Stahle provided equipment and expertise for the reactor operating test. Peter Reagan from Thermo Electron provided the CVD coating for some of the specimens that were tested. John Bevilacqua from The Carborundum Company provided the α-SiC specimens that were tested. Many thanks to Rebecca Bartles and Thomas Storms of Toyo Tanso USA, Inc. for their help in preparing the materials provided by their company.

Finally I would like to thank Jessica Allison and Winston Fan for their help in performing some of the experimental work.

Table of Contents

List of Figures

List of Photographs

List of Tables

1. INTRODUCTION

1.1 Scope and Objectives of this Thesis

This thesis follows on the work done by others in a research group at MIT investigating a new passively safe reactor design, the Passive Pressure Tube Light Water Reactor (PTLWR). Specifically, this thesis presents results of an experimental evaluation of the performance of silicon carbide coated graphite for possible use in the PTLWR. Two fuel designs proposed for this new reactor concept were evaluated for thermal performance using computer models. From the results of these evaluations, and the previous work of the group, a series of tests was established and carried out to examine the possible use of silicon carbide as a protective coating for graphite used in the core of a light water reactor.

The experimental results for the silicon carbide coated graphite are compared to the behaviour of zircaloy and unprotected graphite under the same conditions. Several arguments are made to support the use of silicon carbide as a protective coating for use in LWRs.

1.2 Organization of this Thesis

The basic scope of the work was presented above. Important background information on the PTLWR concept is summarized in Chapter 2. A more complete background is given in Appendix B. Chapter 2 also summarizes background information on zircaloy and silicon carbide use in the nuclear industry. Specific references to corrosion performance in environments typical of reactor operation and accidents are given as a basis for comparing the experimental results presented in Chapter 5.

A brief history of the fuel design for the PTLWR and the results of the analyses performed on two of the proposed fuel designs for this reactor are given in Chapter 3. The experimental test environments for silicon carbide coated graphite are then established in the context of the fuel design evaluation results. Chapter 4 gives the specific experimental setup used to achieve each of the desired test environments, and outlines the test rationale behind certain material choices. Also presented in Chapter 4 is the method and content of data collection. Chapter 5 presents the data and the analysis of the data from the experiments. The analysis concentrates on the implications for SiC use in reactors, specifically for the protection of graphite structural material during normal operation and high temperature loss of coolant accidents. Chapter 6 then gives a summary of the major

findings of this work, and lists several specific items that require additional scrutiny in the future.

The appendices at the end of the thesis supplement the work presented in the main text and are intended primarily to facilitate the extension of this work by supplying details that are necessary for its reproduction. (The appendices are not paramount to understanding the basic conclusions.) As this work follows from work done previously by others, the author understands the desire for clarity and detail, especially when attempting to reproduce or re-analyze earlier conclusions.

2. BACKGROUND

2.1 Brief History and Overview of the PTLWR Concept

The current nuclear power industry is plagued by several disadvantages, both perceived and actual. Two of the most important are the perceived lack of safety of nuclear power plants, and the potentially unrecoverable financial investment in a nuclear plant. Typically these two perceptions are held by vastly different sectors of the population, namely the "general" or vocal public, and the large investors, respectively. Whether these perceptions are in fact true is not at issue, but the successful construction and operation of a nuclear power plant can only be accomplished if both of these concerns are resolved to the satisfaction of everyone involved. While these are certainly not the only factors affecting the design of a new nuclear power reactor, they are two of the most important areas addressed in all new reactor designs.

To accommodate these concerns, in recent years there has been considerable effort to design reactors which utilize passive safety features to prevent the occurrence of severe accidents or to mitigate their consequences. Such an approach leads to a substantial simplification of systems, while enhancing safety. However, the use of passive systems for decay heat removal generally necessitates lower achievable heat transfer capability, which results in lower unit power output, and ultimately in a higher cost per installed kilowatt. This apparent cost disadvantage may be offset by the considerable simplification of the plant if the elimination of redundant and complicated safety components results in a plant that is less expensive to build, operate, and maintain.

A plant that can preserve the simplification benefits that accompany passive safety while running at a high power output of about 1000 MWe should decrease the cost per kilowatt enough to give the plant a decided advantage over smaller passive nuclear plants, and more importantly, make the plant economically competitive with fossil fueled power plants. The Passive Pressure Tube Light Water Reactor (PTLWR) concept was developed at MIT to achieve this goal. The PTLWR is a light water cooled and moderated pressure tube reactor concept, similar to CANDU reactors, but having major differences in fuel design, coolant and moderator, calandria content, and the decay heat removal path to the ultimate heat sink. The design exploits the ability of a pressure tube reactor to operate at a high thermal power output while maintaining a short heat transfer path to the passive decay heat removal system. The main objective of the reactor concept is the capability to survive the total absence of primary coolant without fuel damage. The goals of the PTLWR are:

- Survive loss of primary coolant with no core damage,
- Prevent fast reactivity excursions,
- Achieve inherent reactor shutdown during accidents,
- Minimize technological and economic risk,
- Operate at a high power rating, and
- Produce electricity at a competitive cost.

The achievable operating power level of nuclear reactors is limited by the ability of the coolant system to remove generated heat at the location of the highest power density without exceeding safe temperature limits of the cladding or the fuel. The traditional approach is to establish a nominal power such that these safe limits are not exceeded either during steady state operation or plant transients. To stay within the safe limits in loss of coolant accident scenarios, the most common practice is to replenish with emergency coolant rapidly, to prevent the fuel elements from being uncovered. The approach taken in the PTLWR is based on the requirement that the fuel elements survive, without failure, the high temperatures which result when they become uncovered, thus eliminating the need to supply emergency make-up coolant. An additional constraint on the achievable reactor power results. Specifically this constraint arises because the voided fuel elements must be capable of dissipating the decay heat by natural phenomena, such as conduction, radiation, and convection, without exceeding the safe temperature limits.

One of the major factors affecting the temperature of the voided fuel, is the path length between the hot fuel and the heat sink during the accident. In the PTLWR, this path for heat rejection in the fuel bundles is the distance to the pressure tube wall. Because this path is relatively short, the temperature of the fuel bundles during an accident can be maintained within safe limits for some ceramic fuel materials; however, the prospect of using zircaloy is rather bleak. In the PTLWR, the decay heat passes through the pressure tube, through the gap into the calandria tube, and then through the calandria tube and into the water surrounding the calandria tube. Once the heat reaches the water surrounding the calandria tube, the path to the ultimate heat sink depends on the specific reactor variant being evaluated, both of which are discussed next.

Two variants of the PTLWR were developed, the main physical difference being whether the calandria tubes are maintained wet or dry during normal operation. A picture of the core layout for the wet calandria variant is shown in Figure 2-1. The core consists of a large voided calandria with 740 pressure tubes, each containing a fuel matrix. The fuel matrix shown in Figure 2-1 is only one of the possible configurations, this and one other are evaluated in Chapter 3. Surrounding each pressure tube is a calandria tube, typical of

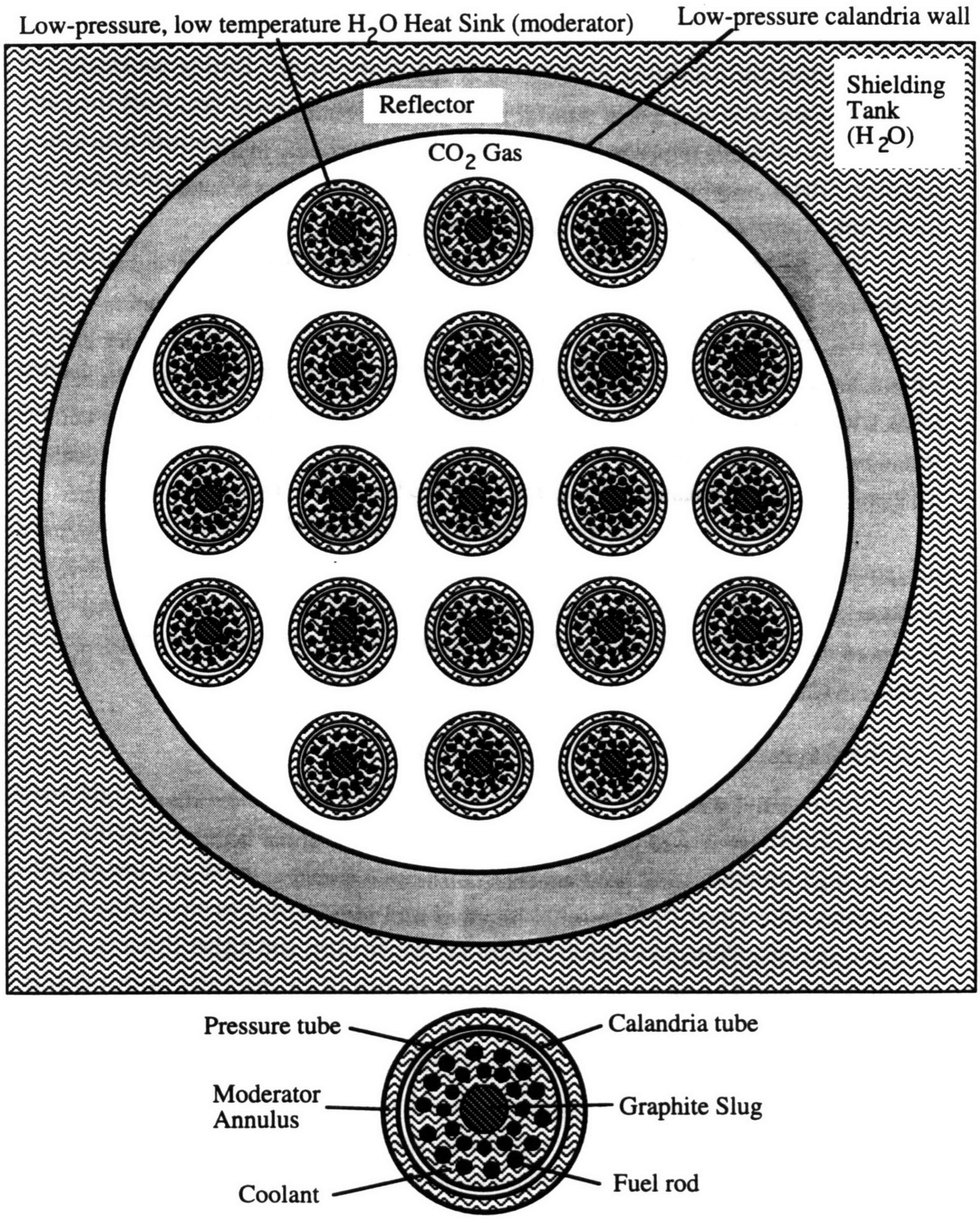

Figure 2-1: Wet Calandria Design Configuration

CANDU reactors. However, outside the calandria tube is a thin light water annulus which is contained by an outer moderator tube. During normal operation, this water annulus provides moderator capability in excess of the coolant water. During accidents, the moderator water acts as a heat transfer mechanism to remove decay heat from the outer surface of the calandria tube to a heat exchanger and ultimately to the ambient atmosphere heat sink. The moderator annulus system is designed to operate via natural circulation and convection to provide a passive cooling mechanism.

The core layout of the dry calandria variant is similar to the wet calandria except for the absence of a moderator annulus. A picture of the dry calandria variant is shown in Figure B-1 in Appendix B The accident decay heat rejection path in the dry calandria variant is established by flooding the calandria with light water, thus wetting the calandria tubes with the water which acts as the immediate decay heat sink. This water boils and later condenses on the containment shell. The outer containment shell surface is cooled by a natural circulation air annulus, thus transferring the heat to the ambient atmosphere.

Appendix B gives a more complete discussion of the PTLWR, including descriptions of the wet and dry calandria variants. The wet calandria variant is developed in detail by Tang [1992], the dry calandria variant is developed in detail by Hejzlar [1994]. A more detailed discussion of the fuel matrix layout for the wet calandria variant can be found in Chapter 3 where two fuel matrix designs are evaluated.

2.2 Background on Zircaloy Corrosion Data

Currently, the zircaloy alloys are the most widely used cladding in light water reactors. Zircaloy is used primarily because of its low thermal neutron absorption cross section, high strength, and good aqueous corrosion resistance. In the last few decades, the zircaloy alloys have continued to improve with respect to corrosion resistance, their strength, and their ability to withstand longer irradiation times and higher fluences. Pellet-clad interaction (PCI) and water side corrosion are two of the mechanisms that degrade cladding performance and durability, especially for high burnup fuel. The use of a pure zirconium layer on the inside of the zircaloy cladding has been successful in limiting PCI. The specialization of zircaloy-2 to boiling water reactors and zircaloy-4 to pressurized water reactors is a direct result of a corrosion problem, specifically hydriding in cladding used in the hydrogen rich waters of a PWR. (This thesis is concerned mostly with zircaloy-4 due to the PTLWR being a PWR application.) The waterside corrosion issues are continually

being addressed by the development of new cladding alloys such as ZIRLO™ [Sabol, 1994].*

The overall operating history of zircaloy is quite impressive, but zircaloy performance during reactor accidents is not as reassuring. Zircaloy, like most metals, begins to oxidize and lose structural integrity at temperatures far lower than those reached by the nuclear fuel pellets during an accident. The melting temperature of zircaloy is approximately 1850°C. While this temperature is high relative to normal reactor operating temperatures, it can be approached during a loss of coolant accident. But more importantly, as the temperature of zircaloy rises, the oxidation rate increases drastically. In this thesis the zircaloy-4 data of interest for comparison are the corrosion rates for normal waterside corrosion in a reactor environment and high temperature oxidation rates in a steam environment.

Over the last thirty years a great deal of experimental work has been performed to determine the oxidation kinetics of zircaloy in hot water. The waterside corrosion rate of zircaloy has been shown to behave in a cyclic manner depending on temperature and the total time of exposure. In general zircaloy has three corrosion regimes: pre-transition, transitory, and steady-state post-transition. The pre-transition regime generally lasts less than 200 days in 360°C water [Peters, 1984]. The transitory regime consists of several sequential periods which generally result in the same weight gain per period, but have decreasing time duration. The steady-state post-transition regime is where the corrosion rate essentially becomes linear with time. Here the cyclic effects are small compared with the average corrosion rate. Peters has shown that predicting the post-transition corrosion rate from short term test data results in an underestimation of corrosion damage [Peters, 1984]. For general operation of a nuclear reactor, long term (>1500 days) corrosion rates are of interest, but for this thesis the short term (<100 days) pre-transition corrosion data is applicable for comparison. According to Peters' data, the equations:

$$\Delta w = K t^{1/3}$$

$$K_{(mg/dm^2/day^{1/3})} = 3665 \exp(-14062 / T)$$

describe the corrosion of zircaloy-4 in the first corrosion period. Here **T** is temperature in Kelvin, Δw is the weight gain in mg/dm^2, and **t** is the exposure time in days. Peters experiments were performed in out-of-pile autoclaves in high-purity, degassed, deionized water.

* Technically speaking, zircaloy is not a trademark or a patented product, but a guideline for alloys developed by Naval Reactors. Therefore, zircaloy should not be capitalized.

There has also been a great deal of experimental work performed to determine the oxidation kinetics of zircaloy in high temperature steam environments. Ballinger studied the kinetics of zircaloy-4 in steam in the temperature range 871°C to 1482°C and found a parabolic corrosion rate [Ballinger, 1976]. Urbanic & Heidrich studied zircaloy-2 and zircaloy-4 in steam from 1050°C to 1850°C and identified a discontinuity in corrosion rate at ~1580°C [Urbanic, 1978]. Leistikow compared the corrosion rates of zircaloy-4 to those of stainless steel No. 1.4970 in the temperature range 600°C to 1300°C and found that zircaloy experiences a break-away to linear kinetics at some temperatures [Leistikow, 1984].

It is generally accepted that the mechanism which governs the oxidation reaction is the diffusion of oxygen through the ZrO_2 lattice. Based on the findings of Urbanic the reaction kinetics of zircaloy vary over three distinct temperature ranges [Urbanic, 1978]. These temperature ranges correspond to changes in the oxidation activation energy of the zirconium which accompany changes in lattice structure. The stable phase of zirconia is temperature dependent: T<890°C monoclinic; 890-1580°C tetragonal; T>1580°C cubic.

The temperature range of interest for this thesis is 900°C to 1300°C and the data from Ballinger will be used. In this temperature range the zircaloy-4 oxidation reaction is parabolic and can be described by the expression:

$$\omega^2 = \mathbf{K_p} t$$

where ω is a measure of the extent of the reaction, $\mathbf{K_p}$ is the parabolic rate constant, and t is the reaction time. For our purposes the extent of the reaction (ω) is measured as the weight of zirconium metal reacted per unit area (mg/cm^2). The rate constant obeys the relationship:

$$\mathbf{K_p} = \mathbf{A}\ \exp(-\mathbf{E} / \mathbf{RT})$$

where $\mathbf{E}$ is the activation energy, $\mathbf{T}$ is absolute temperature and $\mathbf{R}$ is the universal gas constant. According to Ballinger the activation energy is E=33,370 (cal/mole), and $A=3.10 \times 10^5$ (mg^2_{Zr}/cm^4 s).

2.3 Background of SiC / Graphite Corrosion Data

The use of ceramics has been studied for many high temperature applications. A few examples are high temperature gas cooled reactors, first wall materials for a fusion reactor, aircraft or automobile engine parts, and thermal shields such as the tiles on the bottom of the U.S. space shuttles. The result is a wealth of information and data on different ceramics in many challenging applications. One of the most prominent materials tested for the gas cooled reactor and the fusion reactor is silicon carbide. Silicon carbide

has a very slow oxidation rate in steam at elevated temperatures and thus would make a very good structural material for many applications. In a thermal nuclear reactor, SiC does not make an ideal structural material because it has a significant neutron absorption cross section. For this reason the advantages of SiC are usually exploited by applying a thin coating to another material, usually graphite, which has better nuclear properties. The situation where SiC offers the most advantage is in a high temperature oxidizing environment. Several sources of information discussed below show the potential protection offered by SiC in such an accident. The characteristics of SiC in high temperature water have also been studied with less optimistic results.

The behavior of SiC was studied by Hirayama in acidic and alkaline 290°C water to find the corrosion kinetics in these particular situations [Hirayama, 1989]. The results showed that the corrosion of SiC is dependent on pH and on oxygen concentration in the water. The corrosion for a pH 10 solution of LiOH in oxygenated water was found to be quite high since no protective SiO_2 film was formed. There are also indications that the Li ion accelerates the SiC dissolution process. According to these results the dissolution rate of SiC may be too high for our application, however there is no proof that the high dissolution rate is a function of pH alone and not simply the Li ion. There is no published data of SiC tests conducted with a pH control other than LiOH.

In tests to find suitability of materials for fusion blankets, Horn found that the penetration rate for SiC in 10 m/s steam at 1400K (1127°C) was 2 mm/year, increasing to only 6 mm/year at 1600K (1327°C) [Horn, 1979]. This translates to a penetration rate of 0.228 μm/hr at 1127°C and 0.685 μm/hr at 1327°C. Strife and Sheehan performed a study of several ceramic coatings for specific application to graphite to provide oxidation protection at high temperatures. They identified SiC as having the best thermal expansion compatibility and exhibiting a low oxidation rate below 1500°C provided that variability in the coating due to small flaws could be eliminated [Strife, 1988]. Strife also pointed out that the addition of boron to the graphite mixture is advantageous for corrosion protection, but in the case of thermal reactors, the addition of boron is unacceptable due to its high neutron absorption cross section.

The gas cooled reactor relies on a SiC coating applied to the spherical fuel particles (TRISO particles) to aid in the retention of fission products up to temperatures of 1600°C for more than one hundred hours. These small fuel particles (1mm diameter) are then bonded together in a larger (60mm diameter) spherical graphite fuel element for use in the pebble bed HTGR design. The graphite fuel element is subject to rapid oxidation at these high temperatures during an air ingress accident if it is not covered with a protective coating

[Kugeler, 1991]. A coating of SiSiC has been applied to spherical fuel elements and tested in accident environments by Kugeler et al. (The SiSiC coating is an SiC coating layer which contains another 10% of free silicon.) They found that the SiC coating reduces the corrosion of the graphite fuel element to 3 mg/cm^{2}hr in 1400°C air, with no weight loss below 1000°C. The small weight loss observed at 1400°C is the result of microcracks in the coating, while at 1000°C no microcracking occurs. (An improved process has since been developed by this group, see next paragraph.) Kugeler also showed that the SiSiC coating can withstand thermal shocks of 70°C/s without damage if the coating process is followed by a heat treatment at sufficient temperature to allow the free silicon to infiltrate the graphite pores and form an anchoring layer of SiC intermingled with the graphite [Kugeler, 1991]. They also suggested that replacing the fuel element outer graphite shell with a pure SiC shell of 5mm would provide the same corrosion protection with a higher reliability, however this would increase the neutron losses due to absorption. Schulten suggests that enveloping the graphite fuel element with several independent 100μm SiC layers would do away with the effects of microcracking while allowing a simple CVD (chemical vapor deposition) process to be used for large scale production [Schulten, 1993].

An improved SiSiC coating process has been reported by Hurtado et. al. They have developed a process of applying a 150μm - 500μm SiSiC coating to a graphite substrate. After applicable thermal processing, a coating is produced that provides excellent corrosion protection. The tested specimens showed no weight loss after 5 hours in 1400°C air, and an oxidation rate of only 0.16 mg/cm^{2}hr in steam at 1000°C. Thermal shock tests were performed where specimens at 800°C were water quenched to 20°C. After several thermal shocks, the coating showed microcracks throughout the surface, however, the corrosion protection at 800°C was not hampered by the microcracks [Hurtado, 1994a & 1994b].

In a development program for the High Temperature Test Reactor in Japan, Fujii et. al. developed a process which produces a gradual transition from graphite to SiC over a few hundred micrometers [Fujii, 1992]. The resulting graphite/SiC structure is called a functionally gradient material (FGM). The purpose of the FGM was to eliminate a clear junction where differences in thermal and radiation induced expansion would cause stresses between the substrate and coating which could lead to coating failure. To improve the corrosion resistance, the FGM was then coated with 90-140μm of SiC by a CVD process, resulting in a material which was completely enclosed by a SiC protective layer.

Comparison of the corrosion rates of the SiC coated FGM, SiC coated graphite, the uncoated FGM, and virgin graphite were carried out at temperatures of 800°C and 1000°C.

The uncoated FGM showed a lower corrosion rate than virgin graphite, but both were sufficiently high to eliminate these materials from consideration. The SiC coated graphite and SiC coated FGM showed virtually no weight loss in 1000°C air after 5 hours. These specimens were then subjected to thermal cycle tests. For a moderate thermal cycle of 20°C/s heat-up to 1000°C and subsequent slow cooldown, the SiC coating on both the FGM and graphite maintained integrity for ten cycles. A thermal shock test was then initiated where the specimens were heated to a temperature of 1200°C and water quenched. The specimens were subsequently heated and maintained at 800°C for 1 hour to evaluate the protection offered by the coating following the thermal shock. The SiC coating on the graphite showed microcracks and weight loss was observed after the first thermal shock test. The SiC coating on the FGM maintained integrity for several thermal shocks [Eto, 1992; Fujii, 1993]

An issue which must also be addressed is the neutron irradiation damage that occurs in both SiC and graphite. The characteristics of irradiated graphite are dependent on the particular grade and manufacturing processes used. Normally, graphite shrinks at low fluences and expands somewhat at higher fluences. SiC always experiences expansion due to irradiation damage. Clinard studied the irradiation effect on a SiC coated graphite substrate at a fluence of about $2x10^{22}$ n/cm^2 [Clinard, 1983].* The result was a complete delamination of the graphite substrate caused by graphite shrinkage and SiC swelling. This problem must be addressed and successfully circumvented in the future if SiC coated graphite materials are to be used in the PTLWR.

2.4 Background Summary

This chapter presented background on three major topics necessary to understanding the next three chapters. First a brief summary of the passive pressure tube light water reactor (PTLWR) was given to inform the reader of the starting point and objectives of the analyses carried out in Chapter 3. It should be noted that the PTLWR is not developed or justified in this work, rather a small contribution to the overall effort has been attempted. The sections on the corrosion of zircaloy and SiC/graphite are included to inform the reader of the relevant work that has been done concerning materials corrosion problems encountered in the nuclear industry. Some of this data will be used for comparison with the experimental results in Chapter 5.

* This is a very high fast fluence. The current design for the wet calandria variant of the PTLWR will subject the SiC coated graphite to fast fluences close to this value [Mattingly, 1995].

3. WET CALANDRIA WORKING DESIGNS

This chapter presents work done on the fuel bundle designs for the PTLWR. First a brief history of the work performed by Tang and Hejzlar is given. The results of the design work performed by the author are given for two different fuel configurations that are intended to be used in the wet calandria variant of the PTLWR. A set of test environments is then devised using the results of the previous and present design work. Finally a brief chapter summary is included at the end of the chapter.

3.1 History of PTLWR Fuel Design Work

3.1.1 Previous Work

The PTLWR has two variants, the wet calandria and dry calandria, and each variant has unique physical characteristics that govern the fuel configuration used inside the pressure tubes. Specifically, the lattice must remain under-moderated to assure a negative coolant void coefficient. The wet calandria has significantly more water present in the core for moderation than the dry calandria (see Appendix B). Thus the wet calandria design is capable of supporting a higher fuel loading than the dry calandria variant. As a consequence of this and other constraints, the dry calandria fuel designs primarily use TRISO particle fuel, while the wet calandria fuel designs primarily use UO_2 ceramic fuel pellets. There are several additional requirements for the fuel designs used for either variant. These factors are primarily related to core performance during operating and accident conditions. They are summarized below.

The basic requirements for the fuel bundle designs are:

1. Acceptable neutron physics characteristics such as negative coolant and moderator void coefficients, prompt negative Doppler coefficient, and inherent shutdown during an accident.

2. Sufficient heat transfer from the fuel to the coolant during operation to meet normal operating temperature limits on the fuel and the cladding.

3. Sufficient heat transfer from the fuel to the pressure tube surface during accident conditions to meet accident temperature limits.

The third criteria is usually the hardest to meet. Since the philosophy used in this reactor design is to withstand a complete loss of primary coolant without fuel damage, the heat transfer in an accident must take place through a combination of natural convection,

radiation, and conduction through gas and materials. The designer must successfully use fuel material selection and geometric layout to keep the fuel bundle temperatures within safe limits at all times.

One of the paths chosen to accomplish this was to employ extensive use of SiC coated, high density isotropic graphite in the fuel designs. Graphite performs two main functions. First it significantly increases the heat capacity of the fuel bundle. This added heat capacity allows for a significant storage of decay heat early in an accident when the heat generation rate exceeds the rate at which heat is removed from the fuel bundle. Thus the peak temperature reached in the fuel bundle will be reduced. Second, the graphite can act as a high conductivity heat transfer medium to transport heat from the inner fuel bundle to the edge near the pressure tube, thus decreasing the center fuel bundle temperatures. Not all of the fuel designs employ graphite in the same way, but most use graphite to accomplish at least one of the stated functions. The graphite is covered with a SiC layer to prevent water ingress in normal operation and prevent severe oxidation at the elevated temperatures reached during an accident.

Hejzlar developed five possible fuel designs for the dry calandria variant. These are labeled DC-1, DC-2, DC-3, DC-4, and DC-5 [Hejzlar, 1994]. Each has advantages and disadvantages relative to the others which are summarized in Appendix B and in Mattingly [Mattingly, 1995]. The wet calandria design designated WC-5, which is developed in section 3.4 of this thesis, is based on Hejzlar's work with designs DC-1 and DC-2. Designs DC-3, DC-4, and DC-5 are matrix type designs where the fuel is arranged in a solid matrix and enters the pressure tube as one solid piece. See Appendix B for diagrams of these fuel designs.

Tang developed several fuel designs for the wet calandria variant [Tang, 1992]. Three of these designs, designated WC-1, WC-2, and WC-3, are shown in Appendix B. They are also presented in more detail in Mattingly [Mattingly, 1995]. All three of these designs employ a solid matrix configuration with a large volume of non-fuel materials. Several deficiencies in the designs WC-2 and WC-3 led to the development of the WC-4 and WC-5 designs discussed in sections 3.3 and 3.4. Design WC-2 suffered from a high fuel centerline temperature and high cladding temperature during normal operation. Design WC-3, which was developed to alleviate these high temperatures, suffered from high cladding temperature during accidents, and complicated geometry.

3.1.2 Performance Criteria for Acceptable Fuel Designs

Several factors determine whether a fuel design is acceptable for use in the PTLWR. These requirements are presented in detail by Hejzlar [Hejzlar, 1994] and summarized here. The three factors evaluated first for the fuel designs are the void coefficient, the normal operation heat transfer (and temperature) parameters, and the accident heat transfer (and temperature) parameters. If one of these three areas does not meet requirements, then the design is discarded or significantly altered. For our purposes, the void coefficient is required to be negative for both coolant and moderator loss. The operating heat transfer parameters are required to be consistent with established safety limits: namely that the MDNBR be greater than 1.3, and the fuel temperatures and cladding temperatures not exceed safe operating limits which are unique to each material. The accident temperature limits are set by the properties of the specific materials involved. The temperature limits for zircaloy cladding have been established by years of experience and testing. The temperature limits on the graphite and silicon carbide used in these designs have been set at 1300°C. This limit is chosen because it is within the corrosion resistant regime of SiC in a steam environment, and all graphite surfaces are coated with SiC to prevent oxidation. Thus the 1300°C limit should not pose a problem for graphite unless the coating is compromised.

In reality there are several more considerations used to determine whether a design is acceptable. Some of these are Doppler coefficient, in-core pressure drop, fuel utilization, and acceptable fast fluence levels. However, the factors discussed in the previous paragraph are the most important and usually the hardest to satisfy. All of these factors are used to compare the relative performance of a particular fuel design to several others.

3.2 WC-4, Mini-Bundles Contained within a Graphite Matrix

The WC-4 design is shown in Figure 3-1. The matrix consists of a graphite cylinder with six large triangular axial holes (coolant channels). The coolant channels have rounded corners and all exposed surface area of the matrix is coated with SiC. The SiC prevents water ingress during normal operation and also prevents significant oxidation during accident conditions. Each of the six channels is filled with six zircaloy-clad UO_2 fuel pins, for a total of 36 pins in each matrix. Each fuel pin is pressed firmly against a graphite seat by a spring (not shown) to facilitate heat conduction during accident conditions. There is also another variant of the WC-4 design that was studied. Figure 3-2 shows a 30 pin design, where each of the six center-most fuel pins has been removed and

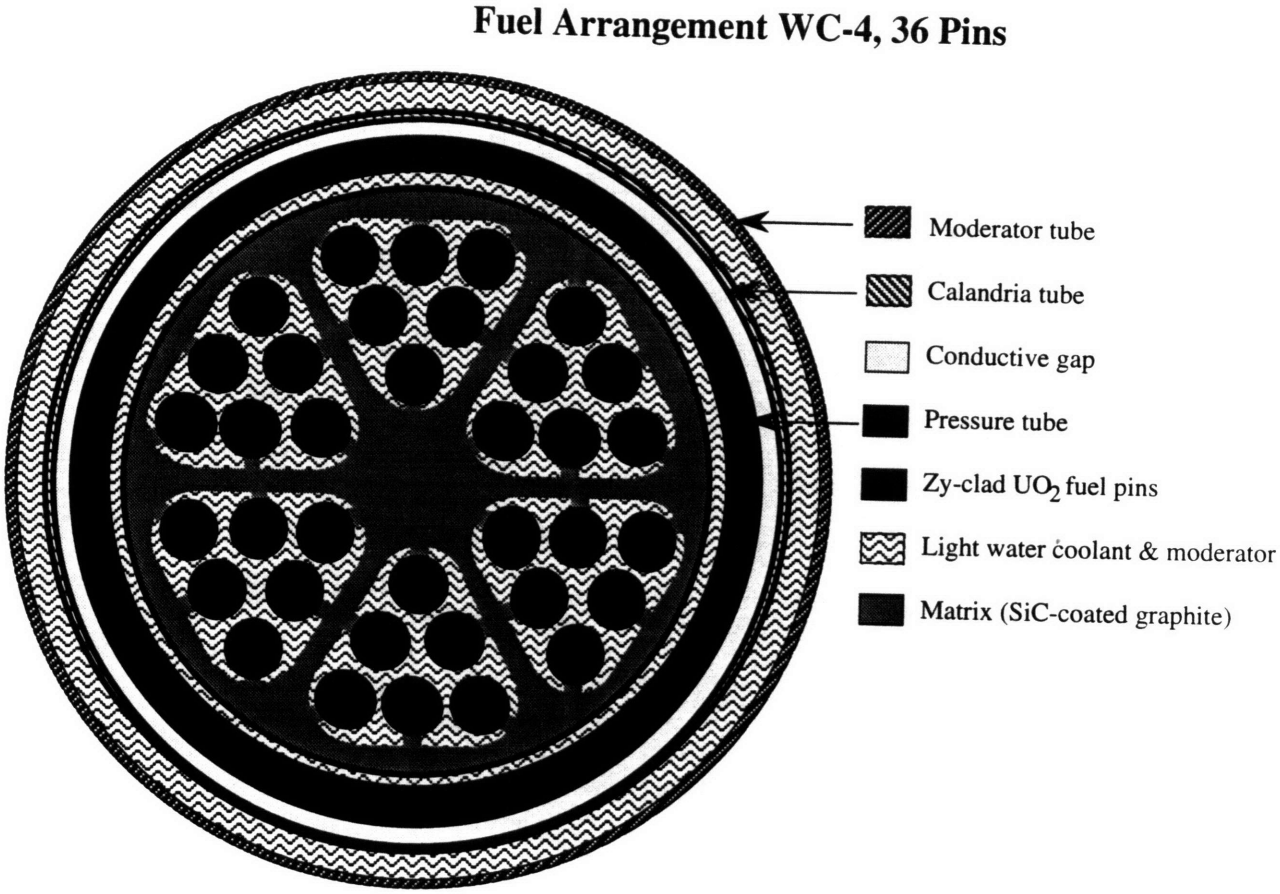

Figure 3-1: WC-4, Mini-Bundles Contained within a Graphite Matrix (36 pins)

replaced with a dummy pin spacer. The heat generation in the remaining 30 pins has been increased by 20% to maintain the same average power production per matrix as the 36 pin design.

During normal operation, the heat generated in each fuel pin is transferred directly to the coolant water flowing around the pin (with a small amount conducting into the matrix and subsequently into the coolant water). Under accident conditions, the decay heat is conducted through the graphite matrix to the outer surface of the graphite cylinder, where it will either conduct to the pressure tube via long runners (not shown), or radiate to the pressure tube. The original design includes six runners that center the matrix in the pressure tube. These runners are intended to provide a conduction path for heat to be transferred from the matrix to the pressure tube. At any given time only two of the six runners can be counted on to contact the pressure tube, and then only a fair degree of

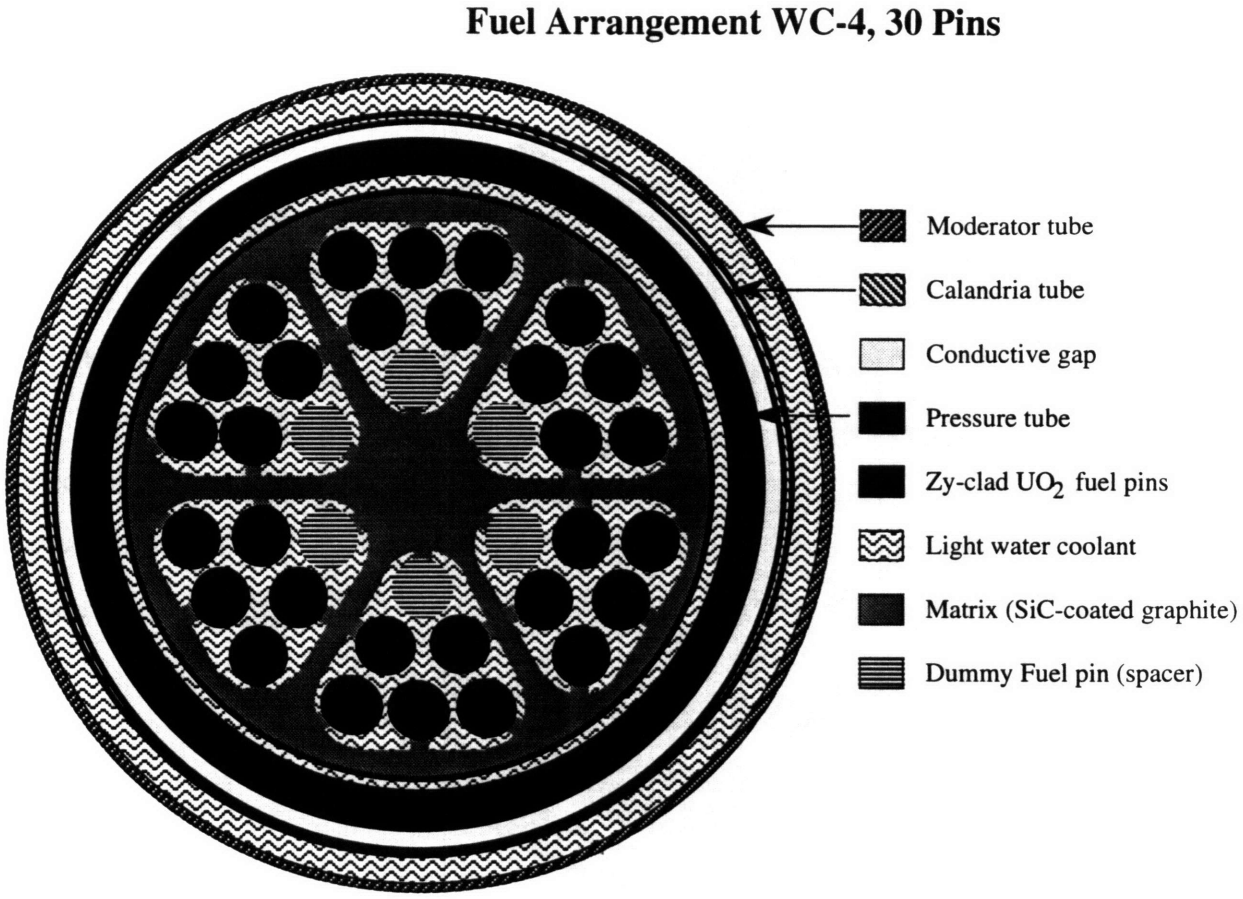

Figure 3-2: WC-4, Mini-Bundles Contained within a Graphite Matrix (30 pins)

contact is present due to contact resistance between the two dissimilar materials and lack of a perfect match between fuel and pressure tube axial bowing. Based on this reasoning, the majority of heat is expected to be transferred via radiation between the matrix and the pressure tube surface.

3.2.1 Performance during Normal Operation

Normal operating conditions for this matrix were simulated at only a preliminary level. The thermal hydraulics of the mini-bundle design are quite complex and there are no existing correlations for the heat transfer coefficient of a small triangular bundle arrangement. All thermal data for WC-4 in this thesis were calculated using the finite element analysis code ADINA-T [ADINA R&D, Inc.]. Full power calculations were done to find the maximum cladding temperature at the junction between the fuel pin and the graphite matrix. The contact between the cladding and the graphite matrix was taken to

have a heat transfer coefficient of 5000 W/m^2°C to account for the significant contact resistance between the two dissimilar materials. This contact conductance is estimated from analogous studies on dissimilar materials [Madhusudana, 1993; Williamson, 1992]. The 5000 W/m^2°C value is based on having a steam or water environment and pushing the fuel rods against the graphite with a pressure of 0.4 MPa (60 psi). This pressure can be exerted by normal LWR fuel spacer grids. All surfaces that are exposed to coolant flow are held at 350°C and a peaking factor of 1.2 was used. The peaking factor of 1.2 is an estimate based on the DC-3 design developed by Hejzlar. No full core physics calculations were performed for WC-4, but for this analysis the value of 1.2 is sufficient [Hejzlar, 1994]. The maximum cladding and fuel temperatures for the full power operating condition are shown in Table 3-1. It is clear that the full power operation is not limiting from a thermal standpoint.

Table 3-1: WC-4 Maximum Temperatures for Full Power

Pins in bundle	Max Clad Temp (°C)	Max Fuel Temp (°C)
30	538	1515
36	506	1258

3.2.2 Performance during LOCA

A second analysis was performed on the WC-4 configuration to assess its ability to transfer decay heat from the fuel to the pressure tube during an accident without exceeding cladding or matrix temperature limits. The details of the thermal model are given in Appendix C.

The LOCA thermal analysis was also performed using the ADINA-T computer code and consisted of a transient calculation starting at normal operating conditions and at time t=0 voiding the pressure tube of all water. Heat transfer between the fuel pins and the matrix is modeled by both conduction into the matrix lands and radiation to the matrix walls surrounding the mini-bundles. Convection between the pins and the matrix was not modeled due to lack of an applicable correlation, however the omission of convective heat transfer should preserve a degree of conservatism. Heat transfer between the matrix and the pressure tube was modeled as radiation only, since the contact between the matrix runners and the pressure tube can not be guaranteed due to pressure tube sagging.

Tang calculated that the moderator system of the wet calandria PTLWR could maintain the calandria tube outer surface at 90°C for both normal operation and accident

conditions; this value is adopted as the boundary condition in this transient analysis. The gap between the pressure tube and the calandria tube is modeled as having an effective conductivity of 2 W/m°C. The value of 2 W/m°C was chosen to be consistent with the analysis of Hejzlar for the DC fuel designs [Hejzlar, 1994].

Figure 3-3 shows the temperature response of WC-4 (with 36 pins) during the simulated LOCA. The figure shows responses for the pressure tube inner surface, the clad temperature of the center-most pin (point where the maximum clad temperature occurs), matrix contacting this center pin, and the matrix surface radiating to the pressure tube. The maximum temperatures for the cladding and the matrix for both the 36 and 30 pin designs are also shown in Table 3-2. For the 36 pin design, the maximum cladding temperature occurs on the six fuel pins nearest the center of the bundle. The maximum matrix temperature occurs at the contact between the six center-most pins and the matrix.

Table 3-2: WC-4 Maximum Temperatures for LOCA

Pins in bundle	Max Clad Temp (°C)	Max Matrix Temp (°C)
30	1010	925
36	1000	945

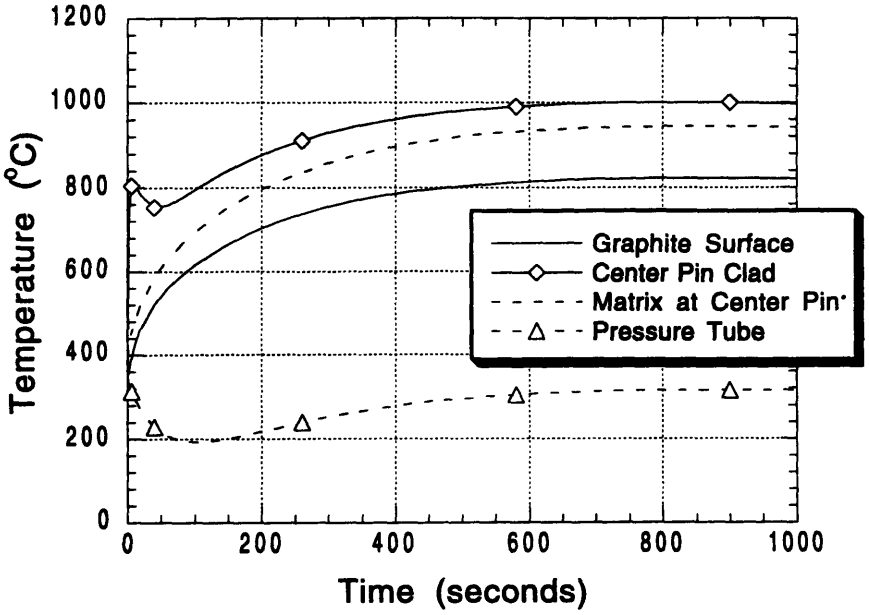

Figure 3-3: LOCA Temperature Response for WC-4 (36 pins)

For the 30 pin design, the maximum cladding temperature again occurs on the fuel pins nearest the center, however in this case there are 12 of these pins in the bundle (because the six innermost pins are not filled with fuel). The maximum matrix temperature occurs where these 12 pins contact the matrix. Notice that the shift from 36 to 30 pins increases the maximum cladding temperature (due to the increased heat generation per pin) but decreases the maximum matrix temperature (due to the contact point with the hottest pins being much closer to the graphite surface).

Both design variants exceed the safe temperature limits for zircaloy cladding, while the matrix temperature remains well below the limiting temperature of 1300°C for the SiC coating. The conclusion reached, based on this result, was to discontinue work on this design and concentrate on a design which will allow radiative heat transfer to take place directly between the fuel pins and the pressure tube. Note, however, that the WC-4 design would be feasible if a new, more rugged cladding material, such as SiC, were used to offset the high temperatures reached during a LOCA.

3.3 WC-5, A Two-Ring Design with SiC-Clad UO_2 Fuel Pins

The WC-5 fuel matrix configuration is shown in Figure 3-4. It consists of a modified CANDU 37-pin fuel bundle. The center pin and the inner ring of six pins have been removed and replaced with a graphite cylinder. The graphite is coated with SiC to protect against oxidation at high temperatures. This cylinder channels water toward the pins during normal operation, and acts as a temporary heat sink during the initial stages of a LOCA. The removal of the inner pins in a CANDU fuel bundle was proposed by AECL in 1977 [Roshd, 1977] to reduce the positive coolant void coefficient. The reasons for removing the pins in the present design are to reduce the path length from the heat source to sink during a loss of coolant accident and to increase the heat capacity of the fuel bundle. The fuel pins are clad in SiC tubes instead of zircaloy due to the high temperatures reached during a loss of coolant accident. The WC-5 fuel matrix design was recommended by Hejzlar as a good candidate for the wet calandria based on the analysis of the design designated DC-2 in his work [Hejzlar, 1994].

SiC-clad UO_2 pellets were tested by British investigators, although for only modest power density [Kennedy, 1974]. Fuel performance was found to be determined primarily by the ability of the silicon carbide tube to withstand stresses. To alleviate the stress on the SiC tube, interaction of the fuel pellets with the cladding caused by fission product induced swelling must be avoided. This may limit burn-up to low values or require more research

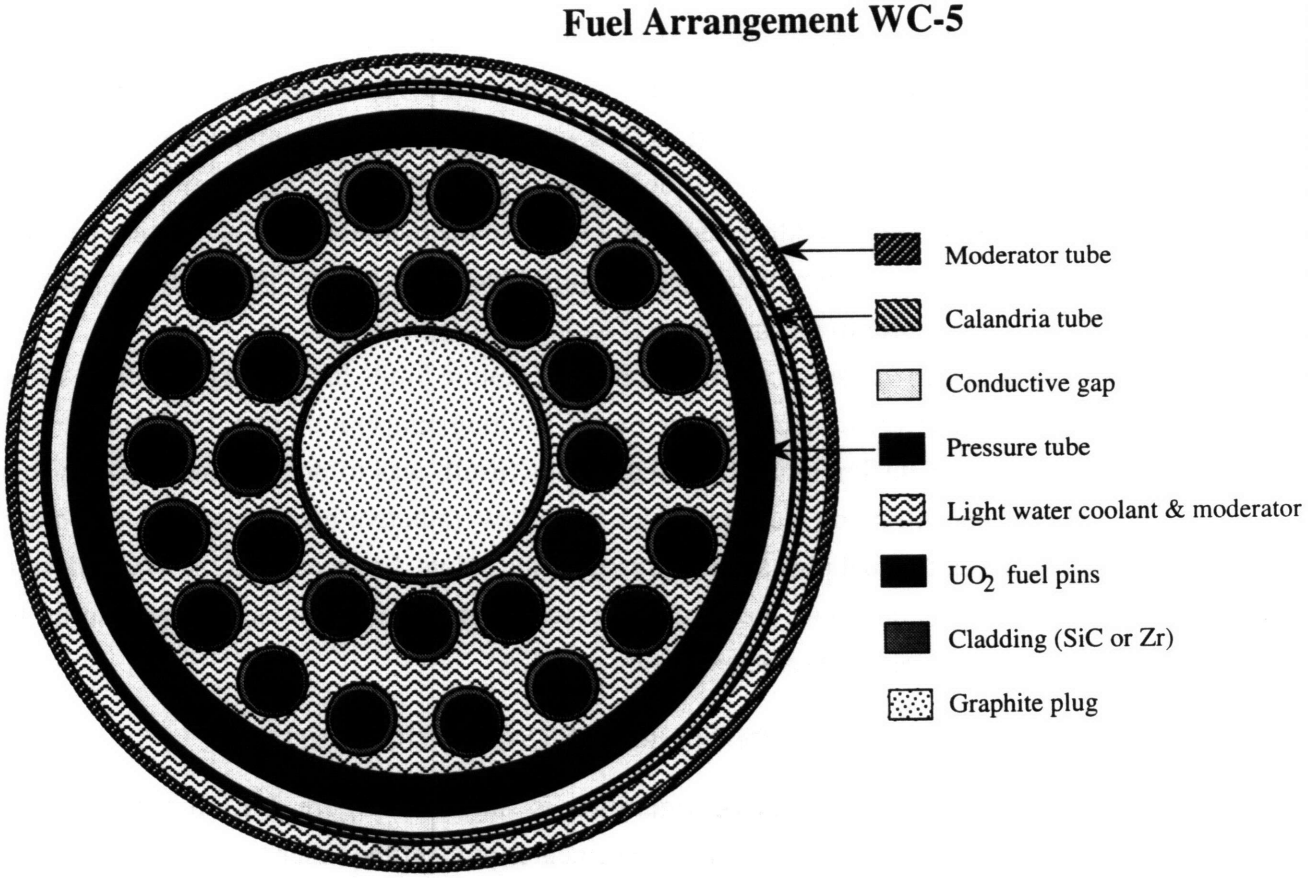

Figure 3-4: WC-5, Two-Ring Design with SiC-Clad UO_2 Fuel Pins

into how to design a conducting gap which would provide some free volume for fuel expansion without strong mechanical interaction with the cladding.

3.3.1 Nuclear Physics

An MCNP model, developed by Hejzlar, was used to calculate the effect of changing the thickness of the moderator annulus. The calculation was performed for a fresh core with initial enrichment of 2%, an infinite lattice in the radial direction and an axial graphite reflector. The results are shown in Figure 3-5. The graph shows that the optimum moderator annulus should be 8 mm thick, hence all subsequent analyses are performed with a moderator annulus of 8 mm and a moderator density of 0.972 g/cm^3. Note that thinner annuli correspond to partial voiding of the 8 mm reference case.

The effects of coolant density changes are shown in Figure 3-6. The operating point of the reactor is roughly at a core-average coolant density of 0.68 g/cm^3, which corresponds to a pressure of 15.5 MPa and an average temperature of 320°C. These

calculations show that this reactor has inherently negative coolant and moderator void coefficients (i.e. positive slope of multiplication factor curve).

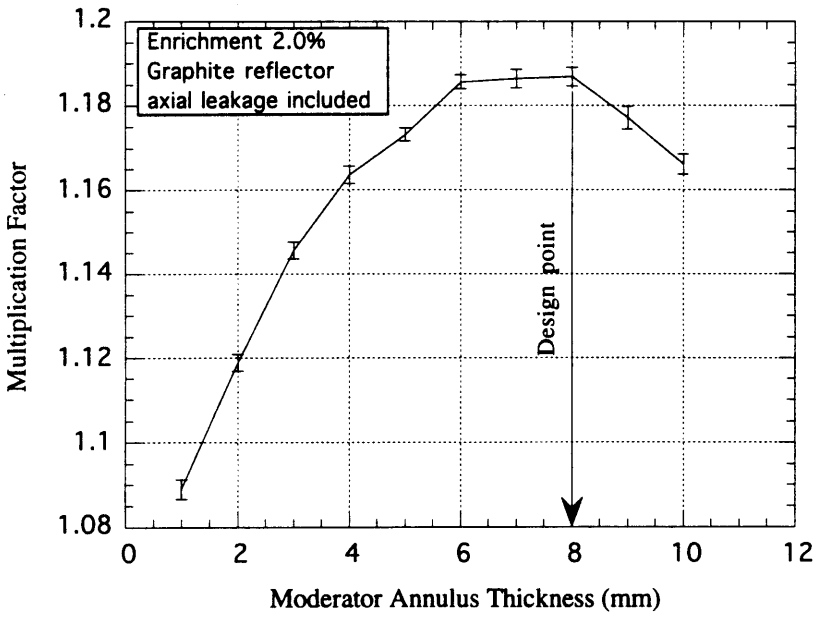

Figure 3-5: Variation of Multiplication Factor with Moderator Annulus for WC-5

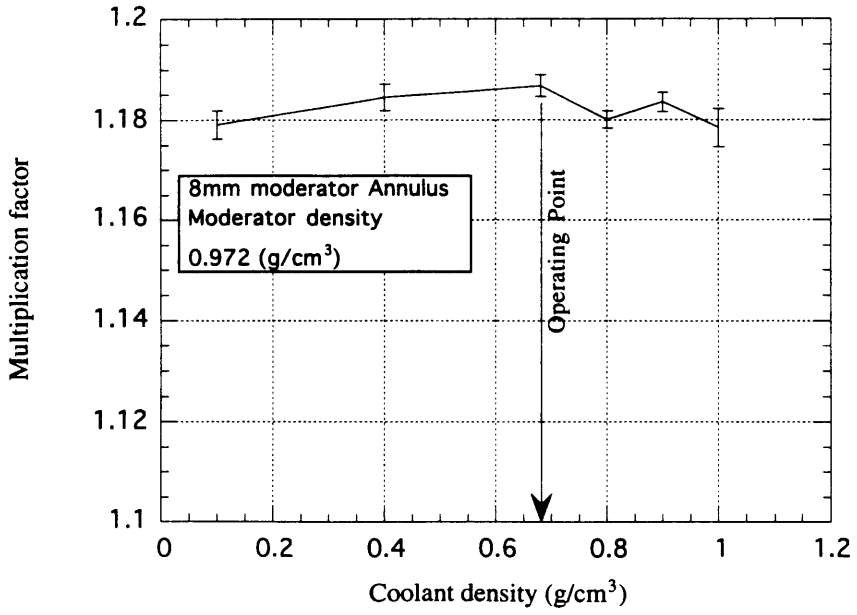

Figure 3-6: Coolant Voiding Behavior for WC-5

The axial power density profile is shown in Figure 3-7. The inner and outer rings of fuel pins have substantially different heat rates. This is due largely to the moderator annulus being located outside of the coolant channel, nearer to the outside ring of fuel rods. As expected the axial profile very closely matches the flat shape of the power profiles calculated for Hejzlar's DC-1 and DC-2 designs. (DC-2 is identical to WC-5 with H_2O in place of the graphite. DC-1 is identical to WC-5 except the fuel in DC-1 is TRISO particle fuel [Hejzlar, 1994]). The pressure tube average power is 263.52 MW/m^3 (per fuel volume) and the axial peak power is 352.40 MW/m^3. This gives an axial peaking factor of 1.34. To obtain a radial peaking factor a full core mockup must be modeled in MCNP. This was not done for WC-5, but was performed by Hejzlar for DC-3. The DC-3 radial peaking factor of 1.06 will be used here as a first estimate to the radial peaking factor for WC-5. This now gives a total peaking factor for the WC-5 fuel design of 1.42. Compared to operating LWRs and CANDUs this peaking factor is an improvement. However, it does place a challenge on the design from a decay heat removal standpoint. One beneficial consequence of the outer ring having a higher power generation is that this ring of pins has a shorter path to dissipate decay heat during an accident. Thus most of the heat in the bundle will be generated close to the pressure tube. This should result in favorable accident performance. In principle it should be possible to reduce the power difference between the inner and outer rings by creating a water channel through the center graphite slug. This would reduce the overall heat capacity of the fuel bundle, but it may be necessary to create a more even power distribution. This option is not evaluated here, but left for future consideration.

3.3.2 Performance during Normal Operation

A detailed thermal hydraulic analysis was not performed on this fuel design. The flow area is decreased by 17% from the normal CANDU 37-pin bundle, and the wetted perimeter is decreased by 8%. These changes are not substantial and performance close to a normal CANDU bundle is expected in terms of pressure drop for the nominal mass flow rate. The heat flux to coolant values for the WC-5 design and the CE-CANDU are shown in Table 3-4 located at the end of this chapter. The peak heat flux to coolant for this design is less than the peak for the CE-CANDU, thus WC-5 is deemed to perform adequately during normal operation. This design will be limited by the removal of heat during accident conditions, not normal operation.

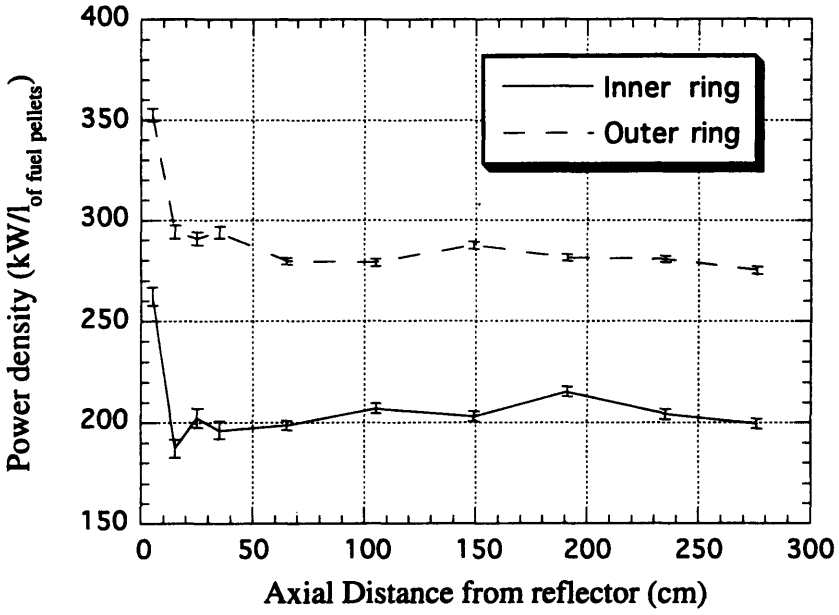

Figure 3-7: Axial Power Density Profile for WC-5

3.3.3 Performance during LOCA

A thermal analysis was performed on the WC-5 configuration to prove the ability of the bundle to transfer decay heat from the fuel to the pressure tube during an accident without exceeding critical temperature limits. The finite element computer code ADINA-T [ADINA R&D, Inc.] was used for this analysis. The details of the thermal model are given in Appendix C.

The ADINA-T thermal analysis program was utilized because of its ability to perform radiation heat transfer calculations while generating discrete view factors between mesh surfaces internally. The thermal analysis consisted of a transient calculation starting at normal operating conditions and at time t=0 voiding the pressure tube of all water and allowing only radiation heat transfer to take place. The normal operating conditions are calculated by holding all surfaces exposed to water at 350°C. The entire pressure tube and the graphite slug are also held at 350°C. Tang calculated that the moderator system could maintain the calandria tube outer surface at 90°C for both normal operation and accident conditions; this value is adopted for the boundary condition in this transient analysis.

The remaining variable is the heat transfer coefficient of the gap between the pressure tube and the calandria tube. Novak has carried out extensive testing of thermal switches, and values of effective conductivity between 2 and 4 W/m°C do not seem out of

reach [Novak, 1995]. (The thermal switch concept involves increasing heat transfer ability with increasing temperature.) For this analysis, gap conductivity values of 2.0 and 4.0 W/m°C were used to calculate bounding results. The value of 2.0 W/m°C was chosen as a lower limit to be consistent with the analysis of Hejzlar for the DC-1 fuel design [Hejzlar, 1994]. The value of 4.0 W/m°C was chosen to be the upper limit for allowable heat loss during normal operation. The CE-CANDU loses approximately 5% of its total heat generation to the moderator during normal operation. A gap conductivity of 4.0 W/m°C corresponds roughly to a 5% heat loss (through conduction only, does not consider gamma heating) during normal operation for the WC-5 configuration.

Figure 3-8 shows the temperature response of the WC-5 fuel matrix with SiC cladding during a LOCA for a peaking of 1.42 and gap conductivity of 2.0 and 4.0 W/m°C. The peak temperatures on the inner ring and outer ring of fuel elements are reached at different times in the accident. Figure 3-8 shows temperature profiles corresponding to the time when the absolute maximum cladding temperature is reached on the inner ring. The peak cladding temperature of 1204°C is reached on the inner ring near the graphite slug when the gap conductivity is 2.0 W/°C at 700 seconds. This temperature is within the range of operability for silicon carbide. Increasing the gap conductivity lowers the peak cladding temperature by only 14°C to 1190°C which is reached at 680 seconds. It can be seen that increasing the gap conductivity does not reduce the maximum temperature much but does succeed in decreasing the length of time elapsed before the maximum temperature is reached.

Figure 3-9 shows several temperatures plotted against time during a loss of coolant transient. For this case all fuel pins have an equal heat generation rate and a peaking factor of 1.42, and the pressure tube-calandria tube gap conductivity is 2.0 W/m°C. The temperatures shown are the cladding temperature on the center-facing and outer-facing surface of both of the rings of fuel rods, the graphite surface temperature immediately adjacent to one of the fuel rods, and the temperature on the inner surface of the pressure tube. This figure clearly shows the benefit of the graphite slug in the center of the fuel channel. For the first 250 seconds of the transient, the inner surface of the cladding on the inner ring of fuel pins is at a lower temperature than the cladding facing outward. This clearly indicates that most of the heat generated in the inner ring of pins during the first 200 seconds is being absorbed in the graphite slug. This is a major advantage over normal CANDU fuel bundles, since the graphite absorbs the first few hundred seconds worth of decay heat until the heat generation rate decreases to the point of being equal with the heat

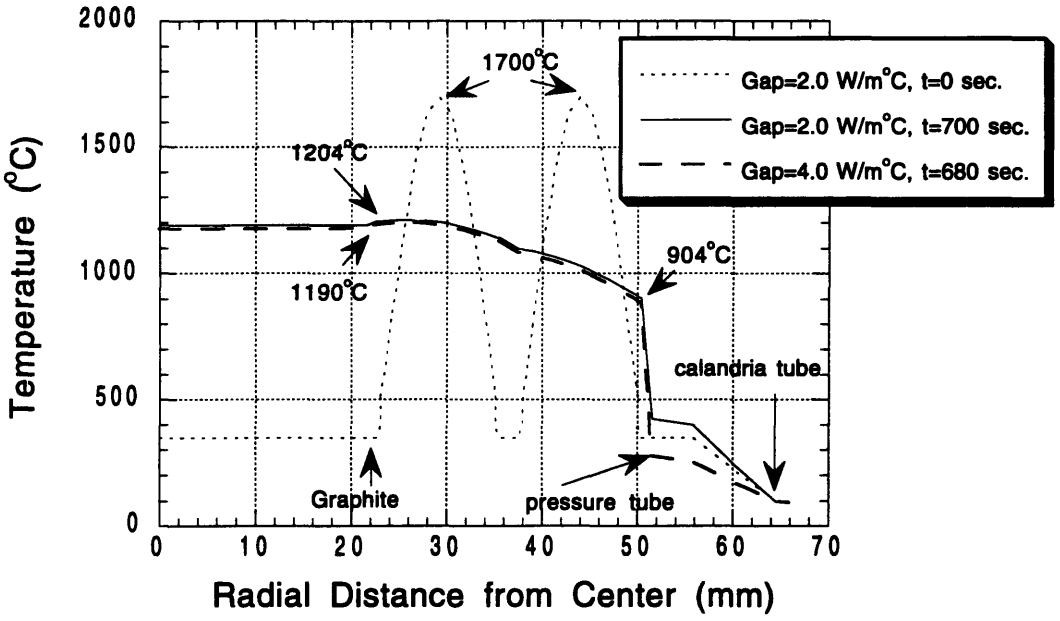

Figure 3-8: LOCA Radial Temperature Performance for WC-5 (SiC Cladding)

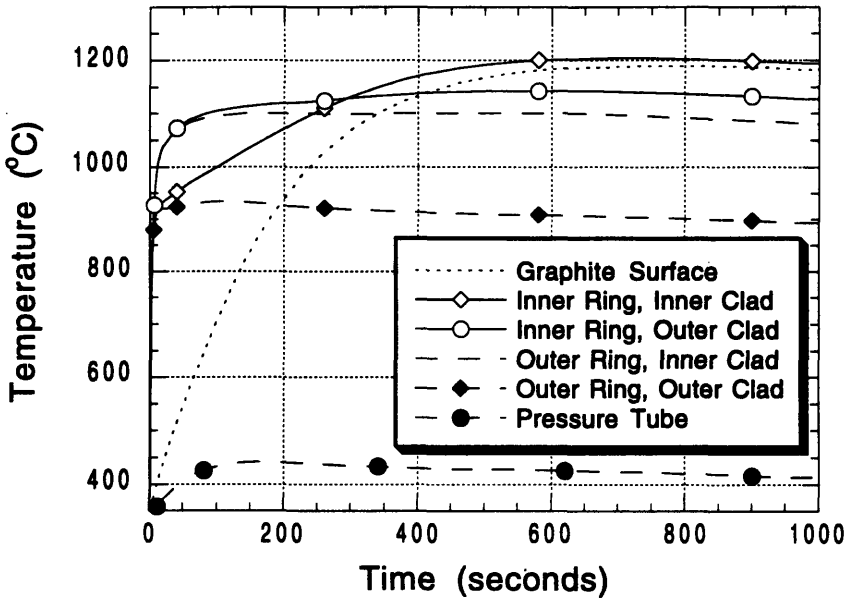

Figure 3-9: LOCA Temperature Performance for WC-5 (SiC Cladding)

removal rate through the pressure tube, thus maintaining temperatures below those that are damaging to the cladding. The actual temperatures encountered in a LOCA are expected to be roughly 70 to 100°C lower than those predicted because the ADINA thermal model did not take into account convective heat transfer involving the steam/air mixture present in the pressure tube.

The maximum cladding and matrix temperatures are summarized in Table 3-3. Included in this table are the maximum temperatures encountered for WC-5 when zircaloy cladding is used. The temperatures encountered are well above the limits for zircaloy cladding.

Table 3-3: WC-5 Maximum Temperatures for LOCA

Cladding material	PT-CT gap (W/m°C)	Max. Clad Temp (°C)	Max. Graphite Temp (°C)
SiC	2.0	1204	1190
SiC	4.0	1190	1175
zircaloy-4	4.0	1196	1181

3.4 Wet Calandria Working Design Choice

Five alternative fuel configurations inside the channels of the wet calandria variant of the passive pressure tube reactor have been proposed and evaluated. (Two in this thesis and three previously by Tang). The options include one bundle-type arrangement in a two-ring geometry, one arrangement with six mini-bundles surrounded by a graphite structure, and three matrix-type fuel designs. Key factors in the areas of reactor physics, thermal hydraulics during normal operation and during loss of coolant accidents, and materials compatibility affecting fuel design were identified, and the design performance was evaluated against these factors.

For loss of coolant accidents, the bundle-type fuel configurations (WC-4, WC-5) provide a less efficient heat transfer dissipation mechanism compared to a matrix-type fuel. Calculations show that the temperatures reached during a LOCA are above tolerable limits for zircaloy cladding. The WC-5 design performs nicely when silicon carbide cladding is employed, and the WC-4 design should also prove acceptable when using silicon carbide cladding.

Design WC-5 with SiC cladding was selected as the most promising working design for the wet calandria variant of the PTLWR. The primary motivation for this choice is the extensive experience with this geometric fuel arrangement in the CANDU. The WC-

5 fuel design is based on currently available technology, and the anticipated performance of the silicon carbide coating for the graphite slug which has been tested as part of this thesis. More research and development in this area is needed, however, to confirm the issues of economical production, and coating behavior after irradiation and mechanical damage in a reactor environment. Further research is also warranted on the SiC cladding technology to reduce the damage caused by pellet-clad interaction, and thus allow increased fuel burn-ups.

Table 3-4 below presents thermal hydraulic data for the matrices studied for the wet calandria reactor. The CE-CANDU is the benchmark design which all others are measured against. The values for WC-2 and WC-3 are included to allow the reader to easily compare designs WC-4 and WC-5 to those previously evaluated.

Table 3-4
Comparison of Thermal Hydraulic Characteristics for the WC Designs

Characteristic	CE-CANDU	WC-2	WC-3	WC-4	WC-5
Average power per fuel channel (MWt)	**5.44**	5.44	5.44	5.44	5.44
Peak power per fuel channel (MWt)	**10.26**	9.79	7.78	6.53	7.72
Total Peaking Factor*	**1.9**	1.8	1.43	1.2	1.42
Average power density in fuel region (W/cm^3 of fuel compact)	**213**	302	302	364	264
Peak power density in fuel region (W/cm^3 of fuel)	**446**	543	543	437	374
Peak heat flux to coolant (W/cm^2)	**114**	195.7	136.8	93.8	105.6
Average heat flux to coolant (W/cm^2)	**59.7**	108.7	95.6	78.2	74.35
Heat transfer surface with coolant (cm^2)	**90,312**	50,038	56,879	69,598	73,226
Total flow area (cm^2)	**34.2**	27.04	27.04	35.2	28.3
Hydraulic diameter (cm)	**0.74**	0.68	1.58	0.56	0.73
Maximum flow rate per fuel channel (kg/s)	**22.1**			22.1	22.1
Average flow rate per fuel channel (kg/s)	**19.05**	32.39	20.96	19.05	19.05
Maximum velocity (m/s)	**9.93**	17.01#	11.41#	9.23	11.5

* Values listed are for a fresh core with uniform enrichment. The peaking factor for the equilibrium core depends on the refueling scheme, and will be different from these values.
# Values of velocity listed for WC-2 and WC-3 are average velocity values.

NOTE: Design WC-1 is not included because no detailed calculations for this design were performed.

3.5 Characterization of Testing Environment

The fuel designs analyzed above for the wet calandria, and those presented by Hejzlar for the dry calandria [Hejzlar, 1994], rely on one key component to be successfully: namely the SiC coating must protect the graphite from the high temperature steam/air environment encountered during an accident. Because this component is essential to the success of the reactor concept, an experimental program was established to examine the performance of SiC coated graphite to be used in this reactor. The test environments for the SiC coated graphite were established using the results of the analyses performed in this chapter. All of the experiments were done in an out-of-core facility since the funding for in-core experiments was not available. This experimental program is a scoping study to determine if further testing is warranted. Thus the lack of irradiated specimens is not a large concern at this time.

3.5.1 Normal Operating Environment

There are two different environments which the graphite must endure. First is the normal operating environment of the reactor. The normal operating environment for this reactor concept has been defined to be high temperature water at 300°-320°C at a pressure of about 15.5 MPa. For our purposes we will use 300°C water at a pressure of 15.5 - 15.9 MPa (2250 - 2300 psig).

The water chemistry has been derived from the water chemistry of PWR and CANDU plants. Since boron is not used for reactivity control in the PTLWR, there is no boric acid included in the water chemistry. Since this reactor is essentially a CANDU, with very little boiling, an overpressure of hydrogen gas is desired to keep the free oxygen concentration in the water low. CANDU reactors generally operate with a water pH of about 10 (@25°C) to help inhibit waterside corrosion and corrosion product transport. The normal pH control agent for CANDU plants is LiOH. Lithium reacts with the SiO_2 layer on the SiC, reducing the corrosion resistance of SiC. For this reason the pH control additive was chosen to be NH_4OH for the PTLWR. Studies by AECL have shown that for corrosion control in the CANDU heavy water reactors and the boiling light water reactor (CANDU-BLW at Gentilly) the important factor is the pH of the water, not the pH additive used to achieve it [Burrill, 1978] [Burrill, 1980].

In normal CANDU plants that use LiOH as the pH additive, the primary water target pD at 25°C is 10.45 [Heitmann, 1993]. This translates to a target pH of 9.58 at 25°C. The acceptable pH range is from 9.43 to 9.93. When using NH_4OH as the pH

additive, the pH at 25°C must be higher since the effectiveness of NH_4OH at high temperatures is less than that of LiOH. The Gentilly reactor water chemistry employed a NH_4OH concentration of 25 mg NH_3 / kg H_2O, which should theoretically give a pH of about 10.1 in our case [Burrill, 1978]. For our test environment a pH of 10.1 at 25°C is defined as the target pH.

Ideally, the experimental environment would have a water flow velocity approximately equal to that encountered in the real plant, 11.5 m/s. However, the facilities available for the tests are not quite this elaborate. The water velocity for this test is essentially zero, however the water is circulated through a charging system which maintains water chemistry and pressure near the desired levels. The lack of water velocity is a drawback to the current test setup, however several studies already document the ability of SiC to successfully withstand high velocity water and steam. For the purpose of this study, the effects of water chemistry and water velocity are considered to be independent of each other. The time frame for the operating conditions test is set at 500 hours. This time was mainly established due to time constraints. It did, however, prove long enough to reveal any weakness in the SiC coating of the test specimens.

3.5.2 LOCA Environment

The second and most aggressive environment that the SiC coating must endure is exposure to steam at the high temperatures that are encountered during a LOCA. Several studies have been completed that show SiC is able to withstand steam/air mixtures at temperatures in excess of 1000°C. A discussion of previous experience with SiC is given in Chapter 2. For the PTLWR, the limiting temperature of the SiC coated graphite was set at 1300°C. Based on the studies discussed in Chapter 2, it is believed that the SiC can successfully protect the graphite at a temperature of 1300°C for the few hours that are necessary.

Based on the fuel performance studies discussed in this chapter, a LOCA for the PTLWR will subject the graphite to temperatures of about 1200°C in a steam environment. The current facilities allow us to raise the test specimens only to 1000°C. This temperature is deemed high enough since subjecting graphite to this temperature will reveal even the slightest flaw in the coating, which is, after all what is being evaluated.

The present literature also made clear that while the potential protection offered by SiC is well established, the main stumbling block to realizing this protection in practice is the coating process used to apply the SiC to the graphite substrate. A poorly applied coating of SiC will spall when the graphite is subjected to thermal cycles. Not only will the

graphite in the PTLWR be subject to mild thermal cycles, such as those encountered during startup and shutdown, but the potential for thermal shock is also present. Thus, in addition to the high temperatures encountered during an accident, the experiments should evaluate the coating performance during a severe thermal shock, which may be encountered if the reactor was inadvertently flooded with makeup coolant.

The accident environment for these experiments is not one, but two different conditions. First the SiC coated graphite will be subjected to 1000°C steam for a period of time necessary to detect any failure in the graphite coating. This time period has been chosen as five hours. This time is justified by a set of experiments which shows that after only a few minutes at temperatures above 650°C, graphite oxidation is severe. These experiments are also discussed in Chapter 5.

The second environment that may be encountered in an accident is thermal shock. To test the susceptibility of the coated graphite to this condition, the specimens will first be tested in the five hour high temperature test, then subsequently subjected to being heated to 1000°C and quenched in room temperature water.

3.6 Chapter Summary

This chapter presented the chronology of events which lead to the experimental program discussed in the remaining chapters. In section 3.1 a brief history of previous work was presented which outlined the development of the PTLWR reactor concept. Sections 3.2 and 3.3 presented detailed analyses of two fuel bundle designs specifically for the wet calandria variant of the PTLWR. Section 3.4 identified the WC-5 fuel bundle design as being the current working design for the wet calandria version of the PTLWR.

The designs analyzed in sections 3.2 and 3.3 rely heavily on SiC to protect the graphite in the fuel arrangement from oxidation during a LOCA. Based on theses analyses a set of experimental environments was established in section 3.5 to test the effectiveness of the SiC coating applied to graphite. Chapter 4 discusses the test rationale, test setup and the data collection used in the experiments.

4. EXPERIMENTAL SETUP

4.1 Summary of Test Rationale

The series of experiments presented in this thesis were performed to determine the ability of a silicon carbide coating to protect graphite from the harsh environment in a LOCA. However, this alone is not enough. In order for the nuclear community to embrace the concept of using SiC coated graphite in reactors, several additional things need to be demonstrated. Therefore, the main aims of the experimental program performed here were the following.

1. Show that SiC has the potential to withstand reactor operating conditions as well as the widely used zircaloy alloys.

2. Show that SiC coated graphite can withstand the challenging environment encountered in a LOCA better than normal zircaloy, after being exposed to normal reactor conditions.

3. Show that SiC coated graphite can withstand the challenging environment encountered in a LOCA much better than plain, uncoated graphite.

A secondary objective of this program was to identify a coating process that is currently available and produces an acceptable SiC coated graphite specimen. This would alleviate the high cost involved in developing a specialized process. Based on the current literature, the company Toyo Tanso USA, Inc. was chosen to provide the graphite for testing, and one type of SiC coating. The graphite tested is IG-110, a high purity, high density, isotropic graphite developed by Toyo Tanso specifically for use in the nuclear industry. (See the Chapter 2 review of SiC and graphite in the nuclear industry.) The coating process used by Toyo Tanso is called PERMA-KOTE and is specifically designed to form a good cohesion between the SiC and the graphite.

To provide a measure of relative performance between different technologies, a second set of SiC coated IG-110 graphite specimens were prepared by Thermo Electron using a chemical vapor deposition (CVD) process. The same type of graphite, provided by Toyo Tanso USA Inc., was used to assure that the results would be as consistent as possible and easily reproducible.

The third type of specimen tested was uncoated ("virgin") IG-110 graphite. The virgin graphite was included in the tests to show the degree of protection offered by each type of SiC coating relative to the damage which results if the graphite is not protected in

any way. The fourth type of specimen tested was sintered alpha silicon carbide. The SiC "sticks" provided by the Carborundum Company were included to show the performance of pure α-SiC in the test environments. The α-SiC stick performance indicates the theoretical degree of protection that can be offered if the coating on the graphite is not compromised in any way, or if SiC is used throughout.

To provide a degree of confidence in the results, three of each type of specimen were included in each test. The next section presents in detail the experiments performed, the test environments for each, and the goal of each experiment. Table 4-1 in the next section summarizes the experiments in an easy to read format. A complete listing of test specimen specifications and ordering information is included in Appendix D.

4.2 Outline of Experiments

As outlined in section 3.5, there are three essential conditions that the SiC coated graphite must survive. The first is the normal operating conditions of the reactor. The second is the high temperatures reached during a loss of coolant accident. The third is the possibility of a quench cooling, with a subsequent heat up back to LOCA conditions. This section outlines in detail the tests performed and the experimental setup used. This experimental program does not test irradiation performance of any of the materials. The radiation effects on SiC coated graphite are a serious problem, but they are beyond the scope of this work.

4.2.1 Reactor Operating Test

This test is to assess the SiC and SiC coated graphite performance in normal reactor operating conditions. The specimens were mounted on a bracket inside an autoclave in positions to maintain a large surface area in contact with the water and to prevent any contact between specimens. The autoclave was placed inside an oven which heated the autoclave to a steady state temperature of 300°C. The autoclave was pressurized with water to 2275 psig. The water chemistry was controlled in an unpressurized charging tank at a nominal pH of about 10.* Hydrogen gas was continually bubbled through the charging tank, and a hydrogen overpressure of between 1.17 and 0.89 psig was maintained.

Because the charging pump flow rate was quite low compared to the volume of the system, a delay in turnover of the system water resulted. The circulation time for water in

* pH 10 was maintained to simulate CANDU BLW reactor conditions. See section 3.5.1 in Chapter 3 for a complete discussion of water chemistry.

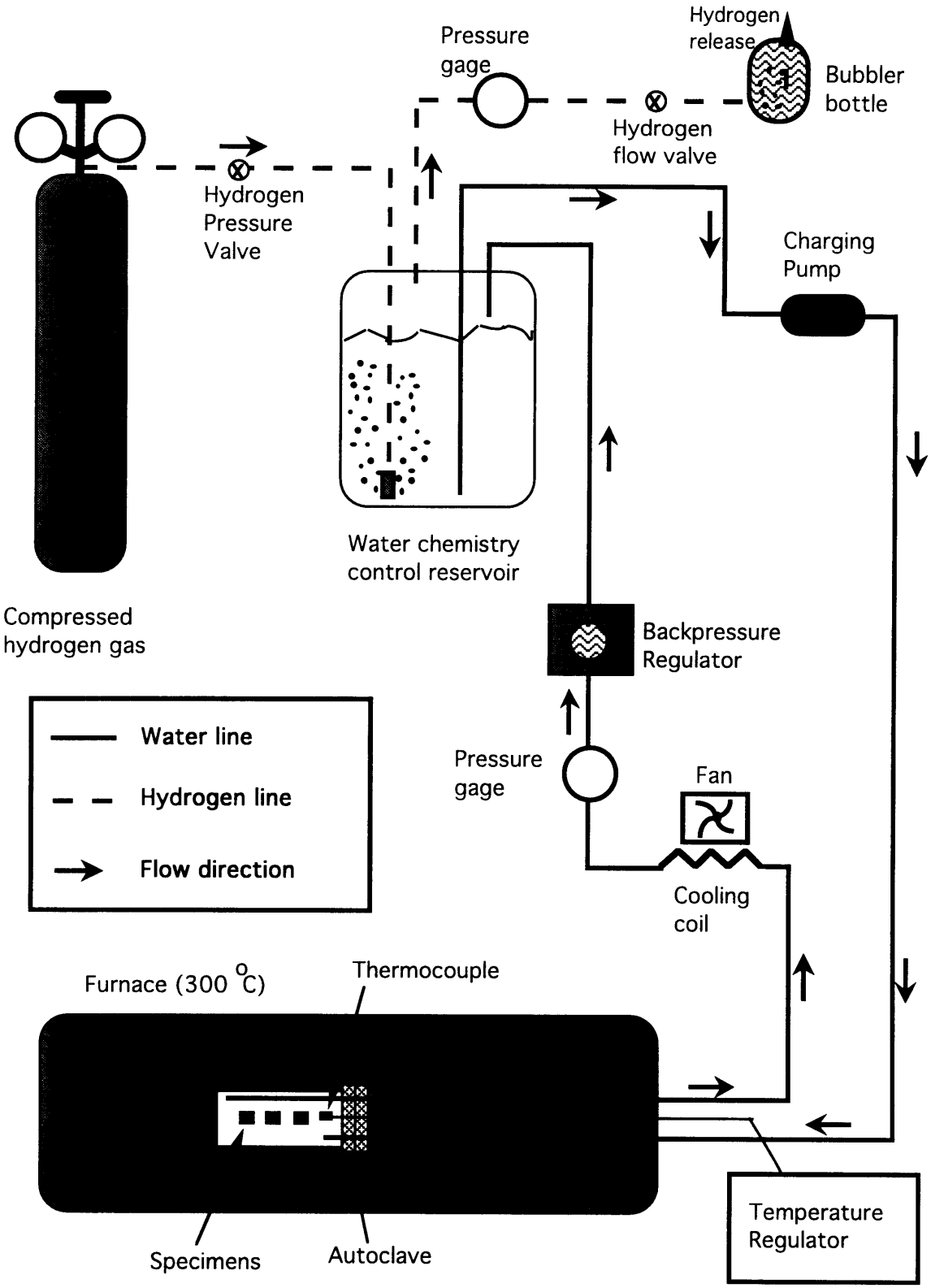

Figure 4-1: Experimental Setup for Reactor Operating Conditions Test

the system was about 2 days. Keeping the pH at the nominal value proved to be difficult, due to this long circulation delay. The pH in the charging tank fluctuated between 9.75 and 10.15.

This test ran continuously for 500 hours (21 days) once a steady state temperature of 300°C was reached. Figure 4-1 shows the general layout of the operating test apparatus. The autoclave was a 1 liter Inconel structure manufactured by Autoclave Engineers. The tubing used was 1/4" outside diameter 316 stainless steel.

4.2.2 High Temperature Corrosion Tests

A series of seven tests were completed in a high temperature LOCA environment. In section 3.5 the temperature for the LOCA environment was identified as being as high as 1300°C, which is the design limit temperature used in the fuel designs WC-4 and WC-5. A test temperature of 1000°C was used in these experiments due to facility constraints. This temperature is, however, sufficient to test the protective nature of the SiC coatings. The specimens were mounted on an alumina firebrick in a fashion to allow roughly 90% of the surface area of the specimens to be exposed to the controlled environment. The specimens and mount were then placed inside an air-tight environmental chamber. The environmental chamber was used to maintain absolute control over the gas mixture and humidity in which the tests took place. The environmental chamber was then inserted into a furnace which heated the assembly to a steady state internal temperature of 1000°C. The temperature inside the environmental chamber was continuously monitored and recorded using a type K thermocouple and a computer system.

The heat capacity of the environmental chamber assembly was sufficiently high to require a substantial heat up and cool down period. A time of 2.5 hours was generally required to heat the test assembly from room temperature to 1000°C, while 4 to 5 hours were required to cool the test assembly to a temperature suitable for handling. During the heat-up and cool-down periods the environmental chamber was flooded with flowing dry nitrogen gas to prevent any unwanted oxidation from taking place. The nitrogen was maintained at a flow rate of between 2 and 4 liters per minute in order to assure that no air was allowed to enter the system inadvertently through the exhaust gas line. The nitrogen gas was standard bottled pre-purified industrial grade nitrogen.

A gas conditioning system was constructed to allow conditioning of the gas (nitrogen or air) prior to it entering the environmental chamber. The gas conditioning setup consisted of a gas flow meter, a gas dryer, a humidifier apparatus, and a mixing chamber where temperature and humidity probes were located. The gas conditioning system for the

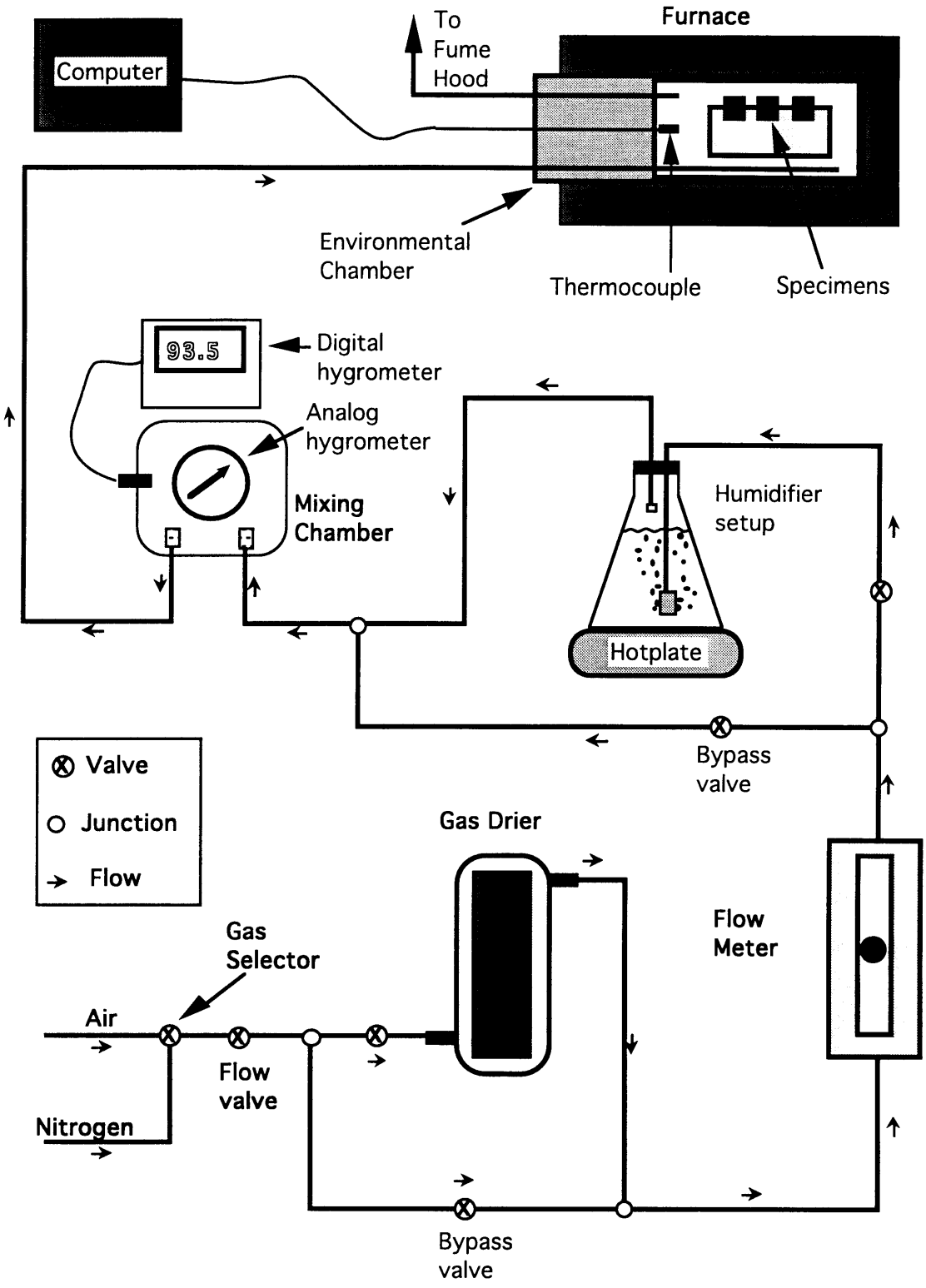

Figure 4-2: Experimental Setup for LOCA Test

LOCA tests is shown in Figure 4-2. To add humidity, the gas was forced through a large bottle of heated de-ionized water. Depending on the gas flow rate and the water temperature, the humidity of the flowing gas could be increased up to saturated conditions at room temperature and pressure. The gas first passed through the drier, through the flow meter, through the humidifier, into the mixing chamber, and finally into the environmental chamber. A system of valves was employed to allow the gas to bypass the drier or the humidifier, however all of the gas passed through the flow meter. The mixing chamber was a necessary component since it was often required to pass most of the gas through the humidifier, while allowing a small amount to bypass directly into the mixing chamber. The mixing chamber assured that the gas was well mixed before it passed into the environmental chamber.

The temperature and relative humidity were measured in the mixing chamber using two methods. An analog hygrometer / thermometer was installed inside the mixing chamber. Readings were taken visually through the transparent surface of the chamber. A digital hygrometer / thermometer probe was also installed in the mixing chamber. The read-out for this probe was located directly above the mixing chamber.

As mentioned previously, the LOCA test series consisted of seven individual tests. Each test is briefly described here. One test was $5^1/_2$ hours in 1000°C dry air at a flow rate of 19 L/min. (heat up and cool down were in dry nitrogen). The test specimens were all previously untested. Four tests were performed for 5 hours in 1000°C humid air at a flow rate of 19 L/min. Upon entering the test chamber the air was saturated with water (at one atmosphere and ~70°F). The first of these consisted of previously untested specimens. The second consisted of specimens that had already been subject to the reactor operating condition test. The third consisted of a previously untested, but damaged specimen (the SiC coating had a large scratch). The fourth consisted of re-testing the first batch after they had been quenched cooled in room temperature water from 1000°C

A single 5 hour test in 1000°C humid nitrogen at a flow rate of 4 L/min. was performed to determine whether the oxygen present in the steam was enough to cause severe damage.

A final LOCA test was performed in dry air. This test did NOT make use of the environmental chamber. Instead uncoated pieces of graphite were placed in the furnace for twenty minutes. The graphite was then checked for weight loss. This process was repeated for temperatures ranging from 600°C to 950°C. This test was performed to show the oxidation damage that occurs at different temperatures when oxygen is available. The

results of this test are to show that the 1000°C tests are sufficient to allow detection of a failure in the SiC coating on the graphite.

4.2.3 Quench Tests

Two quench tests were performed to determine the ability of the SiC coating to withstand the stresses that accompany a very aggressive thermal shock simulation. Because of the slightly different thermal expansion rates of graphite and silicon carbide, a thermal shock will induce stresses between the SiC coating and the graphite substrate. Depending on the ability of the coating process to bond the SiC and the graphite at the interface, the SiC coating may crack or spall, reducing the ability of the coating to protect the underlying graphite from future oxidizing environments. The quench tests were accomplished by heating the specimens for five minutes in air (without the environmental chamber) to 1030°C in the furnace. The specimens were then extracted from the furnace using tongs and immediately plunged into room temperature de-ionized water. This effectively cooled the specimens from 1000°C to 25°C in under two seconds.

Both quench tests were performed on specimens that had been previously tested in the high temperature LOCA tests. One of these groups of specimens had also been previously tested in the reactor operating test. Because of the nature of this type of test, only SiC coated graphite specimens were tested. No purpose would be served for the scope of this thesis by testing SiC sticks or virgin graphite.

4.3 Data Collection

The experiments described in the previous section are all performed to establish the extent of degradation of the test specimens. Four types of analyses were conducted for the specimens. Measurements of the specimen weight, visual examination, optical microscopy, and electron microscopy were conducted.

Weight measurements for all specimens were made before and after each experiment. This provided the mass loss or gain due to water absorption, or graphite oxidation (which may accompany defects in the SiC coating). A large change in mass not only indicates a definite defect in the coating, but also a qualitative indication of the size and severity of the defect.

The surfaces of the specimens were analyzed before and after each experiment using visual observation. Each specimen was carefully scrutinized and any apparent changes or abnormalities were recorded. Special note was taken of color and texture changes. Most specimens were viewed under the optical microscope at a magnification of

Table 4-1: Experimental Test Matrix

Materials for Testing

Pieces	Company	Description	Dimensions	Designators
13	Toyo Tanso	SiC Perma-Kote IG-110	2" x 2" x 1/8"	A1 - A13
12	Thermo Electron	SiC CVD coated IG-110	2" x 1/2" x 1/4"	B1 - B12
12	Carborundum	Silicon Carbide	2" x 1/8" x 1/8"	C1 - C12
28	Toyo Tanso	IG-110 Graphite	2" x 1/2" x 1/4"	D1 - D28

Overall Test Plan

Test	Apparatus	Temp °C	Condition	Length	Cool	Specimens Tested
1	HT Furnace	1,000	Dry Air	5.5 hr	Slow	A1-3, B1-3, C1-3, D1-3
2	HT Furnace	1,000	Humid Air	5.0 hr	Slow	A4-6, B4-6, C4-6, #
3	HT Furnace	1,000	Humid N_2	5.0 hr	Slow	A7-9, B7-9, C7-9, D7-9
4	HT Furnace	1,000	Dry Air	~5 min.	Quench	A2, A5, A8, B2, B5, B8
5	HT Furnace	1,000	Humid Air	5.0 hr	Slow	A2, A5, A8
6	HT Furnace	600-950	Dry Air	1/2 hr	Fast	D11 - D28
7	HT Furnace	1,000	Humid Air	5.0 hr	Slow	Scratched A13
8	Operating Loop Setup	300	NH_4OH, CANDU Chemistry	500 hr	———	A10-12, B10-12, C10-12, D10-12
9	HT Furnace	1,000	Humid Air	5.0 hr	Slow	A10-12, B10-12, C10-12
10	HT Furnace	1,000	Dry Air	~5 min.	Quench	A10, B10

HT Furnace = High Temperature LOCA setup

No D specimens (virgin graphite) were included in test 2 since the D1, D2, and D3 specimens from test 1 were completely oxidized.

Test	Purpose
1 - 3	Find ability of SiC coating to protect graphite in different high temp atmospheres
4	Find ability of SiC coating to withstand thermal shock
5	Find ability of SiC coating to protect graphite after sustaining a thermal shock
6	Find temperature at which graphite starts to oxidize rapidly in dry air
7	Find ability of flawed SiC coating to protect graphite
8	Submit SiC coating to normal operating conditions
9 - 10	Perform tests 2 and 4 on specimens from test 8

100x to 200x. This allowed a more detailed analysis of gross characteristics of the coating, such as texture differences between the different faces that are not apparent to the naked eye. Most defects or noteworthy characteristics were observed using the optical microscope and then scrutinized more carefully using scanning electron microscopy (SEM).

The SEM was used to get a detailed representative picture of what the condition of the specimens were before and after each experiment. The SEM was used to size small cracks, investigate localized breakdowns in the coating, and provide clear pictures of normal and abnormal surfaces for each specimen type.

Several secondary parameters were also recorded during the tests, these were mainly concerned with the test environments. For the reactor operating test, the following additional data were recorded at intervals throughout the 500 hour duration:

1. test chamber temperature (water temperature),
2. water pressure,
3. water pH, and
4. hydrogen overpressure.

For the high temperature LOCA test the following additional data were recorded at intervals throughout the test duration:

1. furnace temperature,
2. environmental chamber temperature (recorded by computer at 10 second intervals),
3. gas and gas flow rate,
4. gas relative humidity and temperature (before entering the test chamber).

This data array assured an accurate record of the test environment that each specimen was subjected to. Thus a complete specimen history was established for future reference. Table 4-2 summarizes the data recorded for each type of experiment.

4.4 Experimental Setup Summary

This chapter outlined the various tests which make up the experimental program. In section 4.1 the rationale is established for the types of tests that were needed and what was judged to be necessary to begin to evaluate SiC coated graphite for consideration for use in a PWR. Section 4.2 details the specific environment that was investigated for each test and indicates how those conditions were met. Table 4-1 gives a summary of each test and its particular purpose in the overall scheme. Section 4.3 outlines the data that were collected for each of the different types of tests. Chapter 5 presents the results for all of the experimental tests discussed in this chapter.

Table 4-2: Summary of Experimental Data Collection

Data Recorded	Operating	LOCA	Quench
Specimen weight before test	X	X	X
Specimen weight after test	X	X	X
Pre/Post Visual Examination	X	X	X
Pre/Post Optical Mircroscopy	x	x	x
Pre/Post Electron Microscopy	*	*	*
Furnace Temperature		X	X
Test Chamber Temperature	X	X	
Water pH	X		
Water Pressure	X		
Hydrogen Overpressure	X		
Gas flow rate		X	
Gas Temperature		X	
Gas Relative Humidity		X	

X = Always recorded,
x = performed for most specimens,
* = performed for select specimens only

5. EXPERIMENTAL RESULTS AND ANALYSIS

This chapter presents the experimental results and the implications that they have on the initial evaluations of the use of SiC coated graphite in a nuclear reactor operating at PTLWR conditions. The performance of the SiC coated graphite is compared to the known performance of zircaloy in the same environments. Section 5.1 presents the weight loss and surface examination data for relevant test specimens. Section 5.2 discusses the implications of using SiC coated graphite in a normal reactor operating environment. Section 5.3 presents behaviors of SiC coated graphite in a high temperature steam environment simulating a LOCA. The final section presents conclusions drawn from the experiments and discusses relevance of this work.

5.1 Experimental Data

The raw weight measurement data recorded for the specimens used in each test is given in Appendix A. The discussions are concerned with general data trends and specific data points.

5.1.1 Reactor Operating Conditions

The reactor operating test subjected specimens to 500 hours (21 days) in 300°C, 15.5 MPa deionized water to which appropriate amounts of NH_4OH and H_2 were added (see section 3.5.1 of Chapter 3). The test specimens were three each of PERMA-KOTE SiC coated IG-110 graphite, CVD SiC coated IG-110 graphite, uncoated IG-110 graphite, and solid α-SiC. Two of the PERMA-KOTE specimens (A11 & A12) gained a significant amount of weight which was attributed to water ingress into the graphite. This water ingress clearly indicated a defect in the SiC coating. One of the PERMA-KOTE specimens (A10) lost a small amount of weight during the test. A careful examination of the A10 surface was completed and the coating was found to be intact, thus this small amount of weight loss was attributed to SiC corrosion. (The coating integrity was confirmed by subsequently testing the specimen in a LOCA environment. No weight loss was observed.) The slight weight loss of A10 was converted to an equivalent penetration and compared to the penetration of zircaloy for the same test conditions.

To convert the A10 SiC weight loss to an equivalent penetration the following manipulation was completed. First the mechanism of weight loss was assumed to be a loss of SiC with no oxide film formation on the surface. If uniform corrosion is assumed, the thickness of the SiC lost is easily calculated. The amount of SiC lost (in moles) is found

by dividing the weight loss by the molecular weight of SiC. (Note again that this does not take into account the possibility of an oxide film on the surface, which is reasonable given the high solubility of CO_2, H_2, and SiO_2 @ pH 10). Next the volume of one mole of SiC was calculated by dividing the molecular weight by the density. The thickness of one mole of SiC was then calculated by dividing the volume of one mole of SiC by the surface area for this specimen. Finally, multiplying the moles of SiC reacted by the thickness of SiC coating per mole gave the penetration depth. The equations used are listed below.

Moles of SiC lost:

$$\mathbf{N}\ (\text{mol}) = (\Delta \mathbf{W} / \mathbf{m}) \qquad (5.1)$$

Thickness of SiC lost:

$$\delta\ (\text{cm}) = \mathbf{N} * (\mathbf{m} / \rho) / \mathbf{SA} \qquad (5.2)$$

Substitution in equation 5.1:

$$\delta\ (\text{cm}) = \Delta \mathbf{W} / \rho / \mathbf{SA} \qquad (5.3)$$

The specific values for the PERMA-KOTE SiC coating and this specimen are listed below.

$\Delta \mathbf{W} = 0.0005$ g

$\rho = 3.2$ g/cm^3

$\mathbf{m} = 40.0967$ g/mole

The dimensions of the A10 specimen were 2" x 2" x 1/8". The surface area was:

$\mathbf{SA} = 2*(2"*2") + 4*(2"*1/8") = 9$ in^2

Converting to compatible units:

$\mathbf{SA} = 58.0644$ cm^2

The penetration of the SiC coating was:

$\delta = 0.0005$ g / 3.2 g/cm^3 / 58.0664 cm^2

$\delta = 2.691 \times 10^{-6}$ cm $= 0.0269$ μm

To compare this penetration to that expected for zircaloy, the corrosion data from Peters will be used [Peters, 1984]. As discussed in Chapter 2, the corrosion data of interest is for the short term pre-transition regime. Peters gives the following equation to represent weight gain on zircaloy specimens in this regime:

$$\Delta \mathbf{w}\ (\text{mg/dm}^2) = \mathbf{K} t^{1/3}, \qquad (5.4)$$

where

$$\mathbf{K}\ (\text{mg/dm}^2/\text{day}^{1/3}) = \mathbf{3665\ exp(-14062 / T)}. \qquad (5.5)$$

The corrosion mechanism for zircaloy that results in this weight gain is the formation of a ZrO_2 film. The weight gain is a measure of the amount of O_2 gained by the film. Dividing the weight gain by the molecular weight of O_2 will give the amount of Zr reacted (in

moles). Once this was determined, the penetration of Zr was calculated similar to that of SiC. Since the weight gain is in units of mg/dm^2, the units of square area were carried through all of the calculations.

Number of moles of Zr reacted per cm^2:

$$n_{Zr}\ (mol/cm^2) = (\Delta w / m_{O_2})*(1dm^2/\ 100cm^2)*(1g/1000mg) \qquad (5.6)$$

Penetration of the Zr:

$$\delta\ (cm) = n_{Zr} * (m_{Zr} / \rho_{Zr}) \qquad (5.7)$$

Equations 5.4 through 5.7 were used to calculate the expected penetration for zircaloy-4. Table 5-1 lists values of weight gain (for a specimen the same size as A10) and penetration calculated for zircaloy-4 from Peters data for several times and includes the experimental values for specimen A10 at day 21. Figure 5-1 shows graphically the expected penetration for zircaloy and the calculated penetration for the SiC layer on specimen A-10. From the figure and the table it is clear that the SiC corrosion rate is substantially less than that of zircaloy for this particular environment.

Table 5-1: Penetration of Zr and SiC for Reactor Operating Test

Time (days)	ΔW_{Zr} (mg) (Peters)	ΔW_{SiC} (mg) (A10)	δ_{Zr} (μm)* (Peters)	δ_{SiC} (μm) (A10)
1	1.775		0.134	
4	2.818		0.213	
8	3.551		0.268	
12	4.064		0.307	
16	4.473		0.338	
20	4.819		0.364	
21	4.898	-0.5	0.370	0.0269

* Calculated here using data from Peters [Peters, 1984]

All of the CVD SiC coated IG-110 graphite specimens in the reactor operating test gained a significant amount of weight due to water ingress. The coating was peeling and flaking off the graphite surface when the specimens were removed from the test apparatus. These specimens were coated with several layers of SiC, but it was unclear how much of the surface was still covered by SiC at the conclusion of the test. From the weight gain it was concluded that the SiC coating was totally penetrated.

The uncoated graphite specimens also gained a significant amount of weight from water ingress. This was to be expected since there is nothing to prevent water from infiltrating the porous structure of the graphite. The solid SiC specimens experienced very little weight change. One SiC specimen remained unchanged, one gained a small amount

of weight and one lost a small amount of weight. The SiC was not expected to gain or lose much weight during the experiment since the surface area and reaction rates are extremely small.

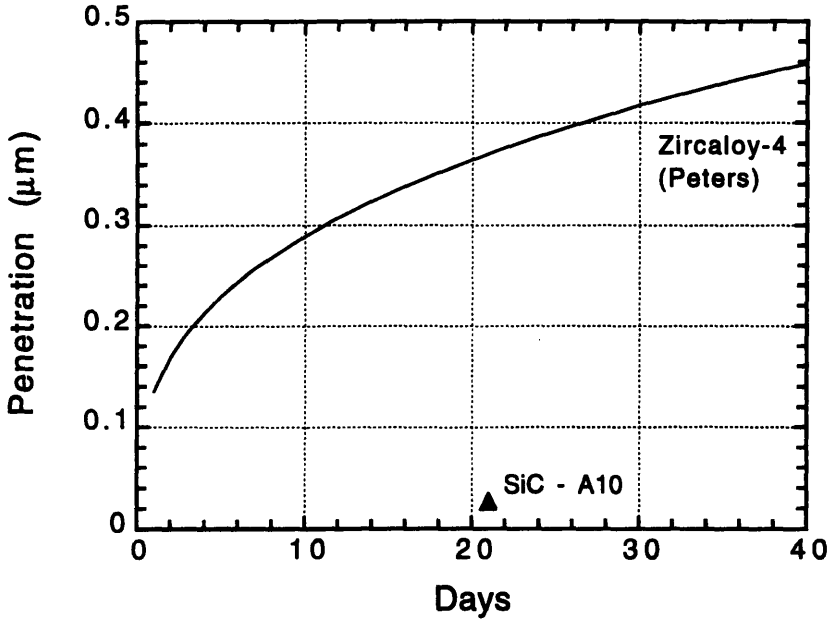

Figure 5-1: Comparison of SiC Penetration to Zy-4 for Operating Test

5.1.2 LOCA Tests

Several high temperature LOCA tests were carried out to determine the ability of SiC coatings to protect the IG-110 graphite in a reactor accident environment of hot steam. The general trend in the weight measurements showed the excellent protection offered by the PERMA-KOTE SiC coated graphite specimens. The CVD SiC coated graphite suffered minor weight loss, which indicated flaws in the coating. The uncoated graphite specimens were completely oxidized in the high temperature steam environment. This result helps to better illustrate the degree of protection offered by even a less than perfect SiC coating. The SiC specimens showed very small weight losses.

In all tests where the specimens were not subjected to the reactor operating test first, the PERMA-KOTE coating remained intact and the graphite suffered no oxidation. A slight weight gain was seen which was attributed to oxide formation on the surface. (It is the very thin layer of SiO_2 which produces the excellent corrosion resistance of SiC in oxidizing environments.) Specimens from the reactor operating test were also tested in the

LOCA environment. A specimen with intact SiC coating (A-10) showed a slight weight gain after the LOCA test. Specimen A11 lost weight due to a hole in the coating. Specimen A12 was destroyed and fragments of the SiC coating were found in the test apparatus. Photo 1 and Photo 2 located at the end of this chapter show the test specimens immediately after the LOCA test where the fragments of SiC coating from specimen A12 are clearly visible. Figure 5-2 shows the weights of the three PERMA-KOTE SiC coated graphite specimens before and after the operating test and after the LOCA test. The graph clearly shows that the SiC coating on specimen A11 provided excellent oxidation protection for the underlying graphite even though the coating was flawed.

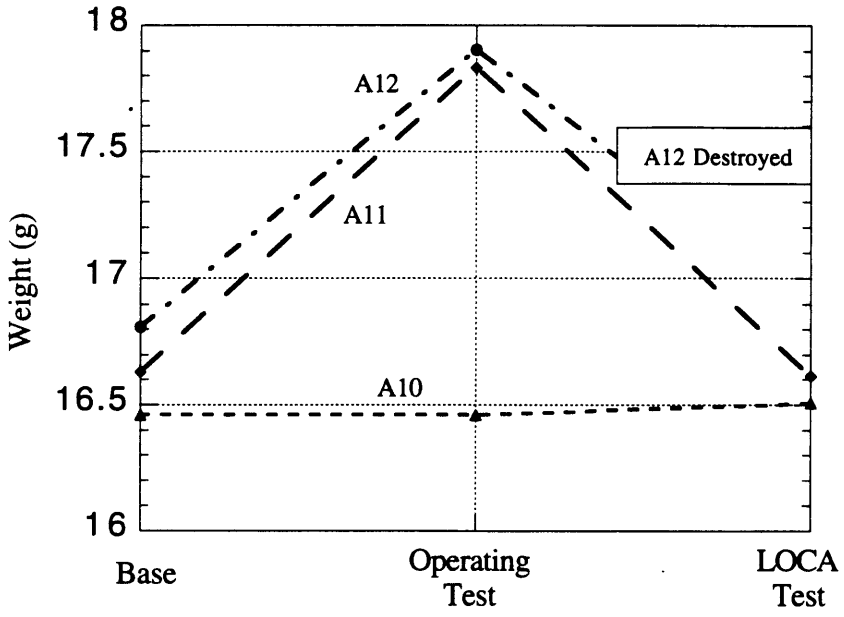

Figure 5-2: Weight Changes of Specimens A10, A11, A12

Two specimens, A10 and A4 were chosen to represent the potential protection offered by the SiC coating. Specimen A4 shows typical results for the PERMA-KOTE specimens that were only subjected to the LOCA test. Specimen A10 is a PERMA-KOTE specimen that experienced the operating test and subsequently was tested in a LOCA environment. Both specimens gained weight during the LOCA test and this weight gain was transformed into surface penetration for comparison to zircaloy. The weight gain mechanism was assumed to be the formation of a thin layer of SiO_2. The reaction was assume to take the following form:

$$SiC\ (s) + 3H_2O\ (g) \longrightarrow SiO_2\ (s) + CO\ (g) + 3H_2\ (g) + 229\ J/mol \qquad (5.8)$$

The first step in calculating the surface penetration was to calculate the amount of SiC reacted (in moles). To determine this, the loss of carbon and gain of oxygen was taken into account. For each carbon lost there are two oxygen atoms gained. Thus for each mole of silicon reacted, a weight gain equal to the difference in the molecular weights of O_2 and C would be observed. Thus the effective molecular weight is:

$$m_e \text{ (g/mol)} = m_{O_2} - m_C \qquad (5.9)$$

Number of moles of SiC reacted:

$$N \text{ (mol)} = \Delta W / m_e \qquad (5.10)$$

Penetration of the SiC coating is then calculated using equation 5.2

$$\delta \text{ (cm)} = N * (m_{SiC} / \rho_{SiC}) / SA \qquad (5.2)$$

The specific values for the A10 and A4 specimens are given below.

m_e = 31.9988 g/mol - 12.0112 g/mol = 19.9876 g/mol

ΔW_{A10} = 0.0493 g

ΔW_{A4} = 0.0023 g

ρ_{SiC} = 3.2 g/cm^3

m_{SiC} = 40.0967 g/mole

SA = 58.0644 cm^2

The calculated surface penetration of A10 and A4 are given in Table 5-2.

The expected penetration of zircaloy-4 in 1000°C steam is calculated for comparison using the results from Ballinger [Ballinger, 1976]. The weight of Zr reacted in an unlimited steam environment is represented by the equations:

$$\Delta w_{Zr} \text{ (mg/cm}^2) = \sqrt{(K_p t)} \qquad (5.12)$$

$$K_p \text{ (mg}^2\text{/cm}^4\text{/sec)} = 3.10\text{x}10^5 \exp(-33{,}370 \text{ (cal/mol)} / RT) \qquad (5.13)$$

where R is the universal gas constant (1.987 cal/mol K), and T is temperature in Kelvin. The penetration of zircaloy is then calculated by dividing the weight of Zr reacted by the density of zircaloy-4.

$$\delta \text{ (cm)} = (\Delta w_{Zr} * (1 \text{ g} / 1000 \text{ mg}) / \rho_{Zr}) \qquad (5.14)$$

The penetration of zircaloy-4 is given in Table 5-2 for several exposure times. The mechanism of zircaloy corrosion is assumed to obey the equation:

$$Zr \text{ (s)} + 2H_2O \text{ (g)} \longrightarrow ZrO_2 \text{ (s)} + 2H_2 \text{ (g)} + 645{,}569 \text{ J/mol} \qquad (5.11)$$

The expected penetration of SiC according to Horn is also used for additional comparison. The expected penetration values for SiC are from experiments carried out in 10 m/s steam at 1127°C [Horn, 1979]. This environment was more punishing than the environment for the LOCA test due to the higher temperature and steam velocity. The values of expected SiC penetration are shown graphically in Figure 5-3 along with the

expected penetration of zircaloy-4 and the calculated values for A10 and A4. Table 5-2 also lists values for certain times. Table 5-2 and Figure 5-3 clearly show the lower corrosion rate of SiC in the steam environment. This low corrosion rate in a highly oxidizing environment is the basis for the protection offered by SiC during reactor accidents.

The performance of SiC coated graphite is shown to be superior to that of zircaloy in a LOCA environment when the coating layer is maintained intact. The specimen A10 experienced a significantly deeper penetration than A4. The only difference in the specimens is that A10 was subjected to the reactor operating test prior to the LOCA test. High temperature water, or the water chemistry, may have sensitized the coating layer causing it to experience greater oxidation in the LOCA environment. Implications of this possibility are discussed in section 5.2.

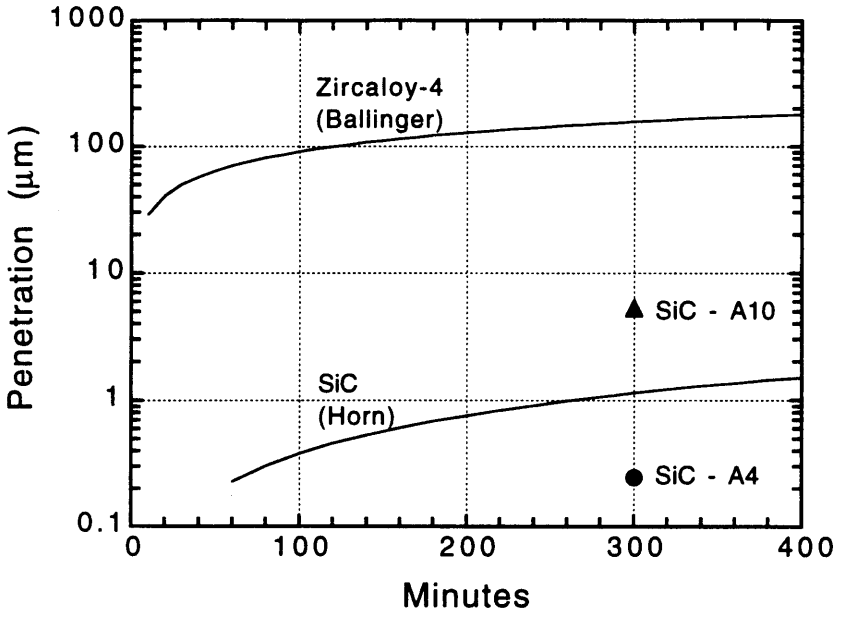

Figure 5-3: Comparison of SiC Penetration to Zy-4 for LOCA Test

The performance of the CVD SiC coated graphite specimens was not as good as the PERMA-KOTE specimens. The coating offered good protection when it remained intact, but the coating showed a great tendency to crack and spall. Figure 5-4 shows the weight gain and loss suffered by these specimens during the operating and LOCA tests respectively.

Table 5-2: Penetration of Zr and SiC for LOCA Test

Time (mins)	δ_{Zr} (μm)* (Ballinger)	δ_{SiC} (μm) (Horn)	δ_{SiC} (μm) (A10)	δ_{SiC} (μm) (A4)
60	70.18	0.228		
120	99.24	0.456		
180	121.55	0.684		
240	140.35	0.912		
300	156.92	1.140	5.323	0.248
360	171.89	1.368		
400	181.19	1.520		

* Calculated using data from Ballinger [Ballinger, 1976].

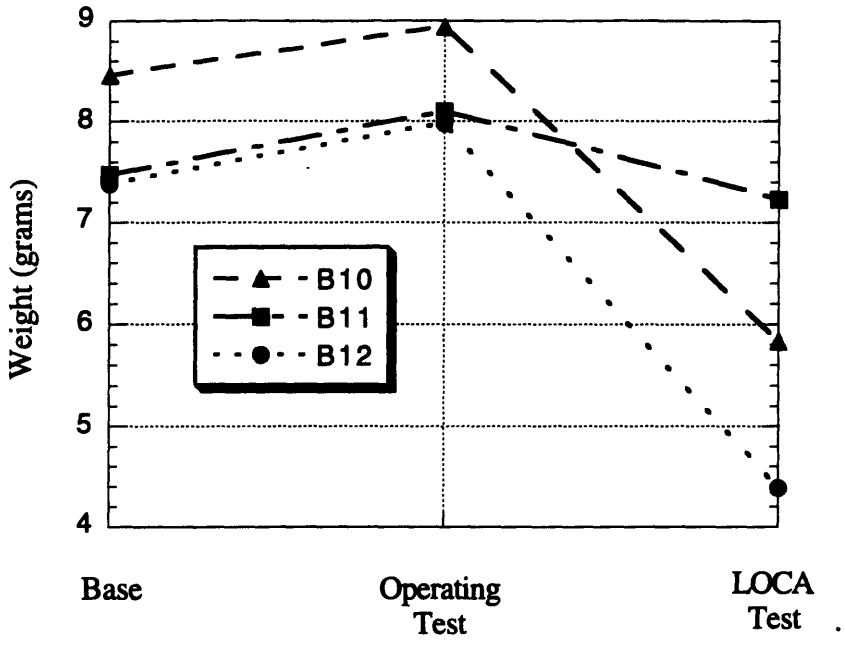

Figure 5-4: Weight Changes of Specimens B4, B5, B6

The uncoated graphite specimens were completely oxidized when they were included in a LOCA test. This shows that unprotected graphite can not be used at 1000°C, but does not indicate at what temperature graphite begins to oxidize rapidly. To determine the minimum temperature at which the graphite must be protected, a separate group of tests was performed to determine the extent of oxidation as a function of temperature for a set exposure time. There were seven tests from 600°C to 950°C at 50°C intervals. The exposure time was 20 minutes in each test. The resulting weight loss as a function of

temperature is shown in Figure 5-5. This figure clearly indicates that above 700°C graphite oxidizes at an unacceptably high rate. At 800°C the oxidation rate seems to have leveled off. This is probably due to a lack of oxygen circulation in the furnace and the small surface area of these specimens. These tests were not performed in the environmental chamber with a forced humidified air flow, thus the amount of oxygen available to the specimens could have been severely limited, nevertheless, the purpose of the experiment was fulfilled.

5.1.3 Quench Tests

The quench tests were performed to test the ability of the SiC coating to withstand thermal shock. The surfaces of the specimens were examined after the quench test and then the specimens were again tested in a LOCA environment to determine the protection offered by a cracked coating. The results show that the PERMA-KOTE SiC coating provided good oxidation protection after being quenched. The CVD SiC coatings did not provide adequate protection after experiencing a quench.

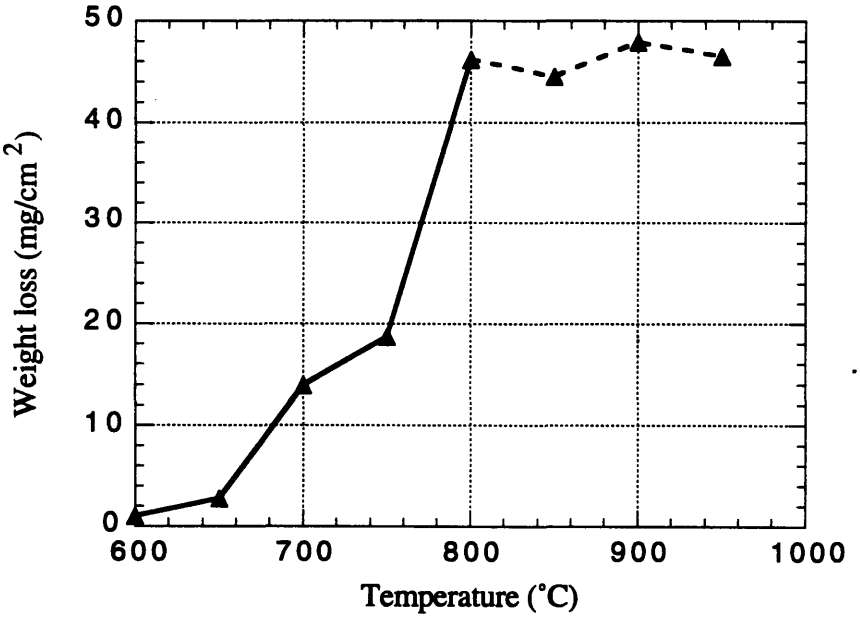

Figure 5-5: Graphite Oxidation Weight Loss for 20 Minute Exposure in Hot Air

Photo 3 (located at the end of the chapter) is an electron micrograph of the intact PERMA-KOTE SiC coating on an as received specimen. Photo 4 (located at the end of the

chapter) shows the coating after it has been quenched in water from 1000°C. The cracks seen in Photo 4 are not visible to the naked eye. The cracks are visible once the specimens have been subjected to the LOCA environment. Photo 5 (located at the end of the chapter) shows a picture of a specimen that has been through a 5 hour LOCA test, quenched, and subjected to another 5 hour LOCA test. The lights streaks are the only indication of any defect in the coating.

Even with these cracks, the SiC coating protects the underlying graphite quite well. Figure 5-6 shows the weight changes for the specimens that were quenched and subsequently re-tested in a LOCA environment. This shows that even with these microcracks, the SiC coating has the potential to protect the graphite in accident conditions.

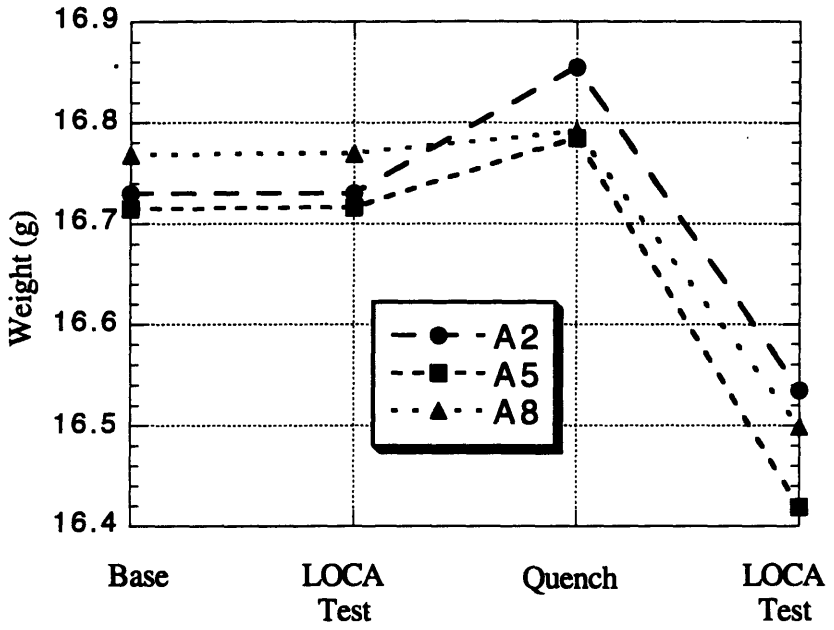

Figure 5-6: Weight Changes of Specimens A2, A5, A8

5.2 Implications for Normal Reactor Operation

The main function of SiC coated graphite in the PTLWR is to increase reactor performance during accident conditions. To do this effectively, the SiC coated graphite must first be able to withstand the normal reactor operating environment with little or no degradation to the SiC/graphite structure, and produce no unwanted effects in the reactor system. In the PTLWR especially, where SiC has been proposed as a cladding material to replace zircaloy, it seems natural to compare the degradation of SiC in reactor conditions to that of zircaloy. As a coating for graphite (or fuel pellets) the SiC must produce a

mechanically sound and chemically stable barrier between the primary system water and the underlying material. To this end, the potential protection offered by the SiC coating was shown by one specimen (A10) in Figure 5-3.*

The main barriers to achieving this protection with an SiC coating were seen to be small defects in the coating. The results from the reactor operating test are discouraging since many of the SiC coated graphite specimens showed water ingress indicating a failed coating. Photo 6 (located at the end of this chapter) is an electron micrograph of a small hole in the SiC coating of specimen A11. Photo 6 was taken after A11 had been subjected to the operating test and subsequently the LOCA test. This hole is located in a fixture mark. The fixture marks are present because the specimen must be supported during the coating process, and thus the specimen is not completely encapsulated during the first coating process. A second coating is necessary to cover the fixture marks from the first coating. Because of this process, the fixture marks are the thinnest layer of SiC on the surface. Under high pressure, it is conceivable that the outer SiC coating, which covers the fixture marks from the underlying coat, will crack and fail, producing a small hole that allows water ingress into the underlying graphite. Obviously, creating a coating method that leaves no indentations or possible voids beneath the SiC layer is one way to produce coatings that are less likely to crack. Several independent layers of coatings may also reduce the failure due to small defects. Another option is to eliminate the graphite substrate altogether and instead use a solid SiC structure. This is an option that will eliminate the problems associated with flaws in a coating, but the disadvantages of the nuclear properties of SiC must be considered.

Another factor that may have aided in the deterioration of the SiC coating in this experiment is the water chemistry. While attempts were made to create an environment where the water was free from boric acid and LiOH, there may have been residual LiOH from previous experiments where normal PWR chemistry was used. LiOH is known to cause accelerated deterioration in hot water environments [Hirayama, 1989]. The combination of lithiated water, very thin SiC coatings at the fixture marks, and the high water pressure may have accelerated the deterioration of the SiC coating and caused coating failures in this test.

The ability of SiC to withstand reactor operating environments has been shown by the performance of specimen A10, and the virtually undetectable deterioration of the solid SiC specimens. The problems associated with small coating flaws have also been

* Alternatively, the degree of development and testing needed was evident by the failure of the other two specimens.

emphasized. One of the major concerns is compatible water chemistry, but since the water chemistry is carefully controlled in reactors as a matter of course, it should not prove difficult to develop a chemistry that will not adversely affect SiC coatings or components in the primary system water.

5.3 Implications for Accident Performance

The performance of the SiC coating in the LOCA environment is much easier to judge than in the normal reactor operating environment. The extremely fast oxidation rate of graphite in air (or steam) at temperatures above 700°C has been shown here (Figure 5-5) and elsewhere [Kugeler, 1991] to be an issue. The PERMA-KOTE SiC coating offered the potential for excellent corrosion protection, especially when compared to the corrosion of zircaloy under the same conditions (Figure 5-3). The CVD SiC coating tested offered good protection in a LOCA, but the coating deteriorated in the normal operating test and in quench tests. This deterioration may be due to thermal mismatch of the CVD SiC and graphite during coating or testing.*

The potential of SiC to serve as a protective coating for structural components is great if the variability in the coating due to small defects can be eliminated. This was one of the major finding of Strife & Sheehan [Strife, 1988] and has been re-emphasized here. The results for the PERMA-KOTE specimens which were quenched and re-tested in a LOCA environment show that even coatings with small flaws can offer considerable protection from oxidation in accident environments.

There are several ways to create more reliable coatings. Schulten proposed using several independent 100μm layers of SiC as a way to create reliable coatings where failure due to microcracking is essentially overcome by brute force [Schulten,1993]. Using several independent layers would allow the use of a simple coating method, where quality control is much easier to maintain. Creating a gradual transition between the graphite and the SiC has been shown to alleviate the stresses between the SiC coating and the graphite substrate during rapid thermal transients. There have been at least three separate processes proposed to produce this type of structure [Fujii, 1992] [Hurtado, 1994]. The subject stresses cause the microcracking that reduces the effectiveness of the coating. Another option is to create a coating which incorporates elemental silicon into the SiC matrix. Upon heat treating, the elemental silicon at the graphite/SiC interface combines with the carbon

* The CVD SiC coating was performed as a complimentary service by Thermo Electron. The graphite specimens were included in coating runs for other components, thus process control for these specimens was not a primary consideration.

substrate to create a SiC interface which embeds in the pores near the interface. The elemental silicon also combines with oxygen near the coating surface; this tends to seal small cracks with SiO_2, thus producing a self healing effect [Kugeler, 1991] [Hurtado, 1994]. The use of elemental silicon may be disadvantageous for the reactor operating environment however.

In addition to cladding or component failure, the amount of hydrogen generation and energy release are also a concern in a nuclear reactor accident. According to equation 5.8, 3 moles of hydrogen gas and 229 Joules are released for every mole of SiC reacted. Equation 5.11 shows that 2 moles of hydrogen and 645,569 Joules are released for every mole of Zr reacted. Table 5-3 and Figure 5-7 show the relative energy release for the oxidation of SiC and zircaloy in the 1000°C steam environment. Table 5-4 and Figure 5-8 show the relative hydrogen gas release for the LOCA test environment. SiC oxidation clearly releases less hydrogen and energy than zircaloy oxidation. This result could help to mitigate the consequences of a reactor accident. However, it must be noted that other metallic core structural material will also oxidize rapidly at these temperatures, releasing large quantities of energy. The elimination of zircaloy cladding improves the situation, but the problem may still exist to some extent, depending on accident progression.

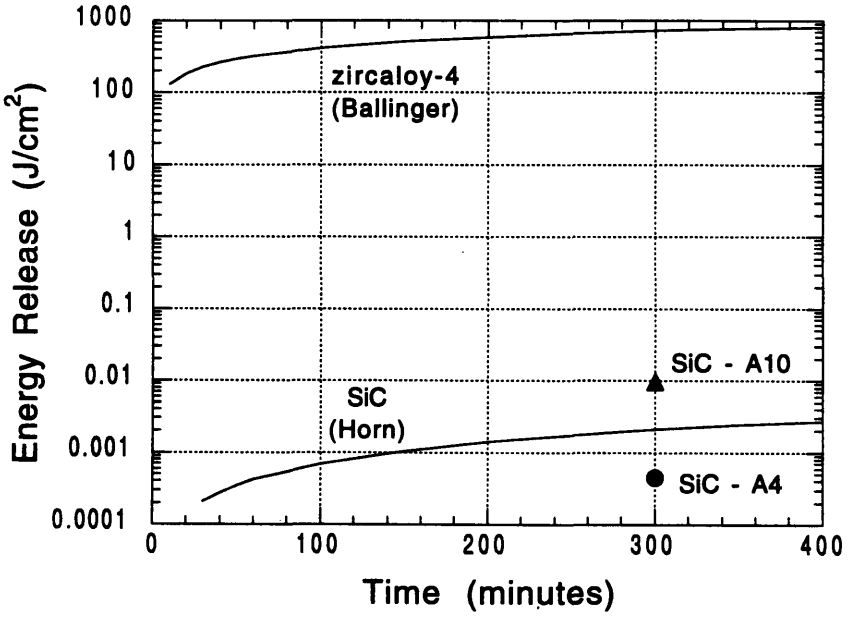

Figure 5-7: Energy Release of Zr and SiC for LOCA Environment

Table 5-3: Energy Release of Zr and SiC for LOCA Environment

Time (mins)	J/cm^2* Zr	J/cm^2 SiC (Horn)	J/cm^2 SiC (A10)	J/cm^2 SiC (A4)
60	322.8	0.418×10^{-3}		
120	456.5	0.835×10^{-3}		
180	559.1	1.253×10^{-3}		
240	645.6	1.671×10^{-3}		
300	721.8	2.088×10^{-3}	9.734×10^{-3}	0.454×10^{-3}
360	790.7	2.506×10^{-3}		
400	833.5	2.784×10^{-3}		

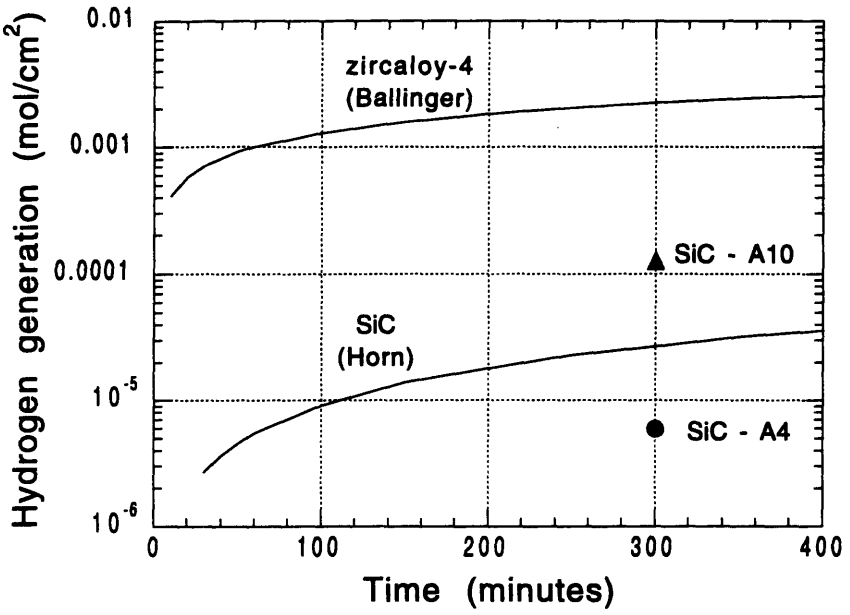

Figure 5-8: Hydrogen Release of Zr and SiC for LOCA Environment

Table 5-4: Hydrogen Release of Zr and SiC for LOCA Environment

Time (mins)	mol H_2/cm^2* Zr (Ballinger)	mol H_2/cm^2 SiC (Horn)	mol H_2/cm^2 SiC (A10)	mol H_2/cm^2 SiC (A4)
60	1.00×10^{-3}	0.55×10^{-5}		
120	1.41×10^{-3}	1.10×10^{-5}		
180	1.73×10^{-3}	1.60×10^{-5}		
240	2.00×10^{-3}	2.20×10^{-5}		
300	2.24×10^{-3}	2.70×10^{-5}	12.7×10^{-5}	0.59×10^{-5}
360	2.45×10^{-3}	3.30×10^{-5}		
400	2.58×10^{-3}	3.60×10^{-5}		

* Calculated using data from Ballinger [Ballinger, 1976].

Based on the results of the experiments reported here and the findings of other researchers, SiC coatings (or structural materials) offer excellent corrosion protection in high temperature steam which is typical of postulated reactor accident environments. Even the deterioration which accompanies small defects can be overcome in most cases, or can be considered adequate protection compared to the rapid corrosion of zircaloy in the same high temperature environment. The PERMA-KOTE process developed by Toyo Tanso USA produced coatings that showed superior performance in almost all cases.

5.4 Analysis Summary

Section 5.1 presented an overview of the data from the experiments performed and compared this data to the known performance of zircaloy for the same test conditions. Section 5.2 and 5.3 discussed the implications for the use of SiC in the reactor operating environment and the accident environment, respectively. Based on the reactor operating and the LOCA tests performed here, the use of SiC as a coating for oxidation protection of graphite or other structural materials shows promise. The potential can best be illustrated by Figures 5-1 and 5-3 which compare the corrosion of SiC to that of zircaloy for both reactor operating environments and LOCA environments.

Obviously the research conducted here does not encompass all of the variables that must be accounted for when evaluating a material for nuclear applications. However, based on this limited analysis, the potential benefits of SiC should be studied more closely in the future. SiC coatings have been studied extensively for use in the high temperature gas cooled reactor, but studies are very limited for SiC coating use in normal light water reactors.

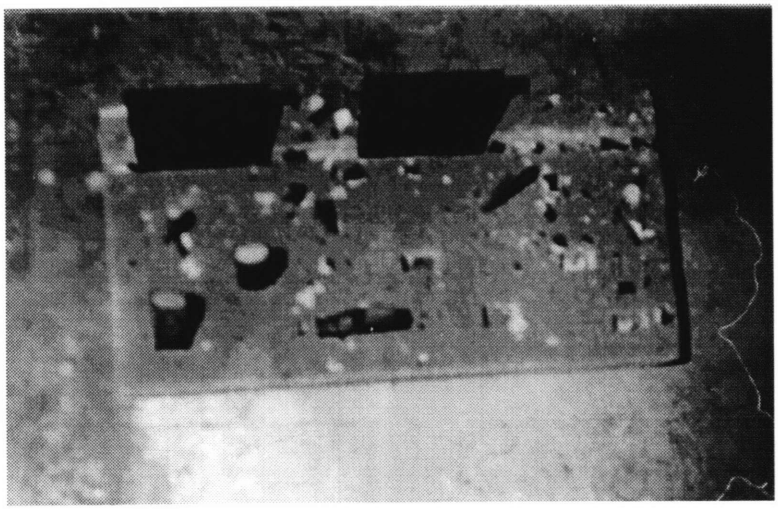

Photo 1: Picture 1 of Specimens Following LOCA Test #9. Fragments of the SiC Coating from Specimen A12 are Visible.

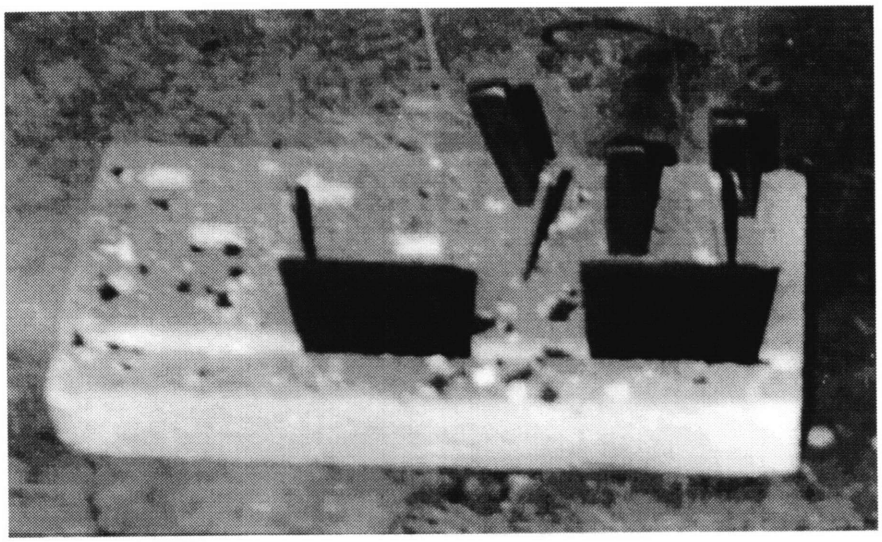

Photo 2: Picture 2 of Specimens Following LOCA Test #9. Fragments of the SiC Coating from Specimen A12 are Visible.

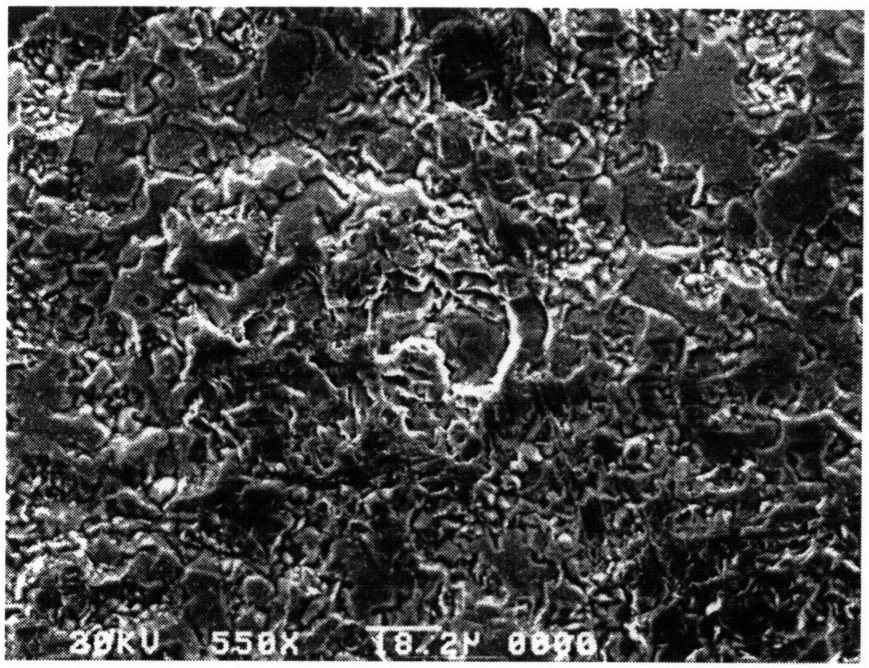

Photo 3: Electron Micrograph (550x) of the PERMA-KOTE SiC Coating of an As-Received Specimen

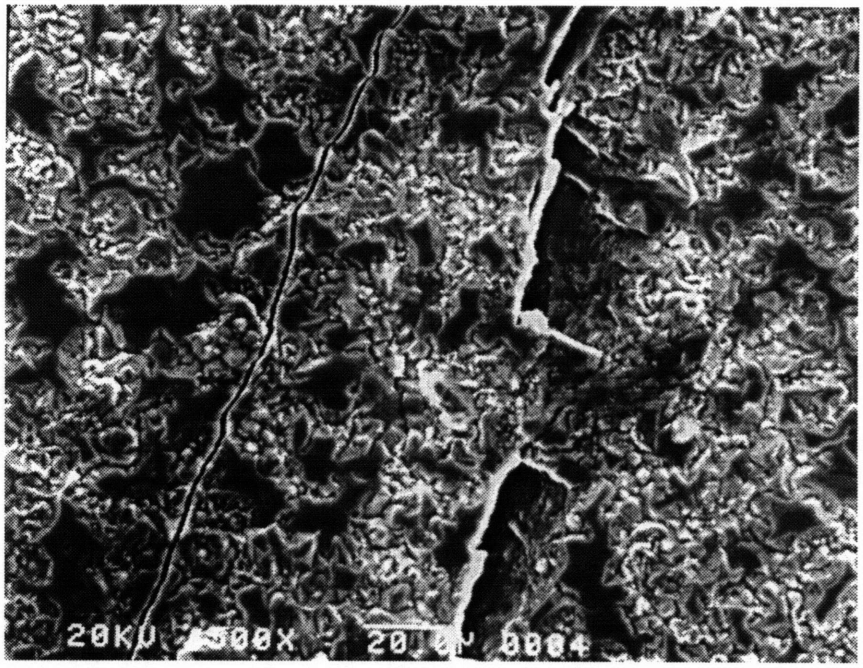

Photo 4: Electron Micrograph (500x) of Cracks in a PERMA-KOTE SiC Coating after a LOCA Test and Water Quench Test

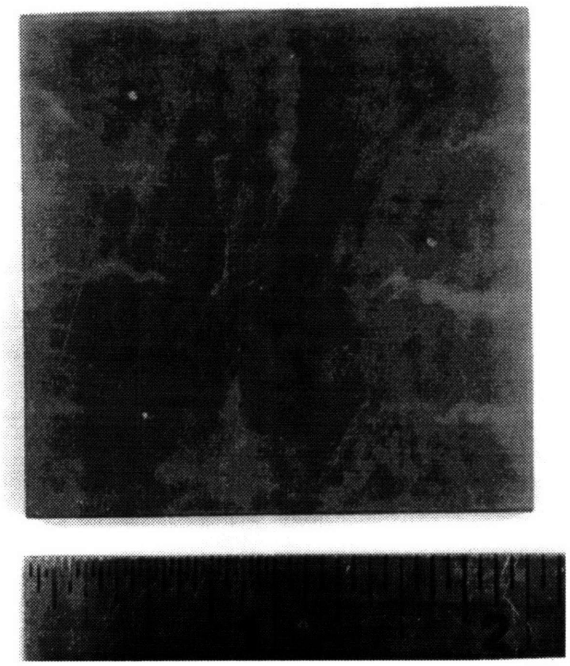

Photo 5: Picture of a PERMA-KOTE SiC Coated Specimen after being Subjected to a LOCA Test, Water Quench Test, and a Second LOCA Test

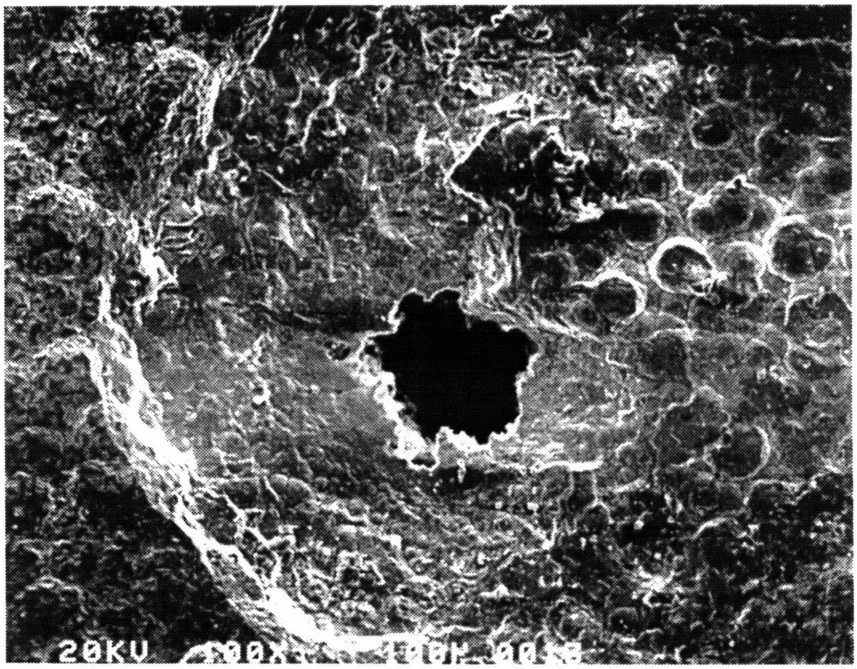

Photo 6: Electron Micrograph (100x) of a Small Hole in the PERMA-KOTE SiC Coating of Specimen A11 taken after the Operating and LOCA Tests

6. SUMMARY AND FUTURE WORK

6.1 Wet Calandria Working Design

Five alternative fuel configurations inside the channels of the wet calandria variant of the passive pressure tube reactor have been proposed and evaluated. (Two in this thesis and three previously by Tang). The options include one bundle-type arrangement in a two-ring geometry, one arrangement with six mini-bundles surrounded by a graphite structure, and three matrix-type fuel designs. Key factors in the areas of reactor physics, thermal hydraulics during normal operation and during loss of coolant accidents, and materials compatibility affecting fuel design were identified, and the design performance was evaluated against these factors.

For loss of coolant accidents, the bundle-type fuel configurations (WC-4, WC-5) provide a less efficient heat transfer dissipation mechanism compared to a matrix-type fuel. Calculations show that the temperatures reached during a LOCA are above tolerable limits for zircaloy cladding. The WC-5 design performs nicely when silicon carbide cladding is employed, and the WC-4 design should also prove acceptable when using silicon carbide cladding.

Design WC-5 was selected as the most promising working design for the wet calandria variant of the PTLWR. The primary motivation for this choice is the extensive experience with this geometric fuel arrangement in the CANDU. This is based on currently available technology, and the anticipated performance of the silicon carbide coating for the graphite slug which has been tested as part of this thesis. More research and development in this area is needed, however, to confirm the issues of economical production, and coating behavior after irradiation and mechanical damage in a reactor environment. Further research is also warranted on the SiC cladding technology to reduce the damage caused by pellet-clad interaction, and thus allow increased fuel burnups.

6.2 Relative Performance of SiC and Zircaloy

Based on the tests performed here, the use of SiC as a coating for oxidation protection of graphite or other structural materials shows promise. The potential can best be illustrated by Figures 5-2 and 5-3 which compare the corrosion of SiC to that of zircaloy for both the reactor operating environment and LOCA environment. Several problems associated with small defects in the coating caused by thermal shock or process imperfections have been

identified and their effects are significant. The PERMA-KOTE SiC coating technology developed by Toyo Tanso USA, Inc. produced a coating which provided excellent protection in the high temperature steam environment of a LOCA. This coating suffered microcracking after being quenched from 1000°C, but subsequent testing in a LOCA environment showed that these small defects did not seriously hamper the ability of the SiC coating to provide good oxidation protection for the underlying graphite.

Several problems associated with SiC use in normal reactor operating environments were identified. The problems with incompatible water chemistry and small defects which allow water ingress were discussed and possible solutions were presented.

6.3 Future Work

The research conducted here does not encompass all of the variables that must be accounted for when evaluating a material for nuclear applications. However, based on this limited analysis, the potential benefits of SiC should be studied in more detail. SiC coatings have been studied extensively for use in high temperature gas cooled reactors, but studies are very limited for SiC coating use in normal light water reactors.

Specific areas for future research are the problems associated with extremely small and extremely large coating defects. Small defects can result in spalling during a rapid heat-up if there is water trapped under the coating which infiltrated through a defect that is too small to allow the flashing water to escape. Large coating defects essentially remove a section of the coating that results in the complete loss of protection. Large coating defects most probably will be caused by rough handling of the material once inside the reactor plant by refueling machines or mishaps during transportation. The reduction of both small and large defects can be reduced by producing a coating that is very tightly coupled to the underlying graphite, and which is sufficiently thick to allow some degradation of the outer layers. The most promising coating process evident to date is the one developed by Hurtado et. al. [Hurtado, 1994] which uses a special slip coating method to create a coating which infiltrates the graphite substrate sufficiently to effect a gradual transition between physical properties. This coating also contains elemental silicon which causes a self-healing mechanism for small defects.

An obvious extension of this research would be the testing of actual size specimens in realistic conditions. This would include increasing the temperature of the LOCA test to 1300°C and increasing the water velocity in the reactor operating test to ~10 m/s. The effect of irradiation is a major variable which is not explored in this thesis, but which has been explored for the use of SiC in the high temperature gas cooled reactor. Regardless of

previous analyses, the effects of irradiation need to be examined for the exact coating process, geometry, and water environment to be used. Finally, the process for coating the full size graphite geometry must be perfected to produce the desired results. From the background information available from industry, it should be possible to overcome this stumbling block.

A simple resolution to the coating problems is to use a solid SiC structure. This option has been employed in this thesis for the cladding, essentially replacing normal zircaloy-4 cladding with SiC cladding. SiC cladding has been evaluated previously, but for only moderate burnups. Stresses caused by pellet clad interaction are problematic and more research is needed to resolve this issue [Kennedy, 1974]. The use of solid SiC structures and matrices for the PTLWR was considered, but the nuclear absorption cross section of silicon is sufficiently high to warrant attempts to perfect the SiC coating of graphite before this option is chosen [Hejzlar, 1993].

REFERENCES

ADINA R&D, Inc., A finite element program for automatic dynamic incremental nonlinear analysis. ADINA-T Users Manual. Watertown, MA.

Almarshad, A.I.A., Klein, A.C., "A Model for Waterside Oxidation of Zircaloy Fuel Cladding in Pressurized Water Reactors," Journal of Nuclear Materials, vol. 183 (1991), pp. 186-194.

Ballinger, R.G., Dobson, W.G., Biederman, R.R., "Oxidation Reaction Kinetics of Zircaloy-4 in an Unlimited Steam Environment," Journal of Nuclear Materials, vol. 62, (1976), pp. 213-220.

Burrill, K.A., Shaddick, A., "Water Chemistry and the Deposition of Corrosion Products on Nuclear Reactor Fuel: A Summary of Experimental Results," AECL-6952, May 1980.

Burrill, K.A., "Corrosion Product Transport in Water-Cooled Nuclear Reactors Part II: Boiling Water with Direct Cycle Operation," Canadian Journal of Chemical Engineering, vol. 56 (1978), pp. 79-86.

Clinard, F.W., Hurley, G.F., Hobbs, L.W., Rohr, D.L., Youngman, R.A., "Structural Performance of Ceramics in a High-Fluence Fusion Environment," Los Alamos National Laboratory Report LA-UR-83-2742, 1983.

Cohen, P., editor, The ASME Handbook on Water Technology for Thermal Power Systems, American Society of Mechanical Engineers, 1989.

Eto, M., Shindo, M., "Development of Advanced Graphite Materials for Nuclear Facilities," International Conference on Design and Safety of Advanced Nuclear Power Plants, Tokyo, October 1992.

Fujii, K., Nakano, J., Shindo, M., "Improvement of the oxidation resistance of a graphite material by compositionally gradient SiC/C layer," Journal of Nuclear Materials, vol. 203 (1993), pp. 10-16.

Fujii, K., Imai, H., Nomura., S., Shindo, M., "Functionally Gradient Material of Silicon Carbide and Carbon as Advanced Oxidation-Resistant Graphite," Journal of Nuclear Materials, vol. 187 (1992) pp. 204-208.

Heitmann, H.G., Handbook of Power Plant Chemistry, CRC Press, Inc., 1993.

Hejzlar, P. "Conceptual Design of a Passive Pressure Tube Light Water Reactor (PTLWR)," Sc.D. Thesis, Nuclear Engineering Department, Massachusetts Institute of Technology, May 1994.
Also published as: MIT Report Number MIT-ANP-TR-023, U.S. Department of Energy Report DOE/ER/75785-4, June 1994.

Hejzlar, P., Todreas, N.E., Driscoll, M.J., "Evaluation of Materials for the Fuel Matrix of a Passive Pressure Tube LWR Concept," MIT Report MIT-ANP-TR-017, U.S. Department of Energy Report DOE/ER/75785-2, December 1993.

Hejzlar, P., Todreas, N.E., Driscoll, M.J., "Passive Decay Heat Removal in Advanced Reactor Concepts," Massachusetts Institute of Technology Report MIT-ANP-TR-003, May 1991.
Also published as : "Passive Decay Heat Removal in Advanced LWR Concepts", Nuclear Engineering and Design, vol. 139 (1993), 59-81.

Hirayama, H., Kawakubo, T., Goto, A., "Corrosion Behavior of Silicon Carbide in 290°C Water," Journal of the American Ceramics Society, vol. 72 (1989), pp. 2049-53.

Horn, F.L., Fillo, J.A., Powell, J.R., "Performance of Ceramic Materials in High Temperature Steam and Hydrogen," Journal of Nuclear Materials, vol. 85 & 86 (1979) pp. 439-443.

Hurtado, A.M., Alkan, Z., Mein, P., "Coating Method for Innovative Graphitic Components with High Corrosion Resistance," Proceedings, Second International Conference on Ceramics in Energy Applications, Institute of Energy Conference, London, April, 1994.

Hurtado, A.M., Mein, P., Alkan, Z., "Development of a High-Temperature Resistant C/SiSiC Compound," Extended abstracts and programme, CARBON '94, Spanish Carbon Group, Granada, July, 1994.

Kennedy, P., Shennan, J.V., "REFEL Silicon Carbide, The Development of a Ceramic for a Nuclear Engineering Application," TRG report 2627(S), October 1974.

Kugeler, A. Hurtado, A., Schröder, B., "Research on the Development of Coated Fuel Elements for High Temperature Reactors," Transactions of the 11th International Conference on Structural Mechanics in Reactor Technology (SMiRT) vol. SD2, Tokyo, August 1991, pp. 399-404.

Leistikow, S., "Comparison of High-Temperature Steam Oxidation Kinetics Under LWR Accident Conditions: Zircaloy-4 Versus Austenitic Stainless Steel No. 1.4970," *Zirconium in the Nuclear Industry: Sixth International Symposium, ASTM STP 824*, D.G. Franklin and R.B. Adamson, Eds., American Society for Testing and Materials, 1984, pp. 763-779.

Madhusudana, C.V., "Thermal Contact Conductance and Rectification at Low Joint Pressures," Int. Comm. Heat Mass Transfer, vol. 20, no. 1, (1993) pp. 123-132.

Mattingly, B.T., Hejzlar, P., Todreas, N.E., Driscoll, M.J., "Fuel Matrices for the Passive Pressure Tube Light Water Reactor", MIT Report MIT-ANP-TR-031, Massachusetts Institute of Technology, June 1995.

Novak, J.P., "Conception and Experimental Investigation of Passive Thermal Switches," S.M. Thesis, Department of Nuclear Engineering, Massachusetts Institute of Technology, June 1995.

Peters, H.R., "Improved Characterization of Aqueous Corrosion Kinetics of Zircaloy-4," *Zirconium in the Nuclear Industry: Sixth International Symposium, ASTM STP 824*, D.G. Franklin and R.B. Adamson, Eds., American Society for Testing and Materials, 1984, pp. 507-518.

Roshd, M.H.M., French, P.M., Jones, R.T., "Nuclear Fuel Bundle Design with Reduced Void Effect," Transactions, American Nuclear Society, vol. 26 (1977), pp. 603-604.

Sabol, G.P., Comstock, R.J., Weiner, R.A., Larouere, P., Stanutz, R.N., "In-Reactor Corrosion Performance of ZIRLO™ and Zircaloy-4," *Zirconium in the Nuclear Industry: Tenth International Symposium, ASTM STP 1245*, A.M. Garde and E.R. Bradley, Eds., American Society for Testing and Materials, 1994, pp. 724-744.

Schulten, R., "The HTR with SiC-technology," Nuclear Engineering and Design, vol. 140 (1993), pp. 261-267.

Shapiro, N.L., Jesick, J.F., "Conceptual Design of a Large Heavy Water Reactor for U.S. Siting," Combustion Engineering Report CEND-379, September 1979.

Strife, J.R., Sheehan, J.E., "Ceramic Coatings for Carbon-Carbon Composites," American Ceramics Society Bulletin vol. 67, no. 2, (1988), pp. 369-374.

Tang, J.R., "Conceptual Design of the Passive Light Water Cooled and Moderated Pressure Tube Reactor (PLPTR)," Sc.D. Thesis, Nuclear Engineering Department, Massachusetts Institute of Technology, May 1992.
Also published as : MIT Report MIT-ANP-TR-013, August 1992.

Tang, J.R., Todreas, N.E., Driscoll, M.J., "Conceptual Design Features for a Passive Light Water Cooled and Moderated Pressure Tube Reactor (PLPTR)," Nuclear Technology, vol. 107, (1994), pp. 49.

Todreas, N.E., Kazimi, M.S., Nuclear Systems I, Thermal Hydraulic Fundamentals, 1st ed., Hemisphere Publishing, 1990.

Urbanic, V.F., Heidrick, T.R., "High-Temperature Oxidation of Zircaloy-2 and Zircaloy-4 in Steam," Journal of Nuclear Materials, vol. 75 (1978), pp. 251-261.

Williamson, M., Majumdar, A., "Effect of Surface Deformations on Contact Conductance," Journal of Heat Transfer, vol. 114, (1992) pp. 802-810.

APPENDICES

Appendix A. Raw Weight Measurement Data*

Table A-1: Test 1 Weight Data (5.5 hours in 1000°C Dry Air)

Specimen	Pre-test (grams)	Post-Test (grams)	Difference (grams)
A1	16.76	16.77	0.01
A2	16.73	16.73	0.00
A3	16.66	16.66	0.00
B1	8.41	8.41	0.00
B2	8.40	8.39	-0.01
B3	8.33	8.31	-0.02
C1	1.77	1.78	0.01
C2	1.82	1.83	0.01
C3	1.83	1.84	0.01
D1	7.26	0	-7.26
D2	7.23	0	-7.23
D3	7.21	0	-7.21

Table A-2: Test 2 Weight Data (5 hours in 1000°C Humid Air)

Specimen	Pre-test (grams)	Post-Test (grams)	Difference (grams)
A4	17.6338	17.6361	0.0023
A5	16.7143	16.7157	0.0014
A6	17.3426	17.3455	0.0029
B4	7.9996	7.9259	-0.0737
B5	7.7738	7.7733	-0.0005
B6	8.1746	8.1473	-0.0273
C4	1.7463	1.7455	-0.0008
C5	1.8411	1.8410	-0.0001
C6	1.8259	1.8257	-0.0002

* The scale used for weight measurements was manufactured by Denver Instrument Company. The scale was an XE Series, Model 100A.

Table A-3: Test 3 Weight Data (5 hours in 1000°C Humid N_2)

Specimen	Pre-test (grams)	Post-Test (grams)	Difference (grams)
A7	16.7547	16.7565	0.0018
A8	16.7675	16.7694	0.0019
A9	16.6059	16.6079	0.0020
B7	8.3045	8.3031	-0.0014
B8	7.3147	7.3140	-0.0007
B9	7.8548	7.8540	-0.0008
C7	1.8407	1.8397	-0.0010
C8	1.8373	1.8369	-0.0004
C9	1.7782	1.7775	-0.0007
D7	7.2189	6.7245	-0.4944
D8	7.2102	6.5379	-0.6723
D9	7.2069	6.5287	-0.6782

Table A-4: Test 5 Weight Data (5 hours in 1000°C Humid Air after quench)

Specimen	Pre-test (grams)	Post-Test (grams)	Difference (grams)
A2	16.8547	16.5343	-0.3204
A5	16.7844	16.4186	-0.3658
A8	16.7913	16.4986	-0.2927

Table A-5: Test 6 Weight Data (Virgin Graphite in Dry Air)

Test	Piece	Temp °C	Pre-Test (grams)	Post-Test (grams)	Difference (grams)
1	A	600	7.2254	7.1934	-0.0320
	B		7.2473	7.2339	-0.0134
2	A	650	7.2161	7.1658	-0.0503
	B		7.2456	7.1741	-0.0715
3	A	700	7.1857	6.7881	-0.3976
	B		7.2399	7.0103	-0.2296
4	A	750	7.1613	6.6475	-0.5138
	B		7.2492	6.9181	-0.3311
5	A	800	7.1905	6.2030	-0.9875
	B		7.2188	6.1218	-1.0970
6	A	850	7.2086	6.2276	-0.9810
	B		7.2050	6.1762	-1.0288
7	A	900	7.2073	6.1076	-1.0997
	B		7.2428	6.1801	-1.0627
8	A	950	7.2100	6.1474	-1.0626
	B		7.2445	6.2065	-1.0380

Table A-6:
Test 7 Weight Data (Coating Defect, 5 hours in 1000°C Humid Air)

Specimen	Pre-Test (grams)	Post-Test (grams)	Difference (grams)
A13	16.4736	14.0832	-2.3904

Table A-7: Test 8 Weight Data (500 hours in 300°C Water)

Specimen	Pre-test (grams)	Post-Test (grams)	Difference (grams)
A10	16.4600	16.4595	-0.0005
A11	16.6312	17.8328	1.2016
A12	16.8097	17.9055	1.0958
B10	8.4591	8.9348	0.4757
B11	7.4742	8.0985	0.6243
B12	7.3768	7.9780	0.6012
C10	1.8212	1.8210	-0.0002
C11	1.8474	1.8474	0.0000
C12	1.7611	1.7612	0.0001
D10	7.2509	7.8333	0.5824
D11	7.2334	7.6533	0.4199
D12	7.2465	7.5808	0.3343

Table A-8: Test 9 Weight Data (5 hours in 1000°C Humid Air after Test 8)

Specimen	Pre-test (grams)	Post-Test (grams)	Difference (grams)
A10	16.4602	16.5095	0.0493
A11	17.8302	16.6136	-1.2166
A12	17.9055	0	-17.9055
B10	8.8667	5.8367	-3.0300
B11	8.0635	7.2264	-0.8371
B12	7.9780	4.3874	-3.5906
C10	1.8210	1.8210	0.0000
C11	1.8473	1.8476	0.0003
C12	1.7612	1.7613	0.0001

Appendix B. Overview of the Passive Pressure Tube LWR

B.1 Overall Design Philosophy

To further enhance the passive safety features of light water reactors, new approaches have been explored which would allow the reactor to withstand the total loss of primary coolant without core damage. Various options for passive decay heat removal from a voided reactor core have been investigated with the concurrent goal of achieving a high reactor power rating during normal operation. As a result, a pressure tube geometry with a solid matrix was identified as the most promising configuration [Hejzlar, 1991]. The feasibility of such a design was evaluated primarily from the point of view of decay heat removal from the fuel to the pressure tube boundary. Further development of this concept resulted in the Passive Pressure Tube Light Water Reactor (PTLWR). The major goals of the PTLWR are listed in table B-1.

Table B-1: Goals for the Passive Pressure Tube Light Water Reactor

• Survive loss of primary coolant with no core damage
• Prevent fast reactivity excursions
• Operate at a high power rating
• Achieve inherent reactor shutdown during accidents
• Minimize technological and economic risk
• Produce electricity at a competitive cost

The PTLWR was designed using the CE-CANDU [Shapiro, 1979] study as the reference point. The CE-CANDU was a Combustion Engineering conceptual design of a large heavy water reactor specifically developed for siting in the United States. The reactor is similar to the Canadian heavy water reactors (CANDU) in many ways with only slight changes made in design specifications and some systems to accommodate the U.S. manufacturing and regulatory standards.

The PTLWR uses the CE-CANDU as a reference design, and any changes are measured relative to the CE-CANDU performance. The basic philosophy adhered to in the PTLWR is to keep all of the ex-core systems exactly the same as in the CE design. The largest innovation in the PTLWR is in the core layout and materials selection. Two of the

most obvious changes are that the PTLWR has a calandria tank filled with gas (CO_2 or N_2) and uses light water as the coolant. The PTLWR core has 740 pressure tubes, each surrounded by a thin calandria tube (same as CE-CANDU), but the fuel arrangement inside the pressure tube is radically different from current pressure tube reactors, due in part to the use of light water coolant. The fuel configurations and materials were developed with primary emphasis placed on:

- achieving a minimum total plant power output of 1000 MWe during normal operation;
- storing appreciable decay heat during initial heat up in an accident; and
- transferring the decay heat from the fuel to the pressure tube surface in the absence of primary coolant without exceeding fuel, clad, or pressure tube thermal limits.

Except for the fuel modularity, which is achieved by using pressure tubes dispersed in a heat sink, all other changes apply to the fuel bundle itself. Thus the fuel matrix is a critical component of the proposed design which deserves special attention.

B.2 Wet and Dry Calandria Form and Function

Two fundamentally different schemes were developed to remove decay heat from the core during a loss of coolant accident. Both designs incorporate the previously mentioned voided calandria. The first design removes decay heat from the core by flooding the calandria with water. This results in boiling of the flooding water and in transferring the decay heat by the steam to the containment. The flooding water also introduces sufficient neutron capture into the core to result in reactor shutdown even if no other shutdown mechanisms were previously initiated. This design is designated the **Dry Calandria** because the calandria tube is maintained dry during normal operation.

The second design utilizes a thin water annulus outside the calandria tube. This is accomplished by the addition of another tube surrounding the calandria tube. This water annulus is part of a separate low pressure moderator system which, during a loss of coolant accident, acts as a heat sink. This design is designated the **Wet Calandria** because the calandria tube is maintained wet during normal operation. Both the wet and dry calandria reactor designs have been developed in detail in earlier reports and will only be summarized here.

A schematic of the dry calandria design is shown in Figure B-1. This design is developed in detail by Hejzlar [Hejzlar, 1994]. The pressure tube employs a solid matrix within which fuel and coolant can be arranged in a variety of ways. The fuel matrix shown

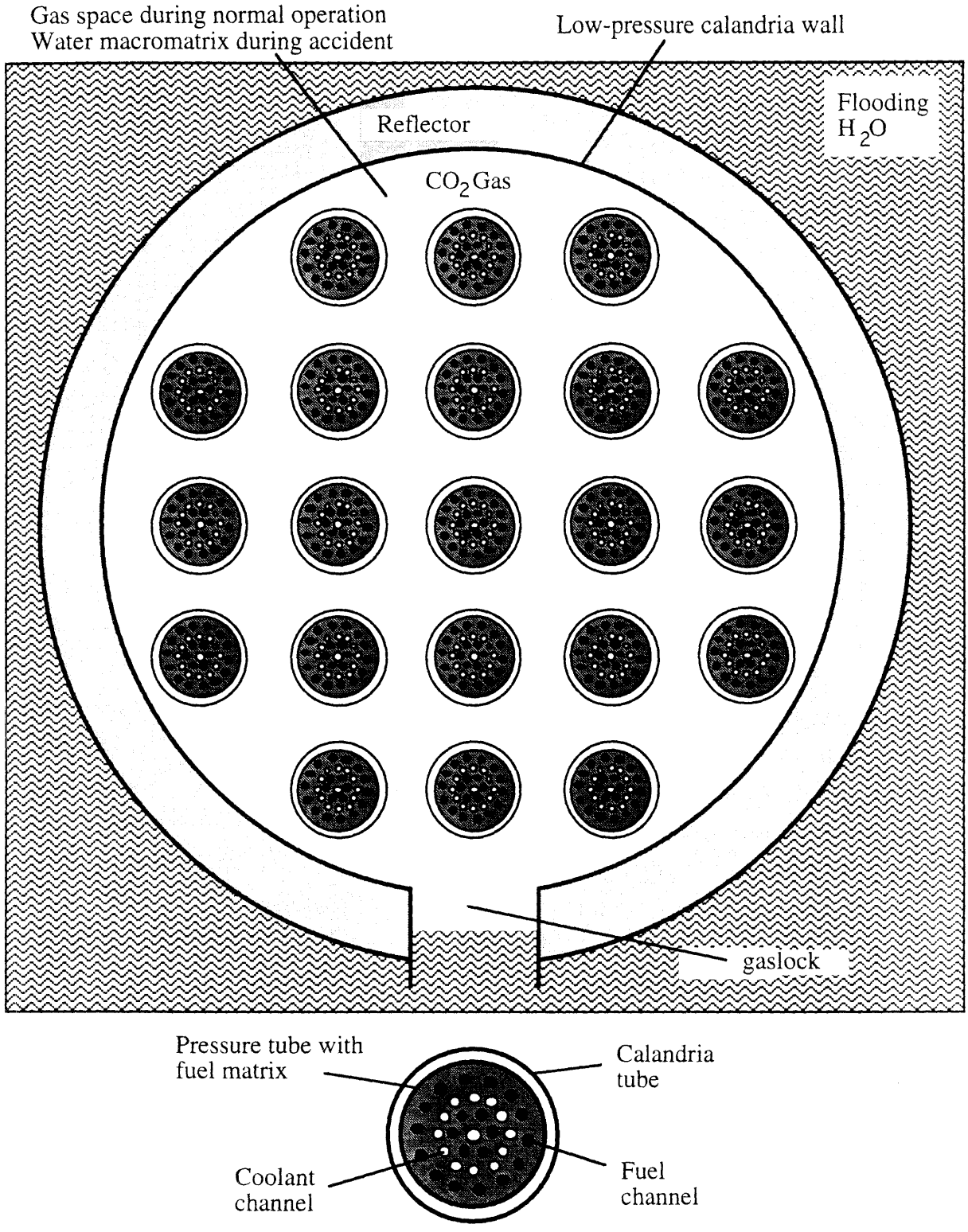

Figure B-1: Dry Calandria Design Configuration

here is only one of several possible designs that have been developed. A calandria surrounded by a solid neutron reflector is submerged in a tank of light water which serves to both cool the reflector and act as a biological shield. The tank and the calandria are both submerged in a large amount of in-containment water. During normal operation this water is kept out of the calandria space by a gas lock. The gas pressure is maintained sufficient to balance the water column outside the calandria. Any disturbance in the primary cooling system (such as loss of coolant or heat sink) beyond the pre-defined envelope of safety limits results in the flooding of the entire calandria space. The flood water serves as an effective heat sink, which transfers the decay heat from the submerged calandria tubes, by boiling/condensing, to the containment walls.

A schematic of the wet calandria design is shown in Figure B-2. This design has been developed in detail by Tang [Tang, 1992]. The pressure tube can again employ a solid matrix with varying configurations of fuel and coolant. The fuel design shown in Figure B-2 is a two-ring design which is only one of the possibilities. The pressure tube is surrounded by a calandria tube, which in turn is enclosed by a light water moderator annulus confined by an outer moderator tube. The gap between the calandria tube and the pressure tube may be equipped with a thermal switch. The thermal switch is a device specifically designed to have an increasing thermal conductivity with increasing temperature. During normal operation the thermal switch conducts a relatively small amount of heat from the pressure tube to the moderator tube. During a LOCA, when the pressure tube temperature is considerably higher, the conductivity of the thermal switch increases substantially to remove a much larger amount of heat from the pressure tube. Two thermal switch designs are presented in Tang [Tang, 1992]. Additional thermal switch designs have been developed and experimentally tested by Novak [Novak, 1995]. An alternative to a complex thermal switch is to tailor the gap conductivity to remove the appropriate amount of energy on a continuous basis. The moderator system is designed to be capable of transferring the desired level of decay heat to the ultimate heat sink by natural circulation during accidents, but can also be tailored to provide heat to a chain of feedwater heaters during normal operation, thus reducing the amount of heat lost. Note that in current CANDU designs all moderator heat (~5% of total from fission) is discarded.

There are some inherent advantages and disadvantages associated with each of these designs. The dry calandria design has inherent shutdown provided by the flooding water regardless of whether other scram systems have caused reactor shutdown. The flooding system is also simple to develop and maintain. However, the critical component of the system is the valve or other mechanism that activates to initiate the flooding process.

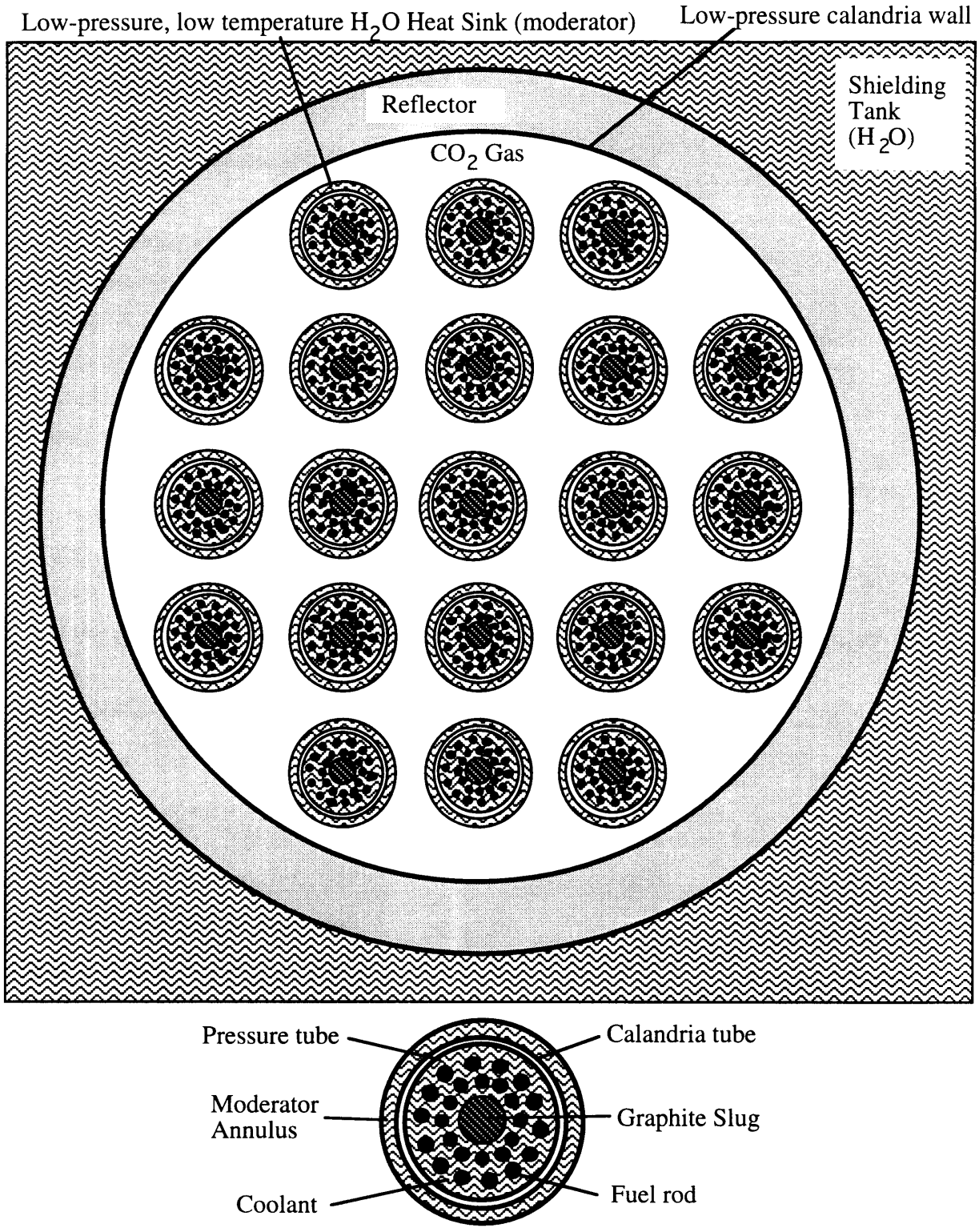

Figure B-2: Wet Calandria Design Configuration

Failure of this redundant/diverse system can cause failure of the decay heat removal process. During normal operation the calandria tubes in the dry design are at a relatively uniform high temperature which helps to reduce the buildup and localization of zirconium hydrides, which cause tube embrittlement.

The wet calandria design benefits from the presence of decay heat removal water at all times, in the moderator annulus outside the calandria tube. Thus there is no need for the flooding system and the vulnerability to operation of the flood initiating valve. (Flooding can also be used in this design as an added safety measure.) This added water annulus significantly increases the moderating capability and allows for a heavier fuel loading in the core. The increased fuel loading causes a decrease in the fast flux and consequently reduces neutron damage to the pressure tubes. However, the present configuration of this low pressure moderating system is vulnerable to failure if it suffers a pipe break, especially since the system removes heat via a natural convection circulation loop.

The factors mentioned above are the primary determinants of whether to use a wet calandria or a dry calandria design. Table B-2 summarizes the points mentioned above.

Table B-2: Advantages and Disadvantages of Wet and Dry Calandria Variants

	Dry Calandria	*Wet Calandria*
Advantages	Flooding provides inherent shutdown High, uniform tube temp reduces localization of Zirc-hydrides Simple ultimate heat sink system	Decay heat sink always present More moderating water, allows higher fuel loading Flooding is optional, not required
Disadvantages	Must initiate flooding with some action	Decay heat system is complex and vulnerable to failure Thermal switch may be complex and costly

The fuel configurations for the wet calandria (WC) and dry calandria (DC) reactors depend on which variant they are to be used in. The basic reason for the split between WC and DC fuel configurations is the neutron physics of the fuel: undermoderation is required to insure negative coolant temperature and void coefficients. The dry calandria has a limited amount of water present for neutron moderation and therefore can not support a large fuel loading based upon criticality requirements. However, the low fuel loading achieved with the TRISO particles does not require more moderation than is provided by

the coolant water in the channel in order to operate at the optimum moderator/fuel ratio. (TRISO particle fuel also provides superior thermal performance during a LOCA.) This low fuel loading results in a high neutron fluence. To reduce the fluence, a higher fuel loading (achieved by using UO_2 fuel pins) can be used, which in turn requires a substantial addition of moderator outside the fuel channel to operate at the optimum moderator/fuel ratio. This increase in the amount of moderator can be provided in the dry calandria design by using additional pressure tubes in the lattice which only carry water. On the other hand, the wet calandria design provides this increase in moderator by the water annulus surrounding the pressure tube. In general all of the WC fuel matrix designs developed by Tang [Tang, 1992] or in chapter 3 can operate in either the wet or dry calandria configurations (based on the neutron physics), but the same is NOT true for all of the DC fuel matrices designed by Hejzlar [Hejzlar, 1994]. However, the optimum performance of the WC matrices can only be achieved by operating these matrices in the presence of sufficient moderator.

For an overview of all fuel designs, see [Mattingly, 1995]. Hejzlar developed the dry calandria variant in detail [Hejzlar, 1994]. Tang developed the wet calandria variant in detail [Tang, 1992]. The next few pages give the fuel designs studied for the PTLWR.

Fuel Arrangement WC-1

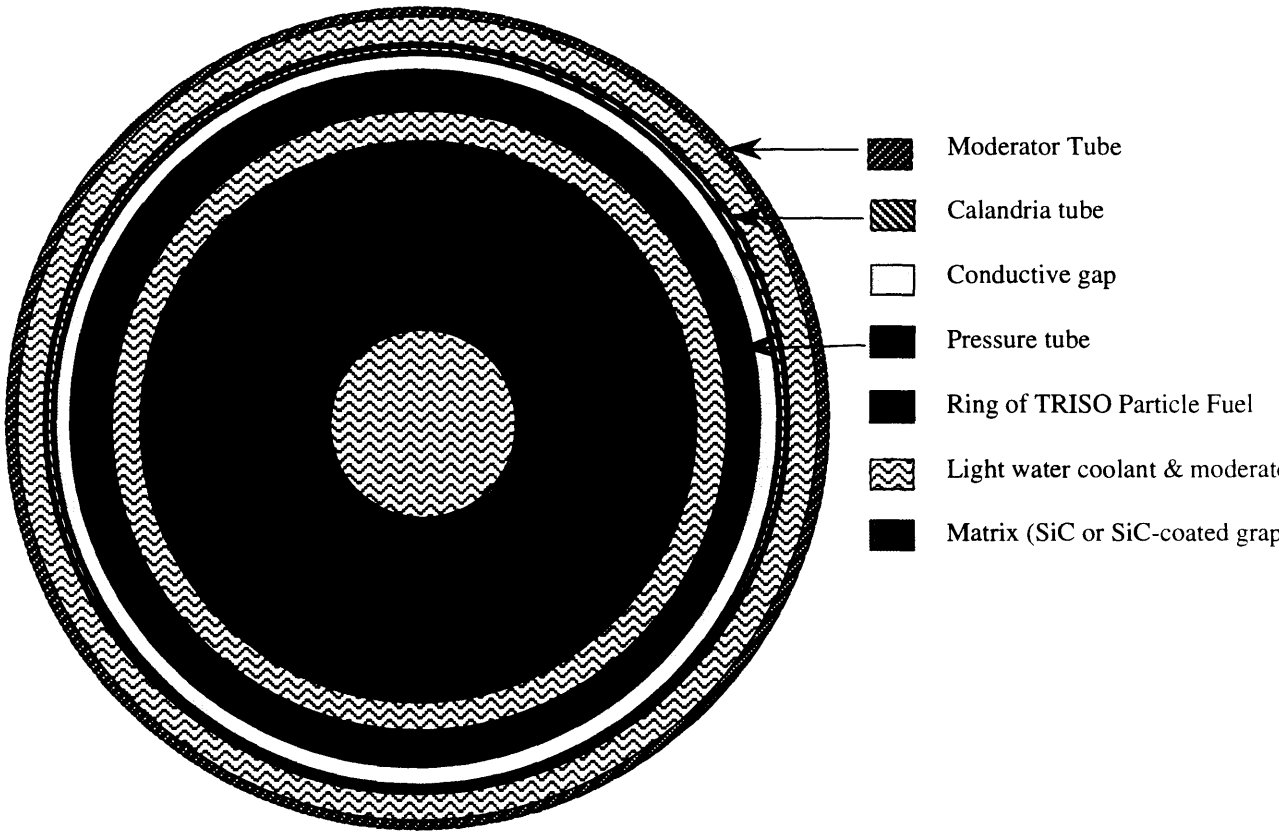

Advantages	Disadvantages
• Uses high conductivity TRISO fuel	• Small heat transfer area
• Matrix takes most of the mechanical loading	• High fuel temperature during normal operation
• No water contacting particle	• Long conduction path between fuel centerline and coolant
• Annular cooling improves heat transfer	

Figure B-3 (from Tang)
WC-1, Graphite Matrix with an Annular TRISO Fuel Ring

Fuel Arrangement WC-2

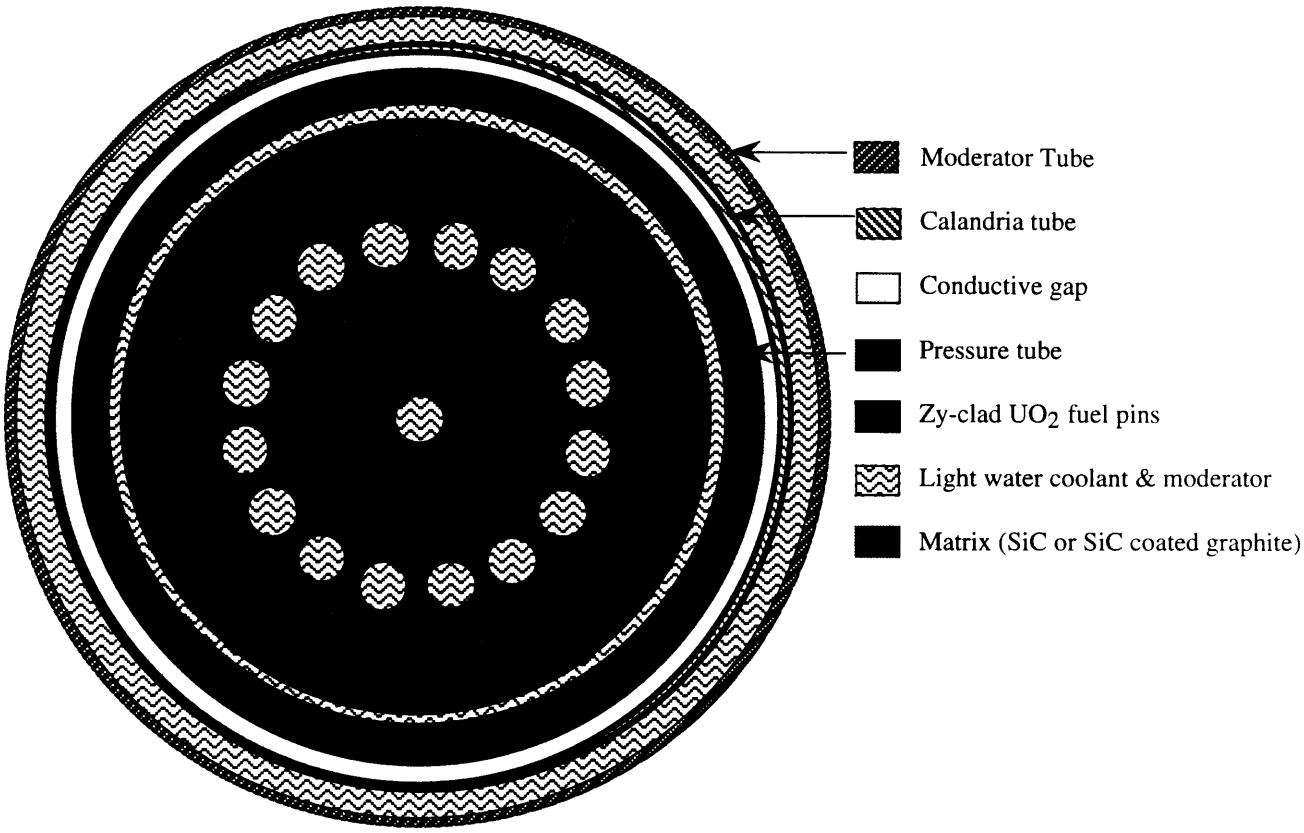

Advantages	Disadvantages
• Uses easily attainable UO_2 fuel pins and Zircaloy cladding	• Low conductivity of fuel along with long conduction path through graphite lead to a high centerline temperature of 2660°C during normal operation
• Matrix takes most of the mechanical loading	• High cladding temperature of 835 °C during normal operation
•No water contacting cladding material	• Difficult to maintain good contact conductance between the Zy cladding and the matrix
	• Small heated perimeter, thus difficult to provide sufficient cooling during normal operation

Figure B-4 (from Tang)
WC-2, Graphite Matrix with Zircaloy-Clad UO_2 Fuel Pins

Fuel Arrangement WC-3

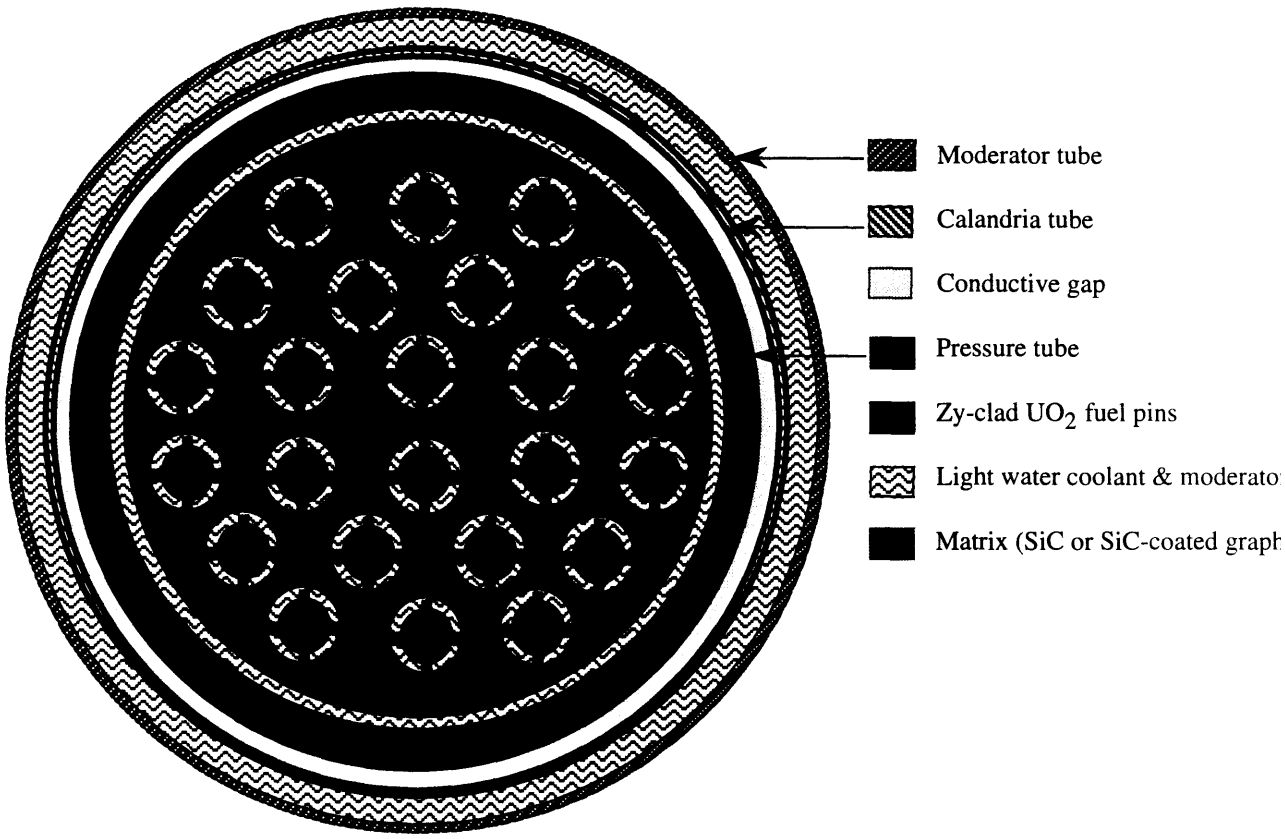

Advantages	Disadvantages
• Uses standard UO_2 fuel pins and Zircaloy cladding	• Small web thickness, stress becomes a critical concern
• Fuel maximum temperature of 1960 °C and clad maximum temperature of 385 °C are both within CANDU experience	• Difficult to manufacture precise fit of fuel into coolant hole
• Heat passes directly from fuel to coolant in normal operation, but conducts through graphite in accident conditions	• Contact resistance between pin cladding and matrix lands can not be well bounded
	• Crevice assisted corrosion between the pins and matrix may become a problem

Figure B-5 (from Tang)
WC-3, Graphite Matrix with UO_2 Fuel in Coolant Channels

Fuel Arrangement WC-4, 36 Pins

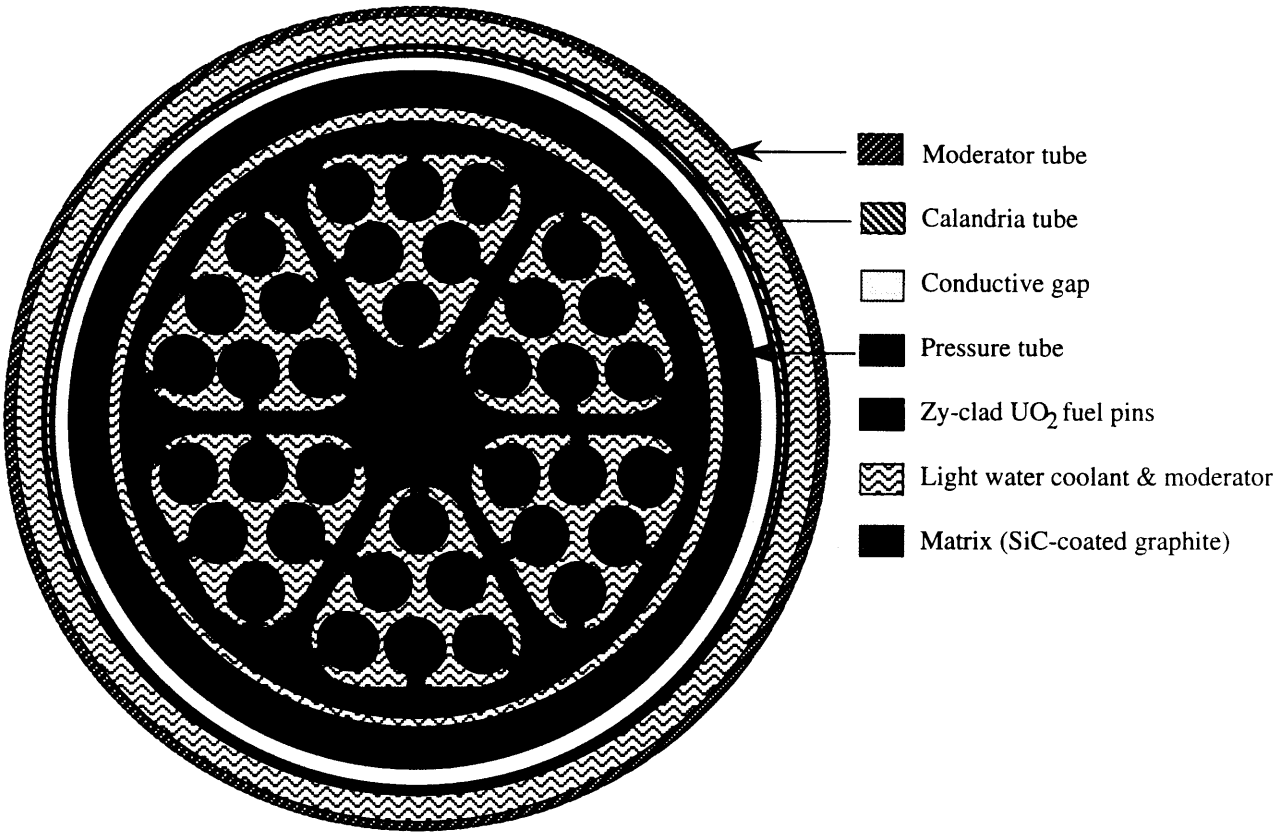

Advantages	Disadvantages
• Uses standard UO_2 fuel pins and Zircaloy cladding	• Relies on contact between pins and matrix at all times to insure satisfactory thermal performance in an accident (spring needed)
• Direct contact between fuel and coolant, no conduction through graphite for normal operation	• Cladding temperature borderline on 1000 °C limit during accident condition
•36 pins instead of 24, more wetted surface for the same core power as the WC-3 design	• Complex design and the structural integrity of relatively narrow graphite spokes during irradiation is questionable
	• Continuous runner contact between pressure tube and matrix for conduction is problematic because of pressure tube sagging. Matrix may get stuck during refueling.

Figure B-6

WC-4, Mini-Bundles Contained within a Graphite Matrix

Fuel Arrangement WC-5

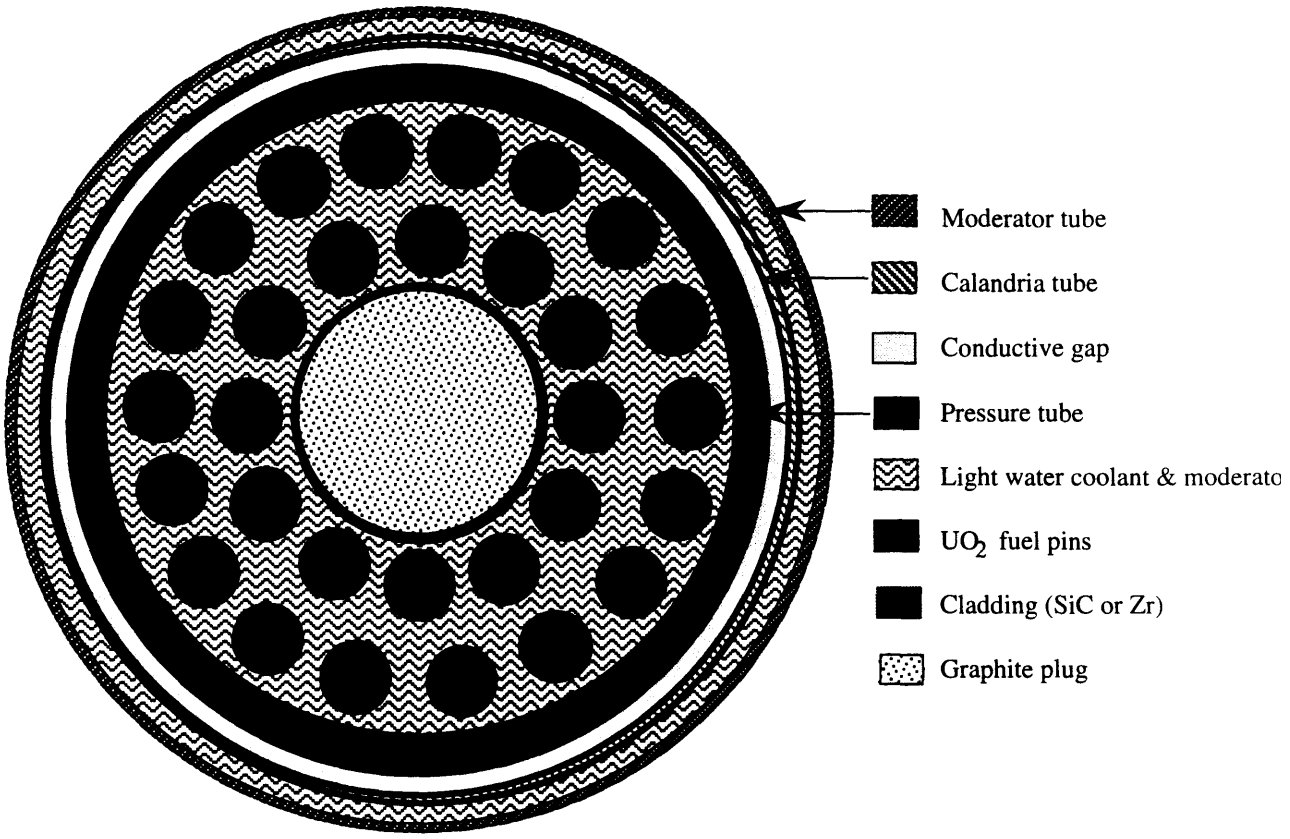

Advantages	Disadvantages
• Uses similar geometry to CANDU, thus the thermal hydraulics are similar	• Low heat removal rate from voided bundle compared to matrix type configurations
• Flatter power density profiles (peaking of 1.42) compensates for removed inner rings, and allows operation at a higher average heat flux than CE-CANDU (74.35 vs. 59.7 W/cm^2)	• Moderate storage capacity, temperature may exceed critical limits for Zircaloy before decay heat generation decreases enough to match the heat removal via radiation to the pressure tube
• Allows radiation of all decay heat to pressure tube, no conduction path is needed	• PCI exerts stress on SiC cladding and limits power rating and burnup
	• Low thermal conductivity of fuel, thus high stored energy

Figure B-7
WC-5, Two-Ring Design with SiC-Clad UO_2 Fuel Pins

Fuel Arrangement DC-1

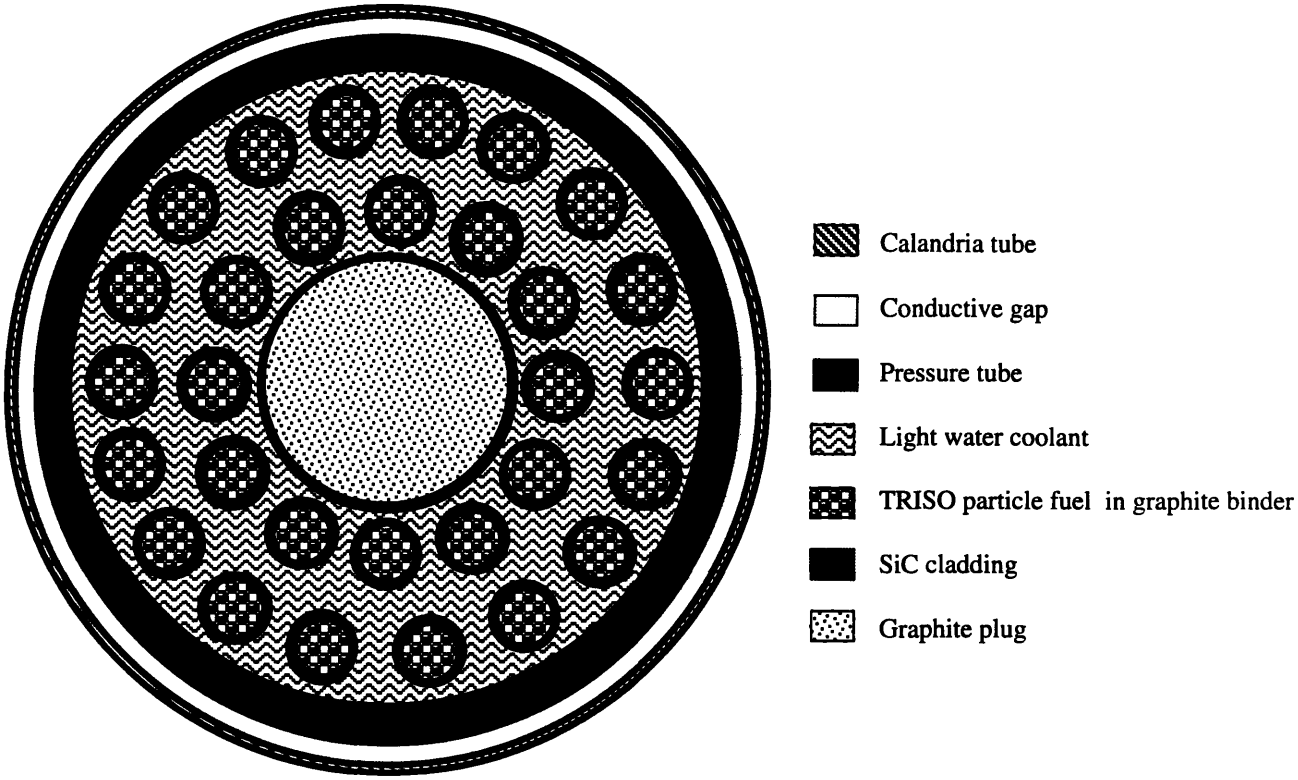

Advantages	Disadvantages
• Uses SiC-clad fuel technology developed in UK for CO_2 cooled reactors which was extensively tested and showed good performance	• Low heavy metal loading, hence high fluence on pressure tube (but less than for matrix-type with particle fuel)
• Uses similar geometry to CANDU, hence the thermal hydraulics are similar	• Low heat removal rates from voided bundles compared to matrix type configuration
• Flatter power density profile allows recovery of power lost by removing inner fuel rods; there is a potential to operate at an even higher power rating	• Low heat storage capability, hence the temperature of the matrix and pressure tube may exceed limits before the upper row of pressure tubes is flooded, establishing the decay heat removal path
• High fuel thermal conductivity, hence low operating fuel temperature and low stored energy	

Figure B-8 (from Hejzlar)
DC-1, Two-Ring Design with SiC-Clad TRISO Fuel

Fuel Arrangement DC-2

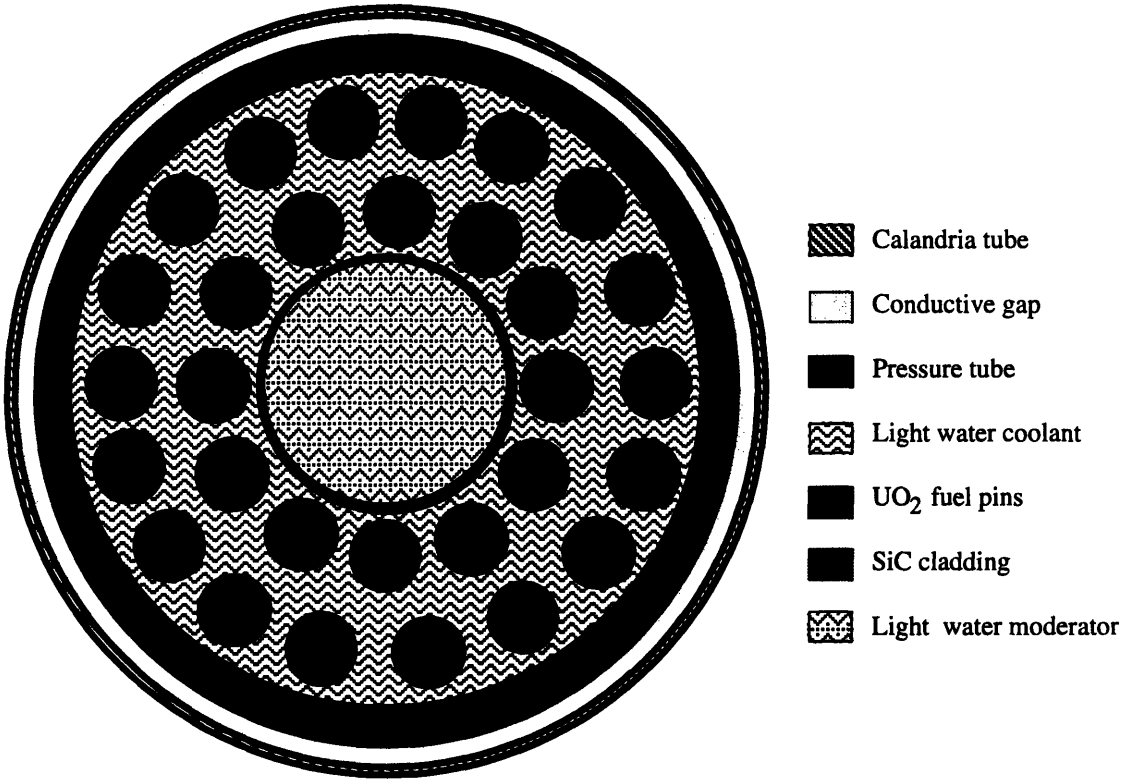

Advantages	Disadvantages
• Uses SiC-clad fuel technology developed in UK for CO_2 cooled reactors	• Low thermal conductivity of fuel, hence high stored energy
• Uses similar geometry to CANDU, thus the thermal hydraulics are similar	• Pellet-clad interaction exerts stress on SiC cladding and limits power rating and burnup
• Flatter power density profile allows recovery of power lost by removing inner fuel rods	• Low heat removal rates from voided bundles compared to matrix type configuration
• High heavy metal loading, hence lower fast fluence on pressure tubes than matrix fuel	• Low heat storage capability, thus limiting temperatures may be exceeded in an accident before the upper row of tubes is flooded
• High conversion ratio	

Figure B-9 (from Hejzlar)
DC-2, Two-Ring Design with SiC-Clad UO_2 Fuel Pins

Fuel Arrangement DC-3

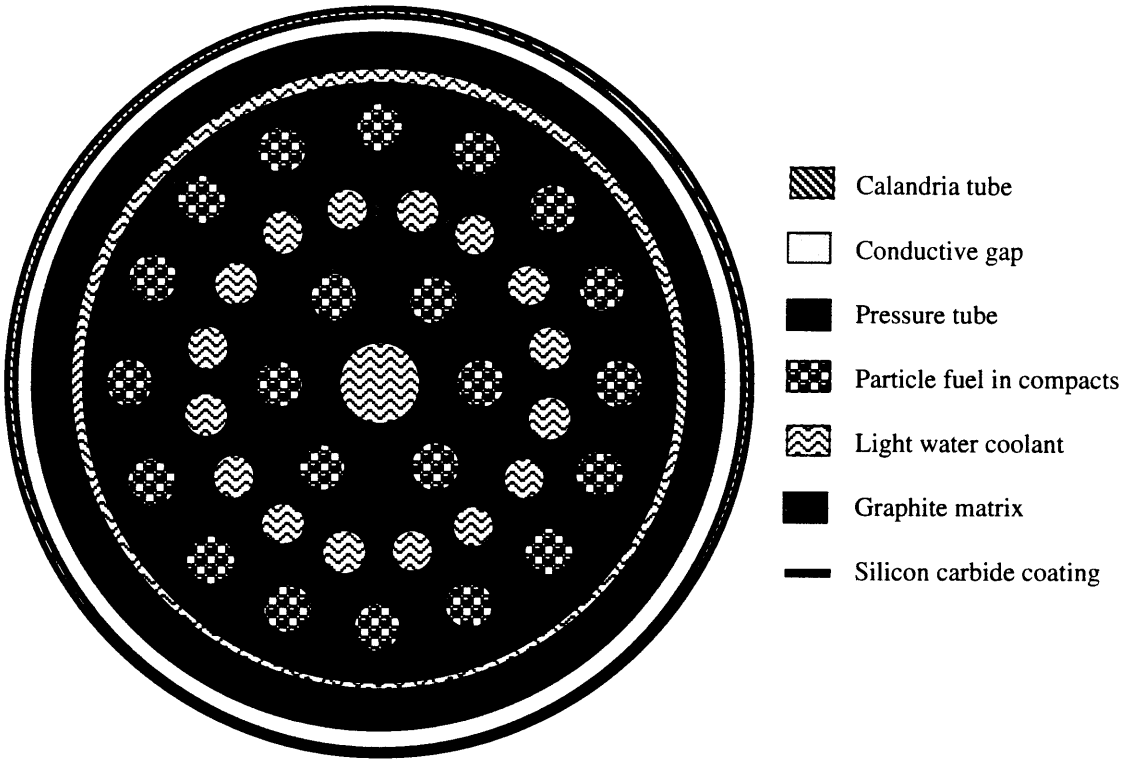

Advantages	Disadvantages
• Uses proven manufacturing technology of MHTGR fuel or HOBEG molded fuel blocks	• Small number of fuel compacts results in relatively high linear heat rate
• High thermal conductivity and storage capability, hence very good performance during LOCA	• Small heavy metal loading results in high fast fluence on pressure tubes
• Heterogeneous arrangement of fuel and coolant combined with voided space outside pressure tubes results in the longest prompt neutron lifetime, and flattest power profile compared with all other DC matrices	• Small heated perimeter, hence difficult to provide sufficient cooling during normal operation

Figure B-10 (from Hejzlar)
DC-3, Graphite Matrix with TRISO Fuel and Coolant Channels

Fuel Arrangement DC-4

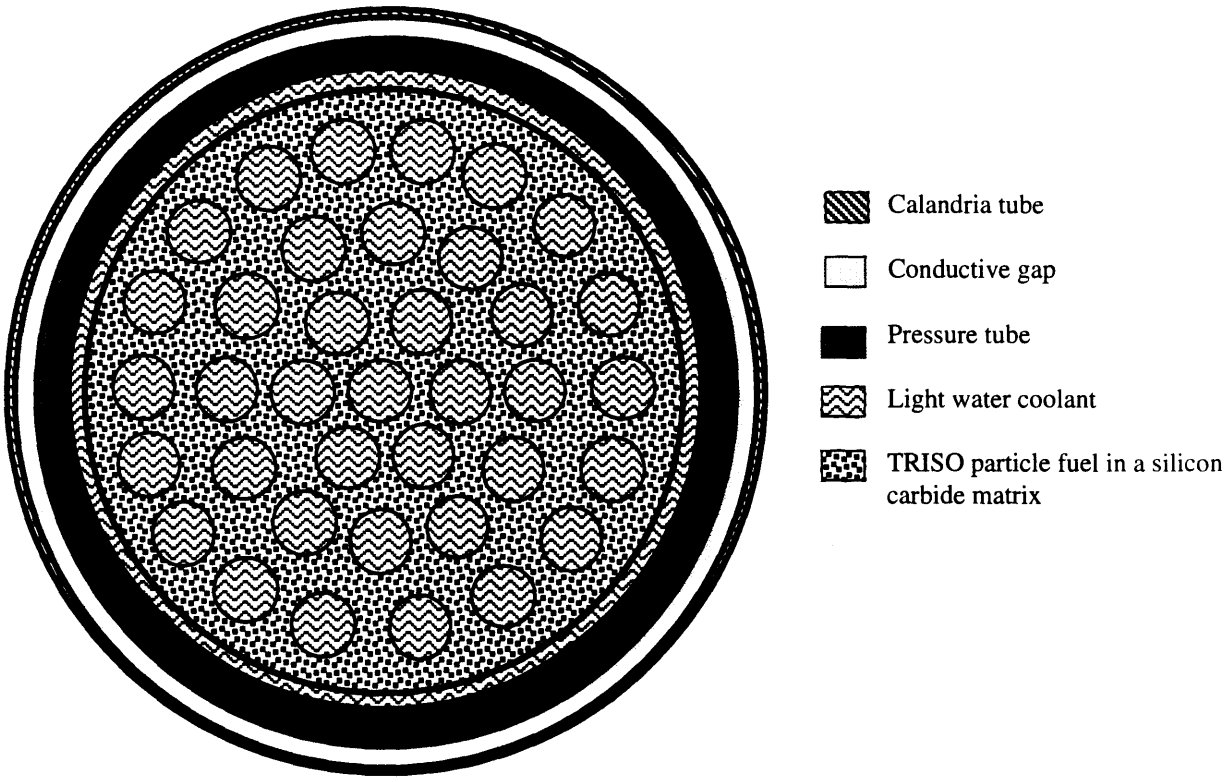

Advantages	Disadvantages
• Based on all ceramic fuel technology developed in UK for CO_2 cooled reactors which showed good fuel performance • High thermal conductivity and storage capacity, thus good performance during LOCA • Large heated perimeter, hence easy to cool during normal operation - large DNBR • Small distance between fuel and coolant and high thermal conductivity, hence low operating fuel temperature	• Low heavy metal loading, hence high fluence on pressure tubes • Requires higher enrichment to overcome parasitic absorption in SiC • Structural integrity of irradiated SiC matrix may be a problem due to decreased thermal conductivity and high thermal gradients

Figure B-11 (from Hejzlar)
DC-4, SiC Matrix with UC Fuel Dispersed Throughout

Fuel Arrangement DC-5

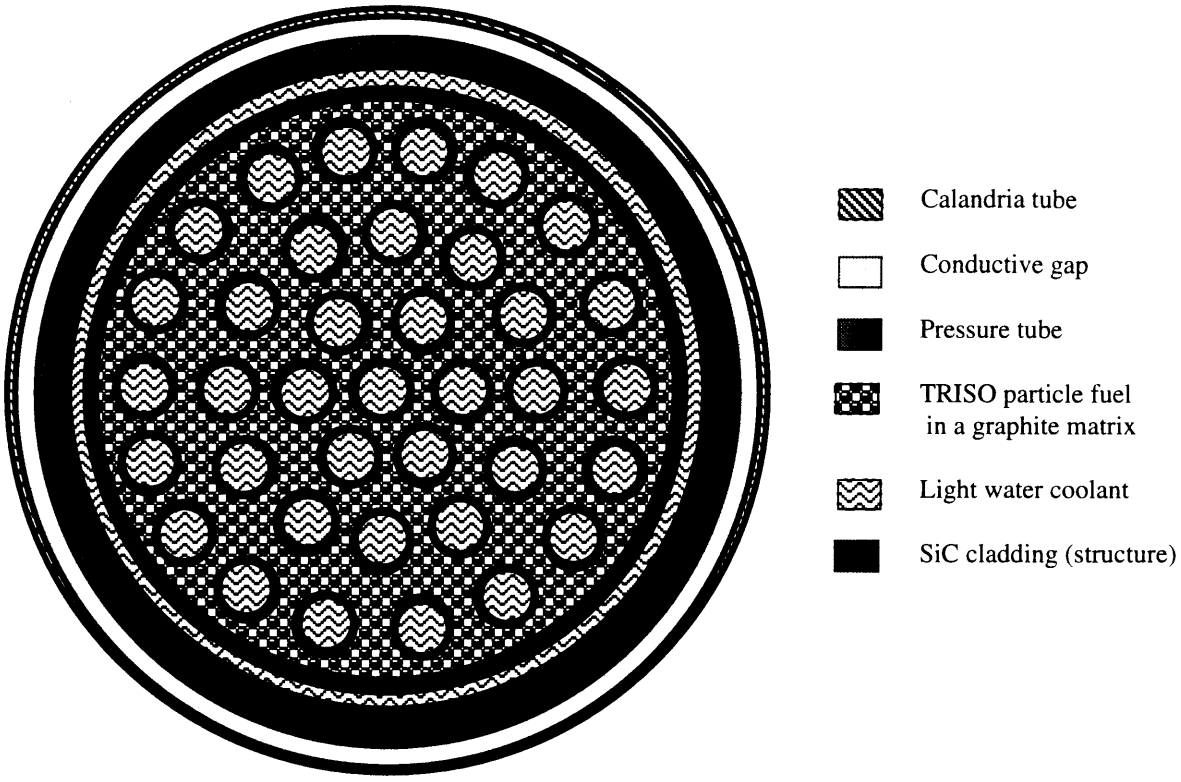

Advantages	Disadvantages
• High thermal conductivity and storage capacity, hence good performance during LOCA	• Non-proven fuel, may be difficult to manufacture with a high quality assurance
• Large heated perimeter, hence easy to cool during normal operation - Large DNBR	• Difficult to ensure the SiC closure plugs remain tight during operation
• Small distance between fuel and coolant and high thermal conductivity, hence low operating temperature	• Difficult to provide good key and dowel coupling between two neighboring elements
• Higher heavy metal loading than for DC-4, hence lower fluence, also requires slightly less enrichment	

Figure B-12 (from Hejzlar)
DC-5, TRISO/Graphite Matrix Surrounded by an SiC Structure

Appendix C. Specifications For WC-4 and WC-5 Designs

C.1 Material Properties Used in the Analyses of WC-4 and WC-5

This section lists the material properties used in the models of WC-4 and WC-5 for ADINA-T computer code.

Table C-1: UO_2 Properties used for Thermal Analysis (Taken from Todreas/Kazimi, 1990)

Temp (°C)	k (W/m°C)	c_p (J/kg°C)
0	9.8	220
200	7.0	220
400	5.0	250
600	4.0	290
800	3.2	300
1000	2.9	310
1200	2.6	320
1400	2.4	330
1600	2.3	340
1800	2.2	350
2000	2.2	370
2200	2.3	400
2400	2.5	450
2600	2.7	500
2800	3.0	500

The density of UO_2 was held constant at:

ρ = 10,421.5 kg/m^3.

This is 95% of the theoretical value.

Table C-2: SiC Properties used for Thermal Analysis (Taken from Hejzlar, 1991)

Temp (°C)	k (W/m°C)	c_p (J/kg°C)
100	10	1130
400	10	1130
1300	15	1130
2000	15	1130

The density of SiC was held constant at:

ρ=3100 kg/m3.

Note this is different from the value of 3200 kg/m^3 (3.2g/cm^3) used in Chapter 5 to calculate penetration.

The emissivity of SiC was held constant at:

ε = 0.9

Table C-3: Graphite Properties used for Thermal Analysis*

Temp (°C)	k (W/m°C)	c_p (J/kg°C)
200	26	450
300	26	1050
400	26	1225
500	26	1400
600	31	1458
700	36	1516
800	39	1575
900	41	1617
1000	41	1658
1100	42	1700
1200	43	1738
1400	43	1775

*These properties were estimated based on data for irradiated H-451 and H-237 nuclear graphites.

The graphite density was held constant at:

$\rho = 1770 \text{ kg/m}^3$

The density of zircaloy was held constant at:

$\rho = 6500 \text{ kg/m}^3$

The thermal conductivity of zircaloy was held constant at:

$k = 13 \text{ W/m°C}$

The heat capacity of zircaloy was held constant at:

$c_p = 330 \text{ J/kg°C}$

The emissivity of zircaloy was held constant at:

$\varepsilon = 0.8$

The zircaloy properties listed above were used to model zircaloy cladding, the pressure tube, and the calandria tube.

C.2 WC-4 Dimensions

Table C-4: WC-4 Fuel Design Dimensions

Parameter	Distance (mm)
Total core length	5940
UO_2 pellet radius	4.715
Pellet - clad gap thickness	0.045
Clad inner radius	4.76
Clad outer radius	5.18
Graphite matrix radius	61.0
Radial distance to center of rod 1	24.41
Radial distance to center of rods 2 and 3	35.66
Radial distance to center of rods 4 and 6	47.46
Radial distance to center of rod 5	45.82
Rod - rod pitch	12.36
Pressure tube inner radius	64.0
Pressure tube outer radius	69.79
Pressure tube thickness	5.79
Calandria tube inner radius	78.45
Calandria tube outer radius	79.97
Calandria tube thickness	1.52
Calandria tube - moderator tube gap	8.0
Moderator tube inner radius	87.97
Moderator tube outer radius	89.47
Moderator tube thickness	1.5

Fuel Rod positions for Table C-4

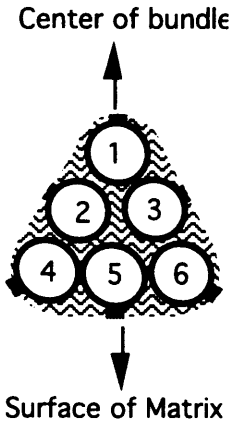

C.3 WC-5 Dimensions

Table C-5: WC-5 Fuel Design Dimensions

Parameter	Distance (mm)
Total core length	5940
UO_2 pellet radius	6.075
Pellet - clad gap thickness	0.045
Clad inner radius	6.12
Clad outer radius	6.54
Graphite slug radius	21.64
Radial distance to center of pellets in inner fuel ring	29.16
Radial distance to center of pellets in outer fuel ring	43.94
Pressure tube inner radius	51.5
Pressure tube outer radius	55.8
Pressure tube thickness	4.34
Calandria tube inner radius	64.5
Calandria tube outer radius	65.9
Calandria tube thickness	1.4
Calandria tube - moderator tube gap	8.0
Moderator tube inner radius	73.9
Moderator tube outer radius	75.42
Moderator tube thickness	1.52

Appendix D. Experimental Specimen Specifications

Specimens	Substrate	Coating Type	Coating thickness
A1 through A13	IG-110 graphite	PERMA-KOTE	~ 0.15 mm
B1 through B12	IG-110 graphite	CVD	~ 0.5 mm

All of the graphite tested was IG-110 nuclear grade graphite supplied by Toyo Tanso USA, Inc. IG-110 is purified IG-11 grade graphite. The A specimens were coated with the PERMA-KOTE SiC coating by Toyo Tanso USA, Inc. prior to being shipped to MIT. Because the specimens were very small, fixturing of the pieces was a problem. To produce a coating which completely encapsulated the specimens, it was necessary to coat the specimens twice. The second coat was applied to cover the areas left bare by the support fixture during the first coating process. This appendix contains copies of some of the company product information.

MIT purchased a small block of IG-110 graphite from Toyo Tanso. MIT subsequently machined several small pieces, some of which were shipped to Thermo Electron for application of the CVD SiC coating. Some of the remaining pieces of IG-110 were used in the tests as virgin graphite.

The α-SiC specimens were supplied by The Carborundum Company. The specific product was called Hexoloy® Sintered Alpha Silicon Carbide. This appendix contains copies of some of the company product information.

Hexaloy® SiC is a registered trademark of The Carborundum Company.

5530 NE 122nd AVE.
P.O. BOX 301368
PORTLAND, OR 97230
TEL: (503) 254-0674
FAX: (503) 254-0723

TOYO TANSO USA, Inc.

QUALITY GRAPHITE / EXCEPTIONAL SERVICE

Toyo Tanso USA is a leading supplier of isotropic, fine grain, ultra high purity graphite products for the worldwide semiconductor industry. Headquartered in Portland, Oregon, Toyo Tanso USA maintains customer support centers throughout the United States.

PRECISION MACHINING is carried out automatically by large capacity CNC turret lathes and milling centers. These machines are operated at very tight tolerance and with excellent repeatability.

TECHNICAL ENGINEERING on site provide expert sales support with design, technical assistance, and analytical capabilities to ensure optimum performance and product life in all applications.

ULTRA HIGH PURIFICATION processes reduce impurities of the graphite to less than 5ppm. Ultra pure graphite parts result in higher performance and improved yields in all semiconductor applications.

SILICON CARBIDE COATINGS AND CONVERSION developed by Toyo Tanso USA provides impervious, contamination free products on graphite substrates for semi-conductor processing environments.

CURRENT SEMICONDUCTOR APPLICATIONS SERVED:

- ISO molded single crystal puller parts
- EPI/CVD susceptors
- Ion implant components
- PECVD plates
- Etch electrodes
- RTP susceptors
- LTO diffusion cassettes
- Sputtering targets
- LPE boats

Toyo Tanso USA, committed to an elevated sense of excellence.

HOME OFFICE
PO BOX 301368
PORTLAND, OR 97230
TEL: (503) 254-0674
FAX: (503) 254-0723

MIDWEST OFFICE
413 VIRGINIA ST.
AUBURN, MI 48611
TEL: (517) 662-2600
FAX: (517) 662-2605

EASTERN OFFICE
4142 MALIBU DRIVE
MEDINA, OH 44256
TEL: (216) 723-4409
FAX: (216) 723-4529

TOYO TANSO USA, Inc.
QUALITY GRAPHITE / EXCEPTIONAL SERVICE

5530 NE 122nd AVE.
P.O. BOX 301368
PORTLAND, OR 97230
TEL: (503) 254-0674
FAX: (503) 254-0723

★★★★ PRODUCT BULLETIN ★★★★

SILICON CARBIDE ENGINEERED MATERIALS—FOR LTO AND DIFFUSION

The superior properties of silicon carbide make it an excellent replacement material for quartz in low temperature and diffusion applications. For the process engineer who is seeking superior process performance and control, **Toyo Tanso Silicon Carbide Materials** should be considered to replace traditional materials.

Wafer carriers manufactured from **Toyo Tanso Engineered Materials** provide many benefits:

Longer lifetime—silicon carbide at high temperatures and in hostile environments will not lose their dimensional integrity, providing more repeatable results, throughout the lifetime of the wafer carrier.

Fewer particles—silicon carbide is a more compatible material, with a higher CTE, allowing the deposited materials to adhere to the wafer carrier, releasing fewer particles.

High purity—the purity of silicon carbide is controlled and consistent from lot to lot, reducing the potential for contamination.

Impervious to most process gases and etchants—further reducing the potential for contamination.

Design flexibility and tolerance capability—the excellent engineering and manufacturing capability of Toyo Tanso allows us to engineer wafer carrier designs with close tolerance limits not available from traditional materials.

Toyo Tanso silicon carbide engineered materials can solve your process problems and reduce your processing costs. For more information about our products please contact:

HOME OFFICE
PO BOX 301368
PORTLAND, OR 97230
TEL: (503) 254-0674
FAX: (503) 254-0723

MIDWEST OFFICE
413 VIRGINIA ST.
AUBURN, MI 48611
TEL: (517) 662-2600
FAX: (517) 662-2605

EASTERN OFFICE
4142 MALIBU DRIVE
MEDINA, OH 44256
TEL: (216) 723-4409
FAX: (216) 723-4529

Introduction

As the first Japanese manufacturer of high density, fine grain isotropic graphite, TOYO TANSO have developped top quality graphite products for wide application range. This brochure is intended to show the basic knowledge and characteristics of our major isotropic grades for those who are selecting the most suitable graphite for given application and also who examine expansion of application of graphite.

Typical Grades / Properties

	Bulk density	Hardness	Specific Resistivity		Flexural Strength		Compressive Strength		Tensile Strength		Modulus of Elasticity		C. T. E.	Thermal Conductivity	
			$\mu\Omega$ cm	$\mu\Omega$·m	kg/cm²	MPa	kg/cm²	MPa	kg/cm²	MPa	kg/mm²	GPa	10^{-6}/°C 10^{-6}/K	kcal/m·h·cW/(m·k)	
IG-11	1.77	55	1100	11.0	400	39.2	800	78.4	250	24.5	1000	9.8	4.6	100	116
IG-12	1.78	60	1250	12.5	470	46.1	900	88.2	290	28.4	1100	10.8	4.7	90	104
IG11P	1.83	60	1100	11.0	470	46.1	950	93.1			1150	11.3	4.6		
IG-14	1.85	60	1000	10.0	460	45.1	850	83.3	280	27.4	1150	11.3	4.7	110	128
IG-15	1.90	60	950	9.5	500	49.0	1050	103.0	300	29.4	1200	11.8	4.8	120	139
IG-43	1.82	55	900	9.0	550	53.9	850	85.3	380	37.2	1100	10.8	4.8	120	139
IG-56	1.77	60	1300	13.0	440	43.1	900	88.2	280	27.4	1050	10.3	4.7	90	104
IG-70	1.85	65	1000	10.0	530	51.9	1000	98.0	320	31.4	1200	11.8	4.6	110	128
IG-73	1.75	65	1300	13.0	450	44.1	1050	102.9	300	29.4	950	9.3	5.5	90	104
ISEM-1	1.70	50	1350	13.5	370	36.3	700	68.6	200	19.6	900	8.8	4.2	80	93
ISEM-2	1.78	55	1100	11.0	420	41.2	850	83.3	250	24.5	1000	9.8	4.6	100	116
ISEM-3	1.85	60	1000	10.0	500	49.0	1050	103.0	300	29.4	1200	11.8	4.6	110	128
ISEM-8	1.77	65	1450	14.5	500	49.0	1100	107.8	330	32.3	950	9.3	5.5	80	93
ISO-61	1.80	75	1500	15.0	650	63.7	1500	147.0	450	44.1	1250	12.3	5.2	60	70
ISO-63	1.83	85	1650	16.5	800	78.4	1850	181.0	580	56.8	1400	13.7	5.5	60	70
ISO-88	1.90	90	1500	15.0	950	93.1	1850	181.0	700	68.6	1300	12.7	6.5	70	81
ISO-90	1.82	75	1350	13.5	770	75.5	1550	151.9	510	50.0	1500	14.7	6.2	70	81
ISO-95	1.90	85	1350	13.5	950	93.1	1900	186.2	630	61.7	1350	13.2	6.5	70	81
SIC-6	1.85	60	1000	10.0	500	49.0	1050	103.0	300	29.4	1200	11.8	5.0	110	128
SIC-10	1.78	55	1100	11.0	420	41.2	850	83.3	250	24.5	1000	9.8	4.8	100	116
SIC-12	1.78	60	1250	12.5	470	46.1	900	88.2	290	28.4	1100	10.8	4.7	90	104
KC-65	1.81	95	2100	21.0	900	88.2	2100	205.8							

Data are typical

Notes
1. CTE data are for the temperature range of 350~450°C.
2. The above grades can be purified (typical ash contents: 10ppm), and/or high purified (2ppm) upon requirement.
3. Conversion to SI units:-
   $\mu\Omega$ cm × 0.01 → $\mu\Omega$·m
   kg/mm² × 0.0098 → GPa
   kg/cm² × 0.098 → MPa
   Kcal/m·h·°C × 1.16 → W/(m·k)

Applications

	Metallurgy						EDM				Semiconductor (Purified Products)				
	Continius Casting Iron Casting	Non-ferrous Meta	Hot Press	Crucible	Heater	Boat Others	Rough Machining	Finishing	Rression Machining	Ultra-Precision Works	Crucible	Heater	SiC PyC Coating	Boat Others	Maximum Block Dimension(mm)
IG-11	○	◎	◎	◎	◎	◎					◎	◎	◎	◎	305×635×2040、φ610×900
IG-12	○	◎	◎	○	◎	○					○	◎	○	◎	432×432×1320、φ1100×610
IG-11P		◎				○									230×540×1000
IG-14		◎				○									230×540×1000
IG-15		◎				○								○	230×540×1000
IG-43		◎	○	○		○					○			○	305×620×1000、φ305×900
IG-56			◎	◎	◎	○					○	◎	○	◎	φ1100×610
IG-70	○	◎	◎	○	○	○					◎	○		○	305×620×1000、φ517×1050
IG-73			○	○	◎	○					○	◎	○	○	305×620×1000
ISEM-1					○	○	◎							◎	305×635×2040、φ1000×700
ISEM-2		○			○	○	◎	○				◎		◎	305×620×1000
ISEM-3		◎			○	◎	○	◎				◎		◎	305×620×1000
ISEM-8						○	○	◎	○					○	305×620×1000
ISO-61						○		◎	◎	○				○	230×540×1000
ISO-63			◎	○		◎		◎	◎	○	○	◎		◎	230×540×1000
ISO-88			◎			◎			◎	◎				◎	75×160×640、φ150×1800
ISO-90						○			◎	◎				○	150×150×610
ISO-95						○			◎	◎				○	75×150×460
SIC-6													◎		305×620×1000
SIC-10													◎		305×620×1000
SIC-12					◎								◎		273×765×765
KC-65						◎									(For jigs for glass to metal sealing)

Notes
1. Other grades for special applications are available upon requests.Please contact our agent or representative for the details.
2. Standard block sizes may change without notice.
3. ◎···Suitable ○···Applicable

Physical Properties (Data are for reference only)

Stress Strain (Grade : IG-12)

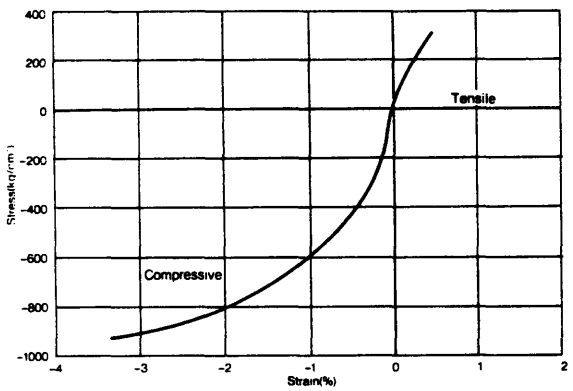

Generally, graphite shows elastic-plastic deformation. However, attention shall be paid to a charactor that fracturing behavior is different between tension and compression.
(Under tensile stress, graphite is not so strong)

Pore Size Distribution

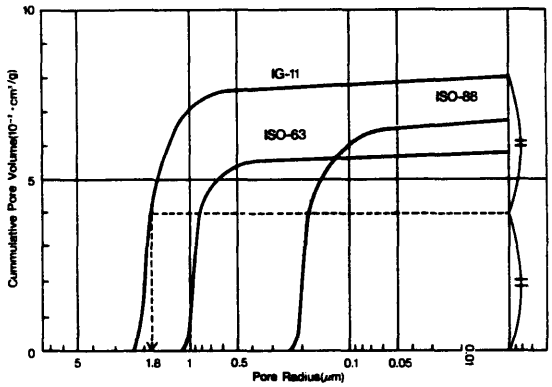

Above data are measured by mercury porosimeter. Pore distribution has a close relation with gas transmittance property and other unique propeties of graphite.

The position at 1/2 of cummulative pore volume indicates an averaged pore radius.

For Example : IG-11

$8/2 = 4 \times 10^{-2} \cdot cm^3/g \rightarrow 1.8\mu m$

Machining Standard

Dimensional Tolerance

Unit : mm

Nominal Dimension			Dimensional Tolerance
0.5	~	6	±0.1
	~	30	±0.2
	~	120	±0.3
	~	315	±0.5
	~	1000	±0.8
	~	2000	±1.2

Tolerance as per JIS B 0405-1977 to be applied, unless otherwise stated in working drawing.

Surface Roughness

Finishing Notation	Machining surface roughness		Finishing Method	JIS B 0601	
	Rmax	Ra		Rmax	Ra
▽▽▽▽	3s	0.75a	Honing Lapping	0.8s	0.2a
▽▽▽	12s	3.0a	Grinder.Lathe Milling cutter	6.3s	1.6a
▽▽	35s	8.75a	Milling cutter.Lathe	25s	6.3a
▽	100s	25.0a		100s	25.0a
~	No prescript		Band Saw	No prescript	

Graphite materials have more porous structure compared with metallic materials. Therefore, surface roughness will appear a little greater than metals.

Manufacturer may change specification without notice

Chemical Properties

Reaction Starting Temperature of Graphite in Gas Atmosphere

Atmosphere	Reaction Starting Temp.	Reaction
The air	380 – 400°C	Oxydation
Water vapor	700 – 750	ditto
CO_2	800 – 900	ditto
H_2	1000 – 1200	Methanidation
N_2	2000 – 2500	Cyanidation
CL_2	2500	(Graphite sublimates)
Ar	3000	(ditto)
Vacuum	2200	(ditto)

Although oxydation starting temperature of graphite is comparatively low in oxydation atmosphere, graphite shows chemical and thermal stability in non-oxydation atmosphere, which expands applications of graphite materials.

Reaction Starting Temperature of Graphite with Other Substances

Substance	Reaction Starting Temperature	Compound
Ar	800°C	Al_4C_3
B	1600	B_4C
Fe	600 – 800	Fe_3C
Na	400 – 450	C-Na intercalation compound (under O atmosphere)
Co	218	CoC, Co_3C
Mo	700	Mo_2C
Ni	1310	Carbunsation into Ni
Si	1150	SiC
Cu	No reaction	
Mg	〃	
Pb	〃	
Sn	〃	
W	1400	W_2C, WC(under H_2 atmosphere)
K	300	C_8K or other intercalation compound
Li	500	Li_2C_2
Be	900	Be_2C(under vacuum or He atmosphere)
B_2O_3	1200	CO_2 + Reduced substance
V_2O_5	438	〃
Fe_2O_3	485	〃
TiO_2	930	〃
SiO_2	1250	SiC 〃
Al_2O_3	1280	Al_4C_3 〃
BeO	960	Be_2C 〃
MgO	1350	〃
ZrO_2	1300	ZrC 〃

Vapor Pressure

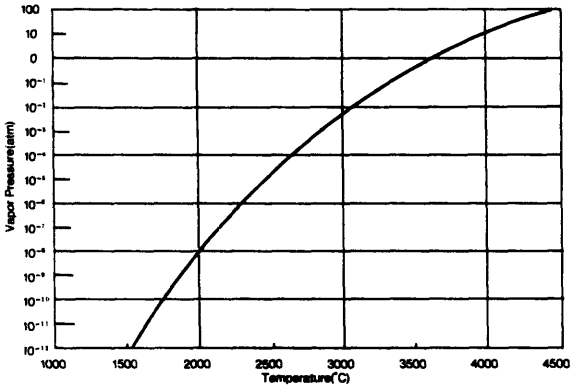

Graphite is a very stable material under 2200°C, but vapor pressure increases under higher temperature and/or lower pressure. Graphite wear by vaporization should be considered in these cases.

Gas Desorption

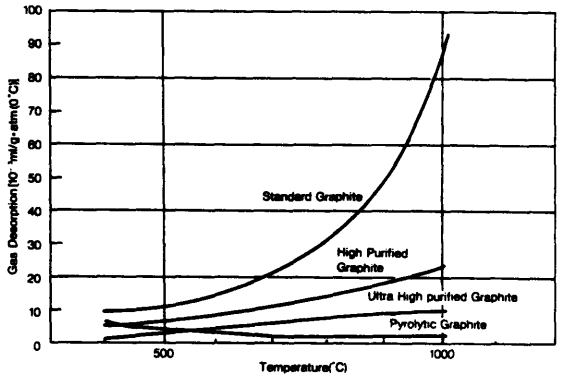

Graphite discharges absorbed gasses under high temperature atmosphere.
Applications such as semiconductor field employ pyrolytic or high purified graphite which discharges less gasses.

Typical Impurity Level (ppm)

– Not Detected

Purity Level		Elements	Al	As	B	Be	Bi	Ca	Cd	Ce	Cr	Cu	Fe	Ga	Ge	Hg	In	K	Li	Mg	Mn	Na	Ni	P	Pb	Si	Sn	Ti	Zn
Ultra High Purity	2ppm		–	–	–	–	–	–	–	–	–	–	–	–	–	–	–	–	–	–	–	–	–	–	–	–	–	–	–
High Purity	10ppm		(0.3	–	–	–	–	–	–	–	–	–	(1.0	–	–	–	–	–	–	(0.1	–	–	–	–	–	(0.1	–	–	–
General Graphite	400ppm		14	–	3	–	–	6	–	–	–	–	26	–	–	–	–	–	–	0.2	–	–	4	–	–	2	–	33	–

The ash content of standard graphite is about 400 ppm but applications such as semiconductor usually call for higher purity. For these requirements, we can reduce impurity level into a few ppm by halogenation treatment at high temperature.

High Temperature Properties (Data are for reference only)

Electrical Resistivity

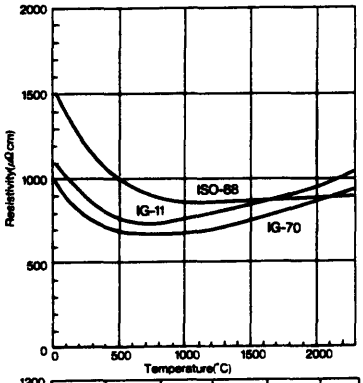

Resistivity at each temperature should be always considered when designing heaters as each grade has each characteristic.

Strength
(Grade : IG-11)

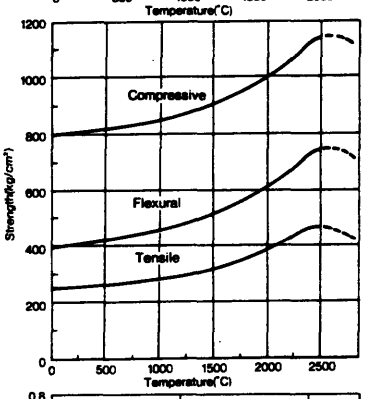

A remarkable feature with graphite compared with other engineering materials is that strength increases according as the temperature rises(till 2500°C) and the maximum strength becomes almost double of that at room temperature. Thus graphite is considered as one of the essential materials in the high temperature applications.

Thermal Expansion

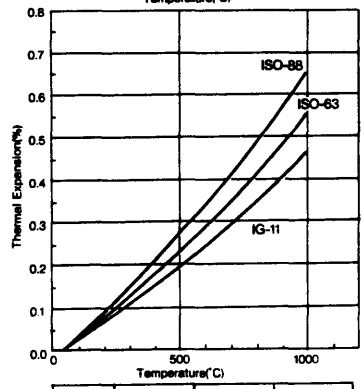

$$\text{C.T.E.}(10^{-6}/^{\circ}\text{C}) = \frac{\text{Thermal expansion ratio (\%)} \times 10^{-2}}{\text{Temperature difference (°C)}}$$

Comparison of C.T.E.

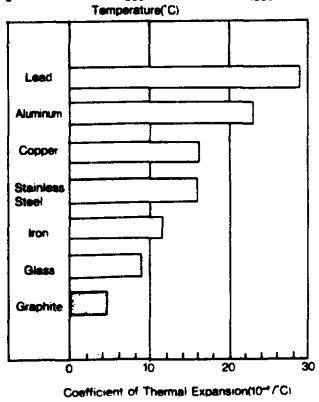

C.T.E. of graphite is much lower than general metallic materials and graphite shows dimensional stability when used at high temperature.

Thermal Conductivity

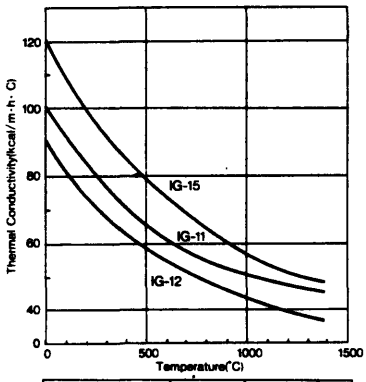

Measurement by Laser flash method

Comparison of Thermal Conductivity

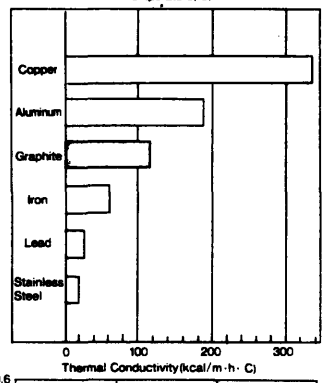

Thermal conductivity of graphite is considerably high and C.T.E. is very low. This brings superior thermal shock resistance with graphite materials. By Wiedemann Franz's law, the relation between thermal conductivity and resitivity of graphite is indicated as below:-

$$\text{Thermal conductivity(kcal/m.h.°C)} = \frac{0.1116 \times 10^6}{\text{Resistivity}(\mu\Omega\text{cm})}$$

Specific Heat

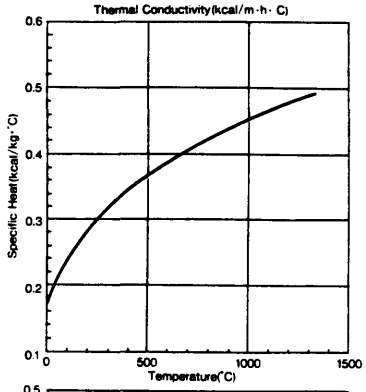

Due to anisotropy of graphite crystals, specific heat of graphite is around 1/3 of general solid. The most of thermodynamic functions are led by this essential incident. Specific heat at high temperature of graphite materials tends to have similar transition regardless of grades.

Conversion to SI units:-
kcal/(kg·°C) x 4.186 X 10^3 → J/(kg·K)

Thermal Diffusivity

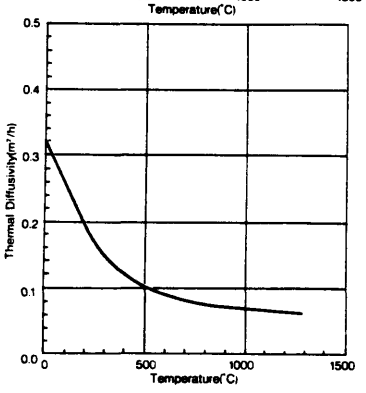

Thermal diffusivity shows thermal transitability of materials. Large thermal diffusivity indicates that the material transfers heat quickly. Graphite has extremely higher thermal diffusivity than other materials.

Conversion to SI units:-

$$\text{Thermal diffusivity } (m^2/h) = \frac{\text{Thermal conductivity(kcal/m.h.°C)}}{\text{Specific heat(kcal kg·°C)} \times \text{Density(g cm}^3\text{)}}$$

PERMA-KOTE
SiC Coated Graphite

PERMA-KOTE is a brand name for our SiC coated graphite which was developed on the basis of the best combination of our own isotropic graphite substrate with fully controlled CTE property and SiC coating technology.

FEATURES

- Excellent heat resistance
- Corrosion resistance
- Impermeability
- High purity
- Thermal shock resistance
- Wear resistance

RESISTANCE OF PERMA-KOTE TO CHEMICALS

Chemical Reagent	Fluid Temp.	Time (Hrs)	Weight Loss (mg/cm^2)
47% HF	25°C	288	Trace
47% HF	80°C	144	−0.10
20% HCl	Boiling Point	288	Trace
36% HCl	Boiling Point	144	Trace
60% H_2SO_4	70°C	144	−0.10
97% H_2SO_4	110°C	144	Trace
50% HNO_3	Boiling Point	144	Trace
61% HNO_3	Boiling Point	144	Trace
50% $HCrO_4$	25°C	288	+0.05
HF+HNO_3(1:1)	25°C	288	Trace
HF+HNO_3(1:1)	80°C	288	−0.10
HNO_3+H_2SO_4	25°C	288	−0.10
Conc. $Na_2Cr_2O_7$/H_2SO_4	25°C	288	−0.15
20% NaOH	25°C	288	Trace
20% NaOH	80°C	288	Trace
H_3PO_4	100°C	192	−0.10
Aqua Regia	80°C	192	Trace

PROPERTIES OF SIC COATING LAYER

Structure	β (3C)
Bulk Density	3.2g/cm^3
Hardness	2,800(Knoop)
Coefficient of Thermal Expansion	4.9x10^{-6}/K (25 – 1350°C)
Electrical Resistivity	14Ω cm
Porosity	0%
Modulus of Elasticity	32,500kg/mm^2

PERMA-KOTE
SiC Coated Graphite

FEATURES

1. Very close to C.T.E. of SiC
   Free from crack and peeling of SiC layer
2. High dense and high purified isotropic graphite
3. Very fine grain graphite
   Very stable properties

SIC-610

CHARACTERISTICS OF SUBSTRATES

Bulk Density		1.85
Hardness	Shore	58
Specific Resistance	$\mu\Omega$cm	1,000
Flexural Strength	kg/cm^2	500
Compressive Strength	kg/cm^2	1050
Tensile Strength	kg/cm^2	280
Modulus of Elasticity	kg/mm^2	1,200
C.T.E. (350 ~ 450°C)	x10^{-6}/°C	5.0
Thermal Conductivity	kcal/mhr°C	110
Oxidation Starting Temp.	°C	550
Ash Content	ppm	20

IMPURITIES

(MeanValue)

Elements	PPM
Fe	4.0
Si	1.0
Ca	<1.0
Li	<1.0
Na	<1.0
K	<1.0
Cu	<1.0
Co	<1.0
Al	<0.5
V	<0.5
Ni	<0.3
Ti	<0.3
B	0.1
Mg	<0.1

SIC-120

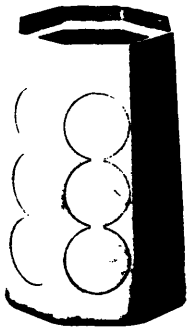

CHARACTERISTICS OF SUBSTRATES

Bulk Density		1.77
Hardness	Shore	64
Specific Resistance	$\mu\Omega$cm	1,500
Flexural Strength	kg/cm^2	500
Compressive Strength	kg/cm^2	1000
Tensile Strength	kg/cm^2	290
Modulus of Elasticity	kg/mm^2	1,100
C.T.E. (350 ~ 450°C)	x10^{-6}/°C	4.9
Thermal Conductivity	kcal/mhr°C	86
Oxidation Starting Temp.	°C	550
Ash Content	ppm	20

IMPURITIES

(MeanValue)

Elements	PPM
Fe	4.0
Si	1.0
Ca	<1.0
Li	<1.0
Na	<1.0
K	<1.0
Cu	<1.0
Co	<1.0
Al	<0.5
V	<0.5
Ni	<0.3
Ti	<0.3
B	0.1
Mg	<0.1

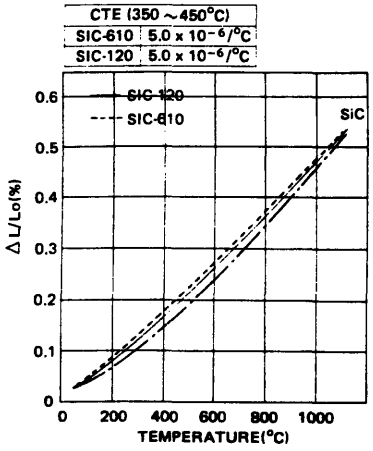

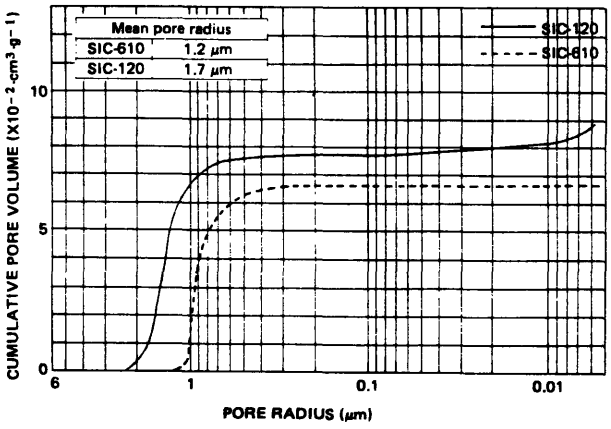

Contact Us for Cost-Effective Structural Ceramics

You can count on Carborundum expertise to help you specify the correct structural ceramic materials to meet exacting component design criteria. Our applications engineering support team has the experience and talent to provide solutions to product design problems. Proven structural ceramic/silicon carbide products, together with proven manufacturing capabilities, are your assurance of world-class supply and quality assurance. Your key to cost-effective part procurement—the Carborundum structural ceramic specialists. For more information, contact one of the offices in our worldwide network.

Mönchengladbach, West Germany

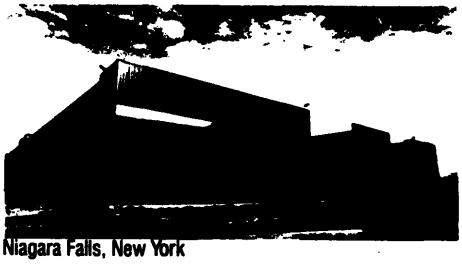

Niagara Falls, New York

CARBORUNDUM

United States
The Carborundum Company
Structural Ceramics Division
P.O. Box 1054
Niagara Falls, New York 14302-1054
Telephone 716 278-6233
Telefax 716 278-3909
Telex 68-54335
Cable (Foreign): Crboinuw

Australia
Carborundum Resistant Materials
326 Settlement Road
Thomastown, 3074, Victoria
Melbourne, Australia
Telephone 61-3-463-0211
Telecopier 61-3-465-6015
Telex 790-38327 (AB: CARBOS AA 38327)

Brazil
Carborundum, S.A.
Rua Santos Dumont, 111
13280 Vinhedo, São Paulo, Brazil
Telephone 55-192-76-3300/3555
Telecopier 55-192-76-3620
Telex 391-191838 (AB: 191838 CARB BR)

West Germany
Carborundum Technical Ceramics GMBH
Gustav-Schoenleber-Strasse 39
D7120 Bietigheim, West Germany
Telephone 49-7142-43284
Telefax 49-7142-42177

Form A-12,047
Effective 7/91 Supercedes 2/90

Hexoloy® Silicon Carbide– The Material Difference

More design engineers are finding out that traditional views of "ceramics" don't apply to Hexoloy silicon carbide products. Hexoloy products are opening new areas of application and design possibilities that are impractical with ductile metals and lesser ceramic materials.

Hexoloy alpha silicon carbide is produced by pressureless sintering the ultra-pure submicron powder derived from the original Acheson process. This powder is mixed with non-oxide sintering aids, then formed into complex shapes by a variety of methods and consolidated by sintering at temperatures above 2000°C (3632°F).

The sintering process results in a single-phase, fine-grain silicon carbide product that's very pure and uniform, with virtually no porosity. Whether submerged in corrosive environments, subjected to extreme wear and abrasive conditions, or exposed to temperatures in excess of 1400°C (2552°F), Hexoloy sintered alpha silicon carbide will outperform other commercially available ceramics or metal alloys, including superalloys.

These properties, plus the others outlined here, make Hexoloy silicon carbide ideal for applications such as chemical and slurry pump seals and bearings, nozzles, pump and valve trim, paper and textile equipment components, armor and more.

Think of all the applications where the properties of Hexoloy silicon carbide materials can make a big difference.

It's hard.

Hexoloy silicon carbide is one of the hardest high-performance materials available, second only to diamonds.

Hardness (Knoop): 2800 kg/mm² at room temperature.

It's strong.

Actual use of Hexoloy silicon carbide parts indicates extremely high strength and excellent resistance to creep and stress rupture at temperatures up to 1650°C (3000°F) for sintered alpha silicon carbide.

Flexural strength (4 pt.): 58,600 psi (404 MPa) at 1500°C.

Fracture toughness: 420 x 10^3 psi/$m^{1/2}$ at 25°C.

Modulus of elasticity (RT): 59 x 10^6 psi (410 GPa).

It's light.

Hexoloy silicon carbide weighs less than half as much as most metal alloys, 40 percent as much as steel and about the same as aluminum.

It's dense.

Densities of fired parts are consistently in excess of 98 percent of the theoretical density of Hexoloy silicon carbide—3.21 g/cm³.

Density: 3.10 g/cm³ minimum.

It's wear resistant.

The extreme hardness and density of Hexoloy silicon carbide make it ideal for applications where parts are subject to high abrasion and sliding wear.

Specific wear rate (pin on disc): SiC vs. SiC 1 x 10^{-9} mm²/kg.

Coefficient of friction (pin on disc): SiC vs. SiC 0.2.

It resists corrosion, oxidation and erosion.

The high density, low porosity and chemical inertness of Hexoloy silicon carbide permit it to function in environments of hot gases and liquids, in oxidizing and corrosive atmospheres, and in strong acids and bases, even at extremely high temperatures.

It resists heat.

The high thermal conductivity of Hexoloy silicon carbide, combined with its low thermal expansion, produces excellent thermal-shock resistance far better than tungsten carbide, aluminum oxide and RB silicon nitride. These properties make it a promising candidate to replace ductile metals in high-temperature gas turbines and diesel engines, as well as heat-exchanger sections.

It can be formed into complex shapes.

New developments by Carborundum researchers in the use of bonding agents and other additives now permit the mass production of complex shapes of Hexoloy silicon carbide by extrusion; pressure forming, with bidirectional or isostatic presses at room temperature; slip casting; and injection molding.

It requires minimum machining.

The as-fired surface finish of Hexoloy silicon carbide parts is excellent (about 64 microinches).

This surface quality, combined with tight dimensional control, yields parts that should require little or no additional machining or finish grinding, depending on application.

It's available.

Silicon carbide is made from two abundant raw materials, silica (sand) and carbon. Worldwide production capacity currently exceeds demand. There are no issues of recurring shortages of critical raw materials that have hindered the production of tungsten carbide and most high-temperature superalloys.

Hexoloy silicon carbide can be mass produced into reliable, complex components at a very competitive cost.

It's up to you.

Where can you use Hexoloy silicon carbide materials? We hope the information in this brochure provides you with some new ideas. And we look forward to helping you explore the possibilities of applying this unique material to your particular requirements.

Physical Properties of Hexoloy® SiC Materials

Physical Properties	Units	Hexoloy SiC Grades—Typical Values			
		SA	SG	ST	KG
Composition* (phases)		SiC	SiC + C	SiC + TiB_2	SiC + Si + C
Density	g/cm^3	3.10	2.5	3.30	2.70
Grain Size	microns	4–6	N/A	5 TiB_2 8 SiC	N/A
Hardness (Knoop)**		2800	N/A	2800	1000
Flexural Strength 4pt @ RT***	MPa x 10^3 lb/in^2	460 60	N/A	448 65	48 7
Compressive Strength @ RT	MPa x 10^3 lb/in^2	3900 560	N/A	N/A	410 60
Modulus of Elasticity @ RT	GPa x 10^6 lb/in^2	410 59	210† 30†	427 61	210 30
Weibull Modulus (2 parameters)		10	N/A	12	N/A
Poisson Ratio		0.14	N/A	0.15	N/A
Fracture Toughness @ RT Double Torsion & SENB	MPa/m x 10^3 lb/in$^2/\sqrt{in}$	4.60 4.20	N/A	8.0 7.3	N/A
Coefficient of Thermal Expansion RT to 700°C	x 10^{-6} mm/mm°K x 10^{-6} in/in°F	4.02 2.20	4.10† 2.30†	4.02 2.20	4.50 2.50
Max. Service Temp (air)	°C °F	1650 3000	1200 2190	1200 2190	820 1500
Mean Specific Heat @ RT	J/gm°K	0.67	0.6†	0.66	N/A
Thermal Conductivity @ RT	W/mK Btu/ft h°F	125.6 72.6	100† 60†	93.0 54.0	112.4 65.0
@ 200°C	W/mK Btu/ft h°F	102.6 59.3	N/A	N/A N/A	90.0 52.0
@ 400°C		77.5 44.8	N/A	38.0 22.0	73.0 42.0
Permeability, RT to 1000°C		All impervious to gases over 31 MPa.			
Electrical Resistivity @ RT**** @1000°C	ohm-cm	10^2–10^6 0.01–0.2	0.01–50 N/A	0.1–1.0 0.1–1.0	N/A
Emissivity		0.9	N/A	N/A	N/A

* Composition Code: Si = free silicon metal; C = free graphite; SiC = silicon carbide; TiB_2 = titanium diboride
** Test Bar Size: 3.2 x 6.4 x 50.8 mm (⅛" x ¼" x ½")
*** Knoop 1000-gm load
**** Dependent upon dopants in Hexoloy SA SiC that will decrease electrical resistivity to a desired range.
† Estimated.

Hexoloy® SiC Material Grades–A Growing Family

Hexoloy SA Silicon Carbide

Hexoloy SA SiC is a pressureless, sintered form of alpha silicon carbide, with a density greater than 98 percent theoretical. It has a very fine grain structure (8 microns) for excellent wear resistance and contains no free silicon, which makes it highly chemically resistant in both oxidizing and reducing environments.

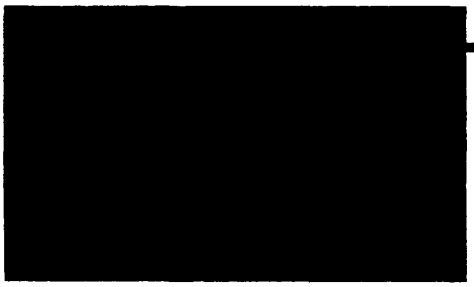

Hexoloy ST Silicon Carbide

Hexoloy ST SiC is a particulate-reinforced, two-phase ceramic composite material with a microstructure consisting of titanium diboride (TiB_2) particles from 1 to 5 microns in diameter in a fine-grain silicon carbide matrix. The TiB_2 particles improve the fracture toughness and strength, while the composite maintains the other desirable properties inherent in the silicon carbide matrix.

Hexoloy SG Silicon Carbide

Hexoloy SG SiC is a unique, patented analogue of Hexoloy SA SiC. It is a sintered silicon carbide and has no free silicon metal. It is electrically conductive, permitting DC-magnetron sputtering rates approximately half that of aluminum. It also has excellent thermal conductivity.

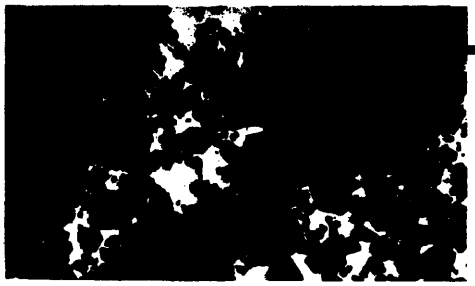

Hexoloy KG Silicon Carbide

Hexoloy KG SiC is a reaction-bonded silicon carbide with free silicon and graphite. Compared with Hexoloy SA SiC, it sacrifices thermal oxidation resistance for improved thermal shock resistance. At very high thermal shock loads, the graphite absorbs uneven expansion, preventing high stress concentrations and failure.

Hexoloy® SiC Design Considerations

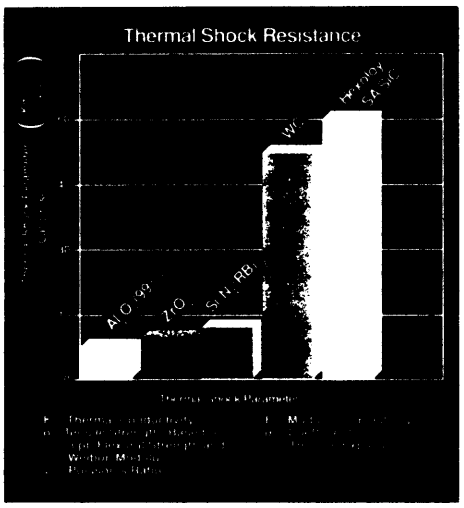

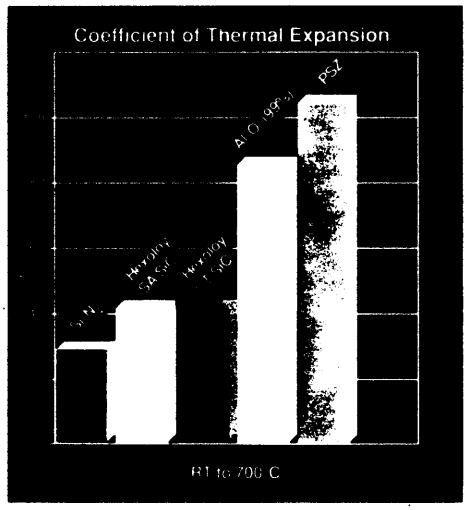

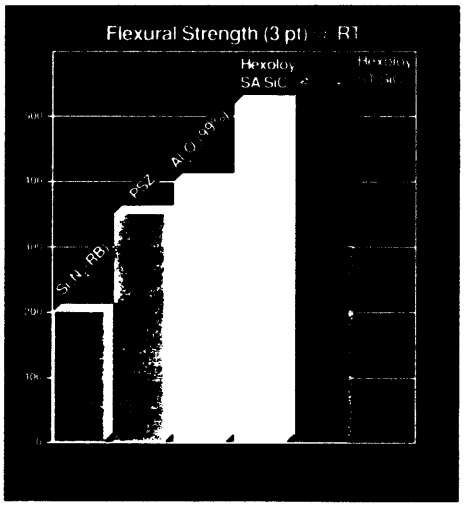

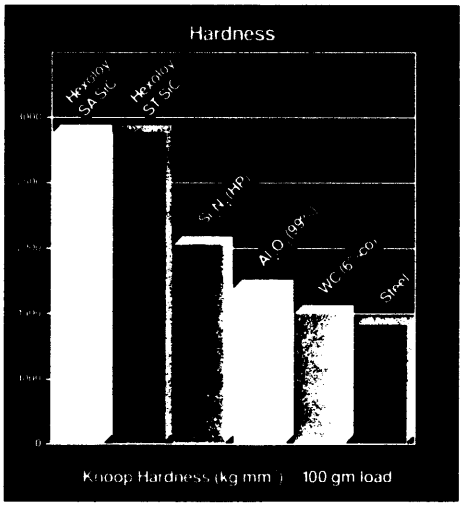

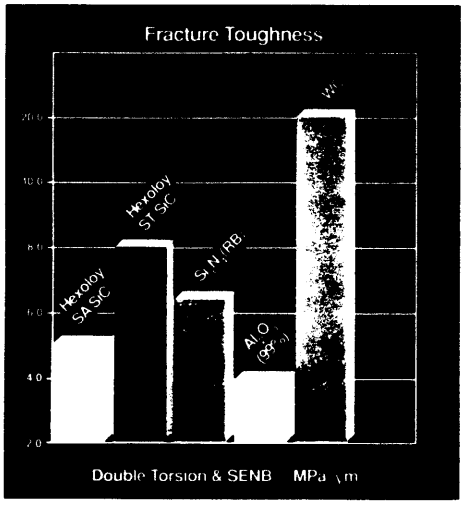

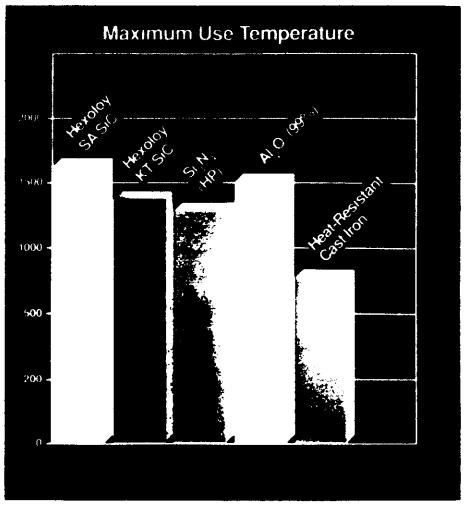

Hexoloy® SiC is a registered trademark of The Carborundum Company

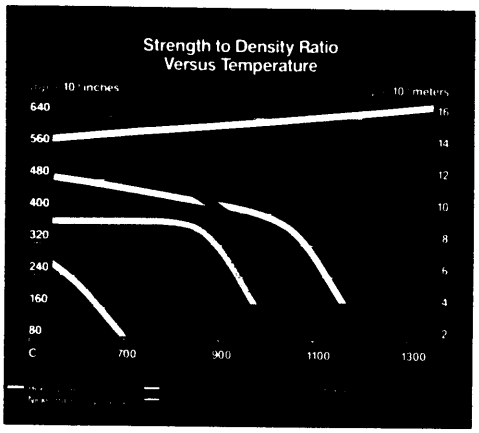

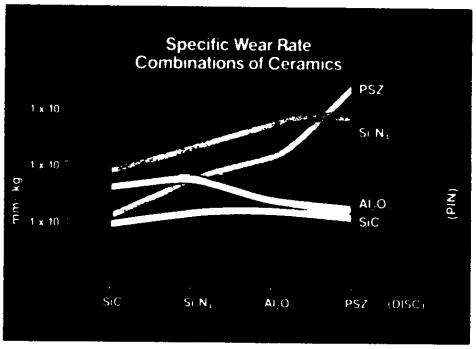

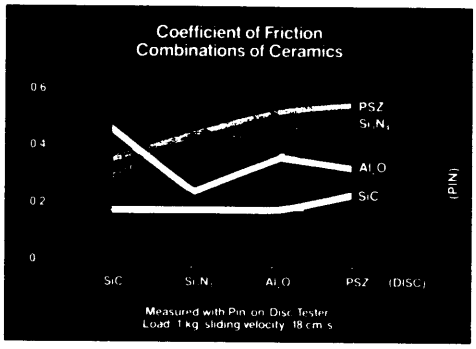

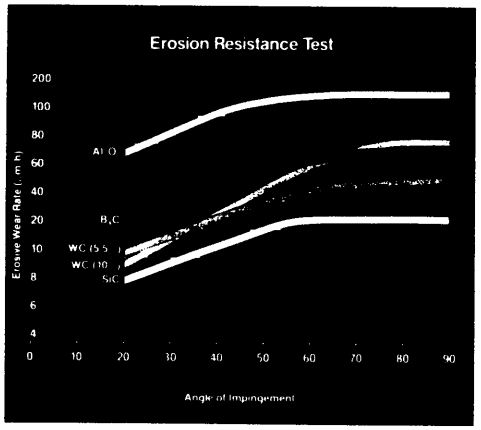

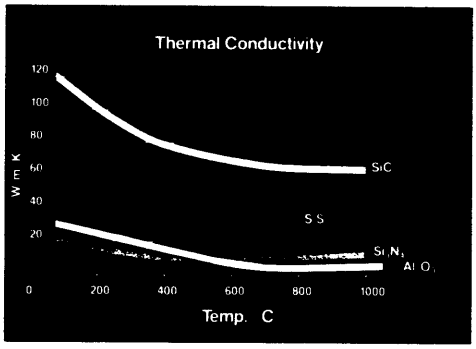

Corrosion Test Results in Liquids

Test Environment* Conc. Reagent (Wt%)	Temp. (°C)	Corrosive Weight Loss (mg/cm² yr)** Hexoloy SA SiC	Hexoloy KT SiC	Tungsten Carbide	Aluminum Oxide
98% H_2SO_4	100	18	550	>1000	550
50% NaOH	100	25	>1000	50	750
5% HF	25	<.02	79	80	200
85% H_3PO_4	100	<.02	88	550	>1000
70% HNO_3	100	<.02	05	>1000	75
45% KOH	100	<.02	>1000	30	600
2% HF	70	<.02	09	850	220
10% HF plus 5% HNO_3	25	<.02	>1000	>1000	160

*Test Time:
**Corrosion Weight Loss Guide:

Hexoloy® SiC is a registered trademark of The Carborundum Company.

Appendix E. Nomenclature

Symbol	Meaning (units)
c_p	Heat capacity (J / kg°C)
δ	Penetration depth (μm)
ρ	Density (grams / cm^3)
ω	Extent of reaction (mg)
K	Weight loss per area per time (mg / dm^2 / $day^{1/3}$)
k	Thermal conductivity (W / m°C)
m	Molecular weight (grams / mol)
N	Moles (mol)
n	Moles per area (mol / cm^2)
R	Universal Gas Constant (1.987 cal / mol K)
SA	Surface Area (cm^2)
T	Temperature (K) (°C)
t	Time (seconds) (hours) (days)
ΔW	Weight change (grams)
Δw	Weight change per area (grams / cm^2)